

Republic of Iraq

Ministry of Higher Education  
and Scientific Research

University of Kufa

Faculty of Engineering

Department of Civil Engineering



# Structural Health Monitoring of Imam Ali Holy Building Using Particle Swarm Optimization Method

A Thesis

Submitted to the Faculty of Engineering at University of Kufa in Partial  
Fulfillment of the Requirements for the Degree of Master of Science in Civil  
Engineering – Structural Engineering

By

**Karrar Hussain Dona**

B.Sc. In Civil Engineering (2018)

Supervised By

**Asst. Prof. Dr. Saad Jabbar Al-Wazni**

1444

2022

بِسْمِ اللَّهِ الرَّحْمَنِ الرَّحِيمِ

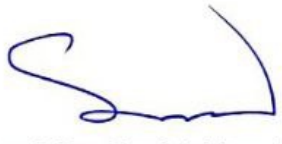
وَقَالَ  
رَبِّ زِدْنِي عِلْمًا

صدق الله العلي العظيم

سورة طه: الآية ١١٤

## Supervisor Certification

I certify that this thesis "**Structural Health Monitoring of Imam Ali Holy Building Using Particle Swarm Optimization Method**" has been prepared by "**Karrar Hussain Dona**" under my supervision at the Department of Civil Engineering in the University of Kufa in partial fulfillment of the requirements for the degree of Master of Science in Structural Engineering.



Signature:

Name: Asst. Prof. Dr. Saad Jabbar Al-Wazni

(Supervisor)

Date: / / 2022

In view of the available recommendations, I forward this thesis for debate by the examining committee.



Signature:

Name: Prof. Dr. Husain Ali Abdul-Husain

(Head of the Civil Engineering Department)

Date: / / 2022

## Linguistic Certification

This is to certify that I have read the thesis entitled “**Structural Health Monitoring of Imam Ali Holy Building Using Particle Swarm Optimization Method**” which was prepared by “**Karrar Hussain Dona**” and corrected every grammatical mistake I found therefore this research is qualified for debate.

A handwritten signature in blue ink, consisting of several fluid, overlapping strokes that form a stylized, cursive name.

Signature:

Name: Shameem Nadhim Al-salami

Date: 6 / 11 / 2022

## Scientific Evaluation Certification

This is to certify that I have read this thesis entitled “**Structural Health Monitoring of Imam Ali Holy Building Using Particle Swarm Optimization Method**” which was prepared by "**Karrar Hussain Dona**" and the thesis is eligible for the debate.

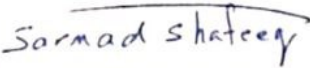
Signature: 

Name: Asst. Prof. Dr. Mohammed Hashim Mohammed

Date: / / 2022

## Scientific Evaluation Certification

This is to certify that I have read this thesis entitled “**Structural Health Monitoring of Imam Ali Holy Building Using Particle Swarm Optimization Method**” which was prepared by "**Karrar Hussain Dona**" and the thesis is eligible for the debate.

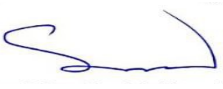
Signature: 

Name: Prof. Dr. Sarmad Shafeeq Abdulqader

Date: / / 2022

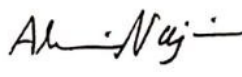
## Certificate of the Examining Committee

We certify as an Examining Committee that we have read this thesis entitled “**Structural Health Monitoring of Imam Ali Holy Building Using Particle Swarm Optimization Method**” and examined the student “**Karrar Hussain Dona**” in its content and what related to it, then found it meets the standard of thesis for the degree of Master of Science in Civil Engineering (Structural Engineering).

Signature: 

Name: **Asst. Prof. Dr. Saad Jabbar Al-Wazni**  
(Supervisor & Member)

Date: / / 2022

Signature: 

Name: **Asst. Prof. Dr. Ali Naji Attiyah**  
(Member)

Date: 2 / 11 / 2022

Signature: 

Name: **Asst. Prof. Dr. Haider Ali Al-Tameemi**  
(Member)

Date: / / 2022

Signature: 

Name: **Prof. Dr. Laith Shakir Rasheed**  
(Chairman)

Date: 3 / 11 / 2022

### Approved by the Head of the Civil Engineering Department

Signature: 

Name: **Prof. Dr. Husain Ali Abdul-Husain**  
(Head of the Civil Engineering Department)

Date: / / 2022

### Approved by the Dean of the Faculty of Engineering

Signature: 

Name: **Prof. Dr. Hasan Mahdi M. Al-khateeb**  
(Dean of Engineering Faculty)

Date: 13 / 11 / 2022



## Acknowledgements

**“In the Name of Allah, The Most Gracious, The Most Merciful”**

Praise Be To Allah, Who enabled me to achieve this  
thesis.

*I would like to express my appreciation and gratitude to my supervisor **Asst. Prof. Dr. Saad Jabbar Al-Wazni** for invaluable guidance, and remarkable suggestions for me to complete this research.*

*My sincere thanks and gratitude to my beloved **mother** who encouraged me and stood by me throughout my life until I reached this stage, and my special gratitude to **my uncles** and **my family** for always being there when I needed them most and for their support to complete my project.*

*I would like also to thank the **Dean of Faculty of Engineering** at University of Kufa, the **Head of Civil Engineering Department**, all the teachers and colleagues for their appreciated support and help throughout my MSc study*

## Abstract

The structure of Imam Ali (as) shrine is one of the historical and important place in Iraq at Najaf. In this study, the proposed SHM technique using the Particles Swarm Optimization (PSO) method was applied for the minaret of Imam Ali. The two minarets of the entire structure are more significant part because of their sensitive for any unexpected loading due to shape and slenderness ratio.

The real dimensions of the minaret structure were taken from the site and the finite element (FE) modeling of the minaret was created using the ANSYS software. The mesh size of 500 mm was suitable for time consuming and accurate results, where the total number of nodes and elements were 5425 and 21685, respectively. For nonlinear static analysis of the minaret, the multilinear isotropic hardening (MISO) material modeling using von Mises was performed. The stress, displacement and crack were extracted from the FE nonlinear analysis of the minaret structure. The maximum von Mises stress is 0.336 MPa in the middle of minaret near fixed part from minaret. The maximum displacement is 1.306 mm on top of minaret dome, while the first crack appeared in the same location of maximum stresses of minaret.

The linear dynamic (modal) analysis using block Lanczos method by ANSYS-APDL software was carried out to extract the dynamic characteristic of the minaret model. The first seven mode shape are adopted with mass participation percentage of 99.5% and natural frequency values ranging around (3.353-29.162) Hz. The shape modes characters are the first, the second and the third bending in x and y axis of the minaret as well as the torsion mode. A parametric study of the FE minaret model was conducted based on modal analysis by using only four modes adopted in order to verify the effect of changing the properties of materials (Modulus of Elasticity and mass density) and the geometry of the minaret on natural frequencies and mode shapes. The results of parametric study proved the

significant effect of modulus elasticity, mass density and the geometry on the dynamic properties of the minaret.

In this study, the SHM technique procedure using the PSO method is proposed by writing subroutine in MATLAB software. Since, it was not available and it is expensive to put sensors and data acquisition devices on the minaret for implementing experimental modal testing on site and for security reasons, the damage scenarios were simulated using the ANSYS software. Therefore, the numerical SHM procedure was implemented using assumed damage scenario to represent the experimental modal analysis of the structure with cracks. To simulate a crack as a damage in the minaret model, the stiffness of a specified element in the FE model was decreased by representing the decrease in Modulus of Elasticity value. This proposed procedure of SHM technique was tested on two types of structures before the minaret model, steel clamped beam and brick masonry wall to reach the efficiency of the adopted proposed SHM technique procedure. The results of the tests proved that the proposed SHM technique is robustness.

For this research, six different scenarios of damage in the minaret structural model were taken with different locations and damage percentages. Three different damage percentages ranged (10, 50 and 90) % were adopted for one location on the top (dome) of the model where the maximum displacement occurred. Also, three locations of damage were selected and distributed in critical stresses regions, near the base, at the end of supported wall in the middle and near the balcony of the minaret model with 90% of damage severity. The proposed SHM technique was carried out to detect those damage scenarios, locations and severities. For damage scenario located on top with severity of 10%, the high convergence of objective function values was gained with small iteration number of 27, but in an area with high stresses on the body of the minaret the high convergence of objective function values was gained with iteration number of 70.

The results of the proposed SHM technique show high efficiency and robustness in detecting damage features for both location and severity for all damage scenarios.

# List of Contents

Title	Page No.
Acknowledgements	<b>I</b>
Abstract	<b>II</b>
List of Contents	<b>V</b>
List of Figures	<b>X</b>
List of Tables	<b>XVII</b>
Nomenclatures	<b>XX</b>
Abbreviations	<b>XXII</b>
<b>CHAPTER ONE: Introduction</b>	<b>1</b>
1.1. General	<b>1</b>
1.2. Structural Health Monitoring	<b>1</b>
1.3. The Shrine structure of Imam Ali	<b>2</b>
1.4. Brick Masonry Structures	<b>3</b>
1.5. Particle Swarm Optimization	<b>3</b>
1.6. Objective of the Research	<b>4</b>
1.7. Organization of the Study	<b>5</b>
<b>CHAPTER TWO: Literature Review</b>	<b>7</b>
2.1. General	<b>7</b>
2.2. Structural Health Monitoring	<b>7</b>
2.3. Vibration Analysis	<b>8</b>
2.4. Vibration-Based Damage Identification Methods	<b>9</b>
2.4.1. Damage detection based on changes in basic modal properties	<b>9</b>
2.4.1.1. Natural frequency changes	<b>9</b>
2.4.1.2. Mode shape changes	<b>9</b>

2.4.2. Damage detection method based on frequency response function (FRF) changes	<b>10</b>
2.4.3 Damage detection methods based on measured flexibility matrix changes	<b>10</b>
2.4.4 Damage detection method based on measured stiffness matrix changes	<b>11</b>
2.4.5 Damage detection method based on updating structural model Parameters	<b>11</b>
2.5. Bricks Masonry Structures	<b>11</b>
2.5.1. Failure modes in Unreinforced Masonry Brick (URM)	<b>13</b>
2.6. Previous Studies of Structural Health Monitoring	<b>16</b>
2.7. Summary	<b>32</b>
<b>CHAPTER THREE: Optimization Problems and Heuristics Methods</b>	<b>34</b>
3.1. Introduction	<b>34</b>
3.2. Optimization problems	<b>34</b>
3.3. Heuristics Optimization	<b>36</b>
3.3.1. Evolutionary Computation	<b>37</b>
3.3.2. Genetic Algorithm	<b>37</b>
3.3.3. Evolution Strategies and Evolutionary Programming	<b>38</b>
3.3.4. Differential Evolution	<b>39</b>
3.3.5. Ant Colony Search Algorithm	<b>39</b>
3.3.6. Tabu Search	<b>40</b>
3.3.7. Simulated Annealing	<b>40</b>
3.3.8. Particle Swarm Optimization	<b>40</b>
<b>CHAPTER FOUR: Finite Element Modeling and Structural Analysis of Masonry Minaret</b>	<b>47</b>
4.1. Introduction	<b>47</b>

4.2. Description and Geometry of Minaret Structure	<b>47</b>
4.3. Material Properties of Minaret Structure	<b>50</b>
4.4. Finite Element Model Using ANSYS Software for Minaret Structure	<b>51</b>
4.4.1. Creating the model	<b>51</b>
4.4.2. Meshing of model	<b>54</b>
4.5. Static analysis of FE minaret model	<b>58</b>
4.6. Modal analysis of FE minaret model	<b>62</b>
4.6.1. Selection the size of mesh	<b>63</b>
4.6.2. Selection the effective modes	<b>65</b>
4.7. Parametric study of FE minaret model under modal analysis	<b>68</b>
4.7.1. Changing Modules of Elasticity	<b>68</b>
4.7.2. Changing Mass Density	<b>70</b>
4.7.3. Changing Height of Minaret	<b>71</b>
4.7.4. Changing Radius of Minaret	<b>72</b>
<b>CHAPTER FIVE: Proposed Structural Health Monitoring Technique of Imam Ali Structure and Verifications</b>	<b>76</b>
5.1. General	<b>76</b>
5.2. Adopted Proposed Technique for SHM	<b>76</b>
5.3. Representing Damage in Proposed SHM technique	<b>78</b>
5.4. Creating of the Subroutine for Proposed SHM Using PSO Method	<b>80</b>
5.4.1. Adopted objective function for PSO method	<b>83</b>
5.4.2. Adopted coefficients for PSO method	<b>84</b>
5.5. Verification of SHM Technique Using PSO Method	<b>85</b>
5.5.1. Test on steel clamped beam model	<b>85</b>
5.5.1.1. First crack scenario of steel clamped beam	<b>87</b>
5.5.1.2. Second crack scenario of steel clamped beam	<b>88</b>

5.5.2. Test on brick masonry wall	<b>90</b>
5.5.2.1. First crack scenario of brick masonry wall	<b>92</b>
5.5.2.2. Second crack scenario of brick masonry wall	<b>93</b>
5.5.2.3. Third crack scenario of brick masonry wall	<b>95</b>
5.5.2.4. Fourth crack scenario of brick masonry wall	<b>97</b>
5.6. Parametric study to select Iteration and Particle Number in Adopted SHM Technique of Minaret	<b>99</b>
5.6.1. Estimation iteration number	<b>99</b>
5.6.1.1 First case	<b>99</b>
5.6.1.2 Second case	<b>100</b>
5.6.1.3 Third case	<b>102</b>
5.6.2. Estimation number of particles	<b>104</b>
5.6.2.1 First Case	<b>104</b>
5.6.2.2 Second Case	<b>105</b>
5.6.2.3 Third Case	<b>107</b>
<b>CHAPTER SIX: Damage Detection Results of Using SHM Technique for Adopted Structural Model</b>	<b>109</b>
6.1. General	<b>109</b>
6.2. Select weighting factors in the Adopted SHM Technique	<b>109</b>
6.3. Damage Detection for Different Scenario Cases (Damage Locations and Percentage) for the Minaret Structural Model	<b>110</b>
6.3.1. First scenario	<b>112</b>
6.3.2. Second scenario	<b>118</b>
6.3.3. Tired scenario	<b>124</b>
6.3.4. Fourth scenario	<b>130</b>
6.3.5. Fifth scenario	<b>136</b>
6.3.6. Sixth scenario	<b>142</b>
<b>CHAPTER SEVENE: Conclusions and Recommendations</b>	<b>149</b>

7.1. Conclusions	<b>149</b>
7.2. Recommendations	<b>152</b>
<b>References</b>	<b>153</b>

# List of Figures

No. of Figure	Title	Page No.
Figure 1.1	Imam Ali holy shrine structure	3
Figure 2.1	Vibration system in a horizontal spring and pendulum is typical	8
Figure 2.2	Bricks masonry historical structures	12
Figure 2.3	Parts of URM wall	13
Figure 2.4	Failure modes in Unreinforced Masonry Brick (URM)	15
Figure 2.5	Comparison between the experimental (solid line) and the theoretical (dot line) dynamic response of a square plate	16
Figure 2.6	Zero noise damage detection, PSO and AP	17
Figure 2.7	Ten percent damage detection via PSO	17
Figure 2.8	Failures occurred at the region between transition segment and cylindrical body	18
Figure 2.9	Evolutionary processes in case 1 of the beam: (a) the best fitness; (b) damage index	19
Figure 2.10	Evolutionary processes in case 2 of the beam: (a) the best fitness; (b) damage index	20
Figure 2.11	Evolutionary processes of example 2: (a) the best fitness; (b) damage index	20
Figure 2.12	Models of Hagia Sophia (right) and the Mihrimah (left) minaret	21
Figure 2.13	Scatter plot of maximum normalized residual displacement versus normalized top displacement for minaret of Mihrimah (left) and Hagia Sophia (right)	22

Figure 2.14	Variation of maximum normalized top displacement with the frequency and the amplitude of sine wave for the case of Mihrimah (left) and Hagia Sophia (right).	22
Figure 2.15	Variation of maximum residual displacement with the frequency and the sine wave amplitude for the case of Mihrimah (left) and Hagia Sophia (right).	23
Figure 2.16	Measuring points of Protiron	24
Figure 2.17	View on vault of Protiron and copper clamp	24
Figure 2.18	Time series of displacements	25
Figure 2.19	Time series of strains	25
Figure 2.20	Damage detection results obtained from PSO and CSS using combination of natural frequencies and mode shapes for a continuous beam	26
Figure 2.21	Damage detection results obtained from PSO and CSS using combination of natural frequencies and mode shapes for a two dimensional truss	26
Figure 2.22	Damage detection results obtained from PSO and CSS using combination of natural frequencies and mode shapes for a frame with three floors and four spans	27
Figure 2.23	Three-dimensional finite elements model of the minaret and meshed state thereof	28
Figure 2.24	Distribution and values of stress occurring in the minaret as a result of analyses	29
Figure 2.25	Numerical and experimental mode shapes of Hafsa Sultan Mosque and Imaret Mosque minaret as examples	31
Figure 2.26	Damage detection of S3 using Combo 3–1 with $h = 3.75$ m	32

Figure 3.1	Basic genetic algorithm iteration flowchart	38
Figure 3.2	Scheme for solving problem by PSO method	42
Figure 3.3	Modification of a searching point via PSO concept	43
Figure 3.4	Flowchart of PSO method in general	45
Figure 4.1	The structure of Imam Ali shrine	47
Figure 4.2	Dimensions of minaret	49
Figure 4.3	Real and ANSYS finite element model of minaret structure	50
Figure 4.4	Finite element of the body of minaret structure	52
Figure 4.5	Finite element of the balcony and upper body of minaret structure	52
Figure 4.6	Steps to drawing parts dome	53
Figure 4.7	Steps to drawing stair of minaret	53
Figure 4.8	Fixed areas in minaret model	54
Figure 4.9	Difference between mapped mesh and free mesh	55
Figure 4.10	two type elements of mesh area	55
Figure 4.11	Types and geometry of element solid65	56
Figure 4.12	Geometry of tetrahedral element	56
Figure 4.13	Elements and nodes of minaret	57
Figure 4.14	Compressive stress-strain curve for brick masonry extracted experimentally	58
Figure 4.15	(a) and (b) transverse displacement in x and y direction, respectively, (c) vertical displacement in z direction and (d) displacement vector of the minaret model	60
Figure 4.16	Von Mises stress of minaret	61
Figure 4.17	Location of cracks in FE minaret model under maximum load	62
Figure 4.18	Convergence of mesh size	65

Figure 4.19	Natural frequency value of first mode with different mesh size	65
Figure 4.20	Extracted mode shapes of adopted brick minaret structure	67
Figure 4.21	Natural frequency value versus Modulus of Elasticity	69
Figure 4.22	Natural frequency value versus mass density	71
Figure 4.23	Changing natural frequency with height of minaret	72
Figure 4.24	Changing natural frequency with base outer radius of minaret	73
Figure 4.25	Natural frequency period of each mode	75
Figure 5.1	General chart of SHM technique	78
Figure 5.2	Damaged element and percentage and location for first, second, third and fourth scenario	79
Figure 5.3	Damaged element and percentage and location for fifth and sixth scenario	80
Figure 5.4	Scheme showing PSO programming in MATLAB	83
Figure 5.5	Steel clamped beam model	85
Figure 5.6	Convergence of objective function for first crack scenario of steel clamped beam	87
Figure 5.7	History of damaged element number and damage percentage for first crack scenario of steel clamped beam	88
Figure 5.8	Convergence of objective function for second crack scenario of steel clamped beam	89
Figure 5.9	History of damaged element number and damage percentage for second crack scenario of steel clamped beam	89
Figure 5.10	Dimension of brick masonry wall	90
Figure 5.11	Damaged elements of brick masonry wall	91

Figure 5.12	Convergence of objective function for first crack scenario of brick masonry wall	92
Figure 5.13	History of damaged element number and damage percentage for first crack scenario of brick masonry wall	93
Figure 5.14	Convergence of objective function for second crack scenario of brick masonry wall	94
Figure 5.15	History of damaged element number and damage percentage for second crack scenario of brick masonry wall	95
Figure 5.16	Convergence of objective function for third crack scenario of brick masonry wall	96
Figure 5.17	History of damaged element number and damage percentage for third crack scenario of brick masonry wall	96
Figure 5.18	Convergence of objective function for fourth crack scenario of brick masonry wall	97
Figure 5.19	History of damaged element number and damage percentage for fourth crack scenario of brick masonry wall	98
Figure 5.20	Convergence of objective function for first case	100
Figure 5.21	History of damaged element number and damage percentage for first case	100
Figure 5.22	Convergence of objective function for second case	101
Figure 5.23	History of damaged element number and damage percentage for second case	102
Figure 5.24	Distribution and convergence of particles towards target (damaged element and severity) in first, 25, 50 and 75 iteration for second case	102
Figure 5.25	Convergence of objective function for third case	103

Figure 5.26	History of damaged element number and damage percentage for third case	103
Figure 5.27	Convergence of objective function for first case	105
Figure 5.28	History of damaged element number and damage percentage for first case	105
Figure 5.29	Convergence of objective function for second case	106
Figure 5.30	History of damaged element number and damage percentage for fsecond case	106
Figure 5.31	Distribution and convergence of particles towards target (damaged element and severity) in first, 25, 50 and 75 iteration for second case	107
Figure 5.32	Convergence of objective function for third case	108
Figure 5.33	History of damaged element number and damage percentage for third case	108
Figure 6.1	The damaged element, damage percentage and damage location of first scenario	113
Figure 6.2	Convergence of objective function for first scenario	114
Figure 6.3	History of damaged element number for first scenario	116
Figure 6.4	History of damage percentage for first scenario	116
Figure 6.5	Distribution and convergence of particles towards damage in first, 25, 50, 75 and 100 iteration	117
Figure 6.6	Ability the first particle to move towards the detected damaged element	118
Figure 6.7	The damaged element, damage percentage and damage location of second scenario	119
Figure 6.8	Convergence of objective function for second scenario	121
Figure 6.9	History of damaged element number for second scenario	121
Figure 6.10	History of damage percentage for second scenario	121

Figure 6.11	Distribution and convergence of particles towards damage in first, 25, 50, 75 and 100 iteration	123
Figure 6.12	Ability the first particle to move towards the detected damaged element	124
Figure 6.13	The damaged element, damage percentage and damage location of third scenario	125
Figure 6.14	Convergence of objective function for third scenario	126
Figure 6.15	History of damaged element number for third scenario	127
Figure 6.16	History of damage percentage for third scenario	127
Figure 6.17	Distribution and convergence of particles towards damage in first, 25, 50 and 75 iteration	129
Figure 6.18	The damaged element, damage percentage and damage location of fourth scenario	131
Figure 6.19	Convergence of objective function for fourth scenario	132
Figure 6.20	History of damaged element number for fourth scenario	133
Figure 6.21	History of damage percentage for fourth scenario	134
Figure 6.22	Distribution and affinity of particles towards damage in first, 25, 50, 75 and 100 iteration	135
Figure 6.23	Ability the first particle to move towards the detected damaged element	136
Figure 6.24	The damaged element, damage percentage and damage location of fifth scenario	137
Figure 6.25	Convergence of objective function for fifth scenario	138
Figure 6.26	History of damaged element number for fifth scenario	139
Figure 6.27	History of damage percentage for fifth scenario	140
Figure 6.28	Distribution and convergence of particles towards damage in first, 25, 50, 75 and 100 iteration	141

Figure 6.29	Ability the first particle to move towards the detected damage	142
Figure 6.30	The damaged element, damage percentage and damage location of sixth scenario	143
Figure 6.31	Convergence of objective function for sixth scenario	144
Figure 6.32	History of damaged element number for sixth scenario	145
Figure 6.33	History of damage percentage for sixth scenario	146
Figure 6.34	Distribution and convergence of particles towards damage in first, 25, 50 and 75 iteration	147
Figure 6.35	Ability the first particle to move towards the detected damage	148

# List of Tables

No. of table	Title	Page No.
Table 2.1	Mihrimah minaret model geometrical properties (left), Haiga Sophia minaret model geometrical properties (right)	21
Table 2.2	Frequency values obtained as a result of numerical analyses	28
Table 3.1	Typical Optimization Problems	35
Table 3.2	damaged elements and damage percentages for different structures	46
Table 4.1	Dimensions of minaret (m)	48
Table 4.2	Material properties of adopted brick minaret model	51
Table 4.3	Finite element properties of adopted brick minaret model.	57
Table 4.4	stress-strain points	58
Table 4.5	inputs for nonlinear static analysis for the FE minaret model	59
Table 4.6	Effect of mesh size on elements number and first natural frequency value	64
Table 4.7	mass participation of modes in x direction	65
Table 4.8	mass participation of modes in y direction	66
Table 4.9	Natural frequencies values and modes characteristic with size of mesh (200)	66
Table 4.10	Natural frequencies values with changing Modules of Elasticity	69
Table 4.11	Natural frequency values with changing mass density.	70
Table 4.12	Natural frequencies values with changing height of minaret	71
Table 4.13	Natural frequencies values versus minaret radius	72
Table 4.14	Natural frequencies values and modes characteristic with size of mesh (500 mm)	74
Table 5.1	Damage element and percentage and location for damage scenarios	78
Table 5.2	Crack scenarios of the steel clamed beam	86
Table 5.3	Modal frequencies for intact, first and second crack scenario for the clamped beam	86
Table 5.4	Material properties of adopted brick minaret model	90

Table 5.5	Crack scenarios of the structural model	91
Table 5.6	Modal frequencies of the masonry wall for intact, first, second, third and fourth crack scenario.	92
Table 5.7	Parameter Description of PSO method for three cases with change in iterations	99
Table 5.8	Parameter Description of PSO method for three cases with change in number of particles	104
Table 6.1	Three different scenarios of damage selecting in sensitivity analysis	109
Table 6.2	Result of <i>Freq</i> and <i>Disp</i> for three different scenario	110
Table 6.3	Damaged element and percentage and location for damage scenarios	110
Table 6.4	Natural frequencies of intact,1 <sup>st</sup> , 2 <sup>nd</sup> , 3 <sup>rd</sup> ,4 <sup>th</sup> ,5 <sup>th</sup> and 6 <sup>th</sup> modes	111
Table 6.5	Input Parameters in SHM technique for damage detection	112
Table 6.6	Material properties of intact and damaged element for first scenario	112
Table 6.7	Material properties of intact and damaged element for second scenario	119
Table 6.8	Material properties of intact and damaged element for third scenario	125
Table 6.9	Material properties of intact and damaged element for fourth scenario	130
Table 6.10	Material properties of intact and damaged element for fifth scenario	137
Table 6.11	Material properties of intact and damaged element for fourth scenario	142

# Nomenclatures

The major symbols are listed below others are indicated with their equations

$(C_{max})$  The maximum weighting coefficient

$(C_{min})$  The minimum weighting coefficient

$h^d$  The distance between the measurements coordinates

$f_i^{scenario-dam}$  The natural frequencies that was extracted from damaged scenario model

$f_i^{updated-dam}$  The natural frequency that was numerically estimate from updated FE model

$s^k$  Current searching point

$s^{k+1}$  Modified searching point

$v^k$  Current velocity

$v^{k+1}$  Modified velocity

$v_{pbest}$  Velocity based on pbest

$v_{gbest}$  Velocity based on gbest

$W_f$  Weighting factors for frequencies

$W_d$  Weighting factor for displacements

$\phi_{n,i}^d$  The local change for curvature between the undamaged structures and damaged structures

$\phi_{n,i}$  The modal displacement for  $i^{th}$  mode shape at the coordinate n

$\phi_{ij}^{scenario-dam}$  The nodes displacement that was extracted from damaged scenario model

$\phi_{ij}^{updated-dam}$  The nodes displacement that was numerically estimate from updated FE model

# Abbreviations

APDL	: ANSYS Parametric Design Language
ANSYS	: Analysis System
DE	: Differential Evolution
E	: Modulus of Elasticity
EAs	: Evolutionary Algorithms
EC	: Evolutionary Computation
EFDD	: Enhanced Frequency Domain Decomposition
EP	: Evolutionary programming
ES	: Evolution strategies
FEM	: Finite Element Model
FRF	: Frequency Response Function
GA	: Genetic Algorithm
IEPSO	: Immunity Enhanced Particle Swarm Optimization
LDV	: Laser Doppler Vibrometer
LTH	: Linear Time History
MATLAB	: Matrix Laboratory
Max.	: Maximum
MD	: Mass Density
MDOF	: Multi Degree of Freedom

Min. : Minimum

MISO : Multilinear Isotropic Hardening

NLTH : Nonlinear Time History

No. : Number

PSO : Particle Swarm Optimization

SA : Simulated Annealing

SDOF : Single Degree of Freedom

SHM : Structural Health Monitoring

SSI : Stochastic Subspace Identification

URM : Unreinforced Masonry Brick

VROTAT : Volume Rotate

VADD : Volumes Add

VGLU : Volumes Glue

# CHAPTER ONE

# CHAPTER ONE

## Introduction

### 1.1. General

The shrine of Imam Ali is the holy place where Imam Ali bin Abi Talib was buried. It is in the holy city of Najaf in Iraq. This city is considered as a holy city for Muslims both inside and outside Iraq. The shrine is considered as one of the oldest historical buildings, as hundreds of years have passed since it was built and by the time, some unexpected problems might occur in the structure. The shrine has a special sanctity for Muslims, as it cannot be demolished or changed, as the sanctity of the old building must be preserved. In this research, the structural health monitoring for the important part of the shrine structure (minaret) is proposed. The structural health monitoring is considered as one of the recent matters especially for the historical and dilapidated buildings which is intended to preserve these buildings as long as possible. The structural health monitoring can be implemented by using the optimization methods, therefore this research adopts the particle swarm optimization method.

### 1.2. Structural Health Monitoring

The old investigation procedures were been carrying out using a simple visual inspection of a structure by an expert engineer and then structural testing is conducted for the purpose of detection any early damage to prevent potential collapse [1]. Nowadays, Structural Health Monitoring (SHM) is the technique of implementation damage identification system to engineering structures and also in the various fields of mechanical and aerospace engineering. This approach based on the dynamic properties of a structure and it is representing the damage as a change in the geometric and/or material properties of these structural systems [2]. In civil engineering, this method is considered very important for such as ancient historical and cultural, dams and bridges structures which are exposed to

continuous damage. The output of SHM process in long term is periodically updated information about the ability of the structure to perform its function. The SHM technique could provide the screening and reliable information regarding the integrity of the structure.

### **1.3. The Shrine Structure of Imam Ali**

Imam Ali is the cousin of the Prophet Muhammad (PBUH), and the building of Imam Ali shrine is one of the historical and ancient buildings as shown in Figure (1.1) with great importance for Muslims at the present time. This structure is located in Iraq, specifically in the southwest region in the province of Najaf which is visited yearly by millions of Muslims from different countries. Firstly, it was built in the year (896 AD) during the reign of King Muhammad (King of Tabaristan). It is consisted of a mausoleum and a dome surrounded by a fortress containing seventy gates. Four construction operations continued after that until the last building which is the current one and it was built in (1614 AD) during the reign of Shah Abbas. The type of the shrine building is the masonry structure and the main units are consisting of clay brick and plaster mortar, the restoration work continued on it until the present time. The masonry structure is brittle and weak when exposed to abnormal load, therefore, it is very important to continuously monitor the shrine structure to control the safety. In this research, one of the two minarets will be adopted to carry out a proposed structural health monitoring technique for detecting the damage as a modern non-destructive testing approach.



Figure (1.1) Imam Ali holy shrine structure

#### **1.4. Brick Masonry Structures**

The brick masonry is one of the oldest structural system used in constructions from ancient times till now. This structural system has high compressive strength and suitable for resisting the bearing loads, but it has low tensile strength. The brick masonry material has quasi-brittle behavior. So, it has low resistant to lateral loads such as wind and seismic load and could lead to an unexpected collapse. For this reason, cracks may appear rapidly and cause the structure's rigidity to decrease, also the nonstructural effects. Thereby, structural health monitoring (SHM) for brick masonry structures, especially for historical buildings, is crucial.

#### **1.5. Particle Swarm Optimization**

The Particle Swarm Optimization (PSO) method is one of the heuristics methods that was discovered by the two scientists (Kennedy and Eberhart, 1995) [3]. This method simulates in its work the movement of bird flocking or fish schooling

searching for food in a specific location, as it has the ability to share information on locations abundant with food among the flock members. The flock of birds spreads in the area to search and takes initial random locations and then begins to search for the best location for food, this movement depends on its velocity and the best location for food that is found. Therefore, the working mechanism of the particle swarm optimization method is through the spread of particles in the search space, and each particle maintains its initial position in the search space at the beginning. After each particle takes a random location, the particles begin to search for a lower (or higher) value for an objective function within the search space. The movement of each particle depends on its velocity and the best position found by this particle or by another particle [3].

### **1.6. Objectives of the Research**

The main objective of the study is to propose new structural health monitoring procedure for the structure of Imam Ali shrine, which has a great importance in the Islamic world. After studying the structural seismic evaluation of Imam Ali Holy Shrine behavior by Khalifa (2021) [4], it became necessary to monitor the structural health of the shrine. However, due to the inability to implement experimental modal analysis in site, setup and connect monitoring devices on the shrine building, the numerical procedures for the minaret structure was adopted and the damage scenarios were simulated for the proposed SHM technique.

#### **The importance of the study includes:**

- 1- Making finite element model of the minaret in an external file and making a non-linear analysis (static analysis) using the Analysis System software (ANSYS) by ANSYS Parametric Design Language (APDL) method to extract the places of high stress and the places where cracks occur.
- 2- Conducting a modal analysis of the minaret using the ANSYS program by APDL method and making a parametric study of the minaret to reveal the effect

of changing the modulus of elasticity, mass density and geometry of the minaret on the natural frequencies and mode shapes.

3- Creating the damage scenarios for the minaret by reducing the modulus of elasticity in the selected elements of finite element model of the minaret.

4- Creating a subroutine in MATLAB software linked with ANSYS software to carry out the proposed procedures of structural health monitoring technique by using Particle Swarm optimization method.

### **1.7. Organization of the Thesis**

The overview of this study is provided below and along with a brief summary of each chapter:

- **CHAPTER ONE:** Introduction

This chapter introduces the general idea about the structural health monitoring, the shrine of Imam Ali in Iraq in Najaf city, particle swarm optimization method, aim of this study and the organization of this study.

- **CHAPTER TWO:** Literature Review

This chapter shows the structural health monitoring and vibration dynamic analyses. Also it gives an idea about modal analysis, applications of modal analysis and mathematics for modal analysis, and reviews of bricks masonry structures and failure modes in Unreinforced Masonry Brick (URM), ANSYS and MATLAB software. In the end the previous studies that are relevant to structural health monitoring and optimization methods were reviewed.

- **CHAPTER THREE:** Optimization Problems and Heuristics Methods

This chapter describes the optimization methods, its application and use in structural health monitoring, as well as showing the type of heuristics optimization, finally the particle swarm optimization method is presented.

- **CHAPTER FOUR:** Finite Element Modeling and Modal Structural Analysis of Masonry Minaret.

This chapter describes the dimensions of the adopted model (the minaret), and the method used for conducting a finite element model of minaret, the type of construction of the minaret and the materials from which it was built, and material properties of minaret. Then the nonlinear analysis (static analysis) and dynamic analysis of the model are presented as well as the dynamic characteristics (natural frequencies and mode shapes).

- **CHAPTER FIVE:** Structural Health Monitoring Technique for Imam Ali Structure and Verifications

This chapter explains how to program the optimization technique (Particle Swarm Optimization Method PSO) in MATLAB. Also, it explains how to represent the damage and create a scenario file for the damage. After the end of programming the technique and linking it to ANSYS software, it was tested on two models, the first on a steel clamped beam and the second on a brick masonry wall.

- **CHAPTER SIX:** Damage Detection Results for Adopted Structural Model Using SHM Technique

In this chapter, the PSO technique is applied to the approved model (minaret). Three different location of damage are taken, as well as three different percentages of damage, and the results are extracted and discussed.

- **CHAPTER SEVEN:** Conclusions and Recommendations

The most significant findings from this study are outlined in this chapter along with various recommendations and ideas for additional research on structural health monitoring for historical masonry structures.

# CHAPTER TWO

# CHAPTER TWO

## Literature Review

### 2.1. General

The subjects covered in this chapter include structural health monitoring (SHM), vibration dynamic analysis, methods of performing dynamic analysis, modal analysis, vibration-based damage identification methods, bricks masonry structures, Failure Modes in Unreinforced Masonry Brick (URM), ANSYS software, MATLAB software and some literature reviews on these topics.

### 2.2. Structural Health Monitoring

For a long time the qualitative and non-continuous methods were used to determine the service of structures, such as the railroad wheel-tappers who used the sound of a hammer striking the train wheel to select if there is a damage. Later, the SHM is suggested to facilitate the task of detecting damage and determining its location and its amount [2].

SHM means the analysis and observation of a system over time using periodically sampled response measurements to observe changes of the geometric and material properties of engineering structures such as bridges, buildings and historical buildings. The output of this process in the long term SHM, is periodically updated information about the ability of the structure to perform its intended. After happening the events, such as blast loading, earthquakes or storms. The SHM provide the screening and reliable information regarding the integrity of the structure.

The SHM process involves selecting the sensor types, number and locations, excitation methods, and the data acquisition/transmittal/storage hardware commonly. There are two techniques in the field of SHM.

1- Static based techniques

2- Vibration based techniques which is subdivided into two aspects. First the direct problem, by suggesting models for damage to determine the dynamic characteristics. Second the inverse problem, by using dynamic characteristics to determine damage characteristics.

Damage can be defined as changes that take place to the system that adversely affect its performance in current or future time. So the SHM is not meaningful without a comparison between two states of the system, one of them is assumed to represent the initial state and often undamaged.

In this study the vibration based technique was depended by using modal analysis.

### 2.3. Vibration Analysis

Vibration is a movement that is repeated. The repetition may or may not continue. Vibration can be considered as a transition between the kinetic and potential energy. The mass is responsible for kinetic energy while the spring is responsible for potential energy [5]. The Figure (2.1) shown a mass connected to a horizontal spring. Also the pendulum is a typical example of a vibration system. But it doesn't have a spring-like component for potential energy. In fact, the mass has dual role for both potential and kinetic energy. There are two type from systems vibration depending on number of degree of freedom (single and multi) [6].

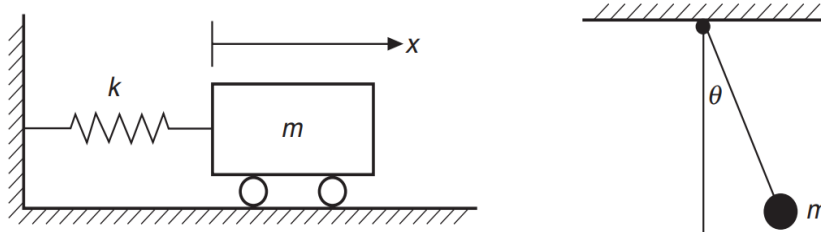


Figure (2.1) Vibration system in a horizontal spring and pendulum is typical [7]

## **2.4. Vibration-Based Damage Identification Methods**

In the last decade, the researches in vibration-based damage identification methods are expanding rapidly. There are many methods to detect, locate, and characterize damage in structural and mechanical systems by investigating changes in measured vibration response [7].

### **2.4.1. Damage detection based on changes in basic modal properties**

In this section, the modal properties are defined as resonant frequencies and mode shape vectors [7].

#### **2.4.1.1. Natural frequency changes**

The natural frequency is one of the most important fundamental dynamic characteristics of the structure. The natural frequency mainly depends on ratio between mass and stiffness of structure. So can use this change to detect the damage by using some techniques [8].

The changes in structural properties cause changes in vibration frequencies which are used for damage detection and health monitoring. Also the resonant frequencies have statistical variation much less than random error sources compared with other modal parameters. The frequencies generally cannot give spatial information about structural changes, except at higher modal frequencies [7].

#### **2.4.1.2. Mode shape changes**

When the damage occurs in a structure, it also cause change in the mode shapes, this change can be used to detect and locate damage in structure and estimate the mode shapes by using modal analysis from Finite Element Model (FEM) [8].

The general formula for the absolute change in mode shape curvatures by using the central difference approximation is:

$$\phi_{n,i}^d = \frac{\phi_{n-1,i} - 2\phi_{n,i} + \phi_{n+1,i}}{h_d^2} \quad \dots \quad 2.1$$

$\phi_{n,i}^d$  - The local change for curvature between the undamaged structures and damaged structures.  $\phi_{n,i}$  - The modal displacement for  $i^{th}$  mode shape at the coordinate  $n$ ,  $n \pm 1$  - the estimation coordinates of points after and before the certain point,  $h^d$  - the distance between the measurements coordinates [8].

#### **2.4.2. Damage detection method based on Frequency Response Function (FRF) changes**

The Frequency Response Function (FRF) introduces the linear dynamic system by equivalent expression. So any change in mass or stiffness for structure will cause change in the acquired FRF response of the structure. This changes can be used to detect the damage [8].

#### **2.4.3. Damage detection method based on measured flexibility matrix changes**

It is another method for damage identification that uses the dynamically measured flexibility matrix to assessment changes in the static behavior of the structure. The flexibility matrix relates resulting structural displacement and applied static force. The flexibility matrix can be estimated by the mass-normalized measured mode shapes and frequencies [7].

Using flexibility matrices to detect damage by the flexibility matrix synthesized using the modes of the damaged and undamaged structure or from FEM. Because of the inverse relationship to the square of the modal frequencies, the flexibility matrix is most sensitive to changes for lower-frequency modes of the structure [7].

#### **2.4.4. Damage detection method based on measured stiffness matrix changes**

In this case, the dynamically measured stiffness matrix is used, and it is pseudoinverse of the dynamically measured flexibility matrix [7]. Also it can detect damage and its location by estimating the dynamically measured damping and mass matrices with stiffness matrix [8].

#### **2.4.5. Damage detection method based on updating structural model Parameters**

This method is based on the modification of structural model matrices such as stiffness, mass and damping to reproduce as closely as possible the measured static or dynamic response from the data. This methods solve for the updated matrices (or perturbations to the nominal model that produce the updated matrices) by forming a constrained optimization problem based on the structural equations of motion, the nominal model, and the measured data. Comparisons of the updated matrices to the original correlated matrices are provided [7]. The differences in the various algorithms are classified for:

- 1- The objective function with parameters.
- 2- The constraints on the problem.
- 3- The implemented optimization method.

In this study, this method was adopted due to the ability to solve complex problem of structural analysis.

### **2.5. Brick Masonry Structures**

The masonry brick is one of the important materials used in structures from ancient times till now. The masonry brick has high compression strength and suitable to resist the loads but it has low tensile strength. The masonry with bricks is quasi-brittle. So it has low resistant to lateral loads such as wind load and seismic load, so it may cause a sudden collapse of the building. For these reasons,

the cracks may happen suddenly and may cause reduced stiffness of structure. So the structural health monitoring SHM is very important for brick masonry structures especially for ancient buildings. Figure (2.2) shows some buildings from Unreinforced Masonry Brick.



Figure (2.2) Bricks masonry historical structures

The masonry structures are built from bricks and mortar as a binder material. This type of structure is called Unreinforced Masonry Brick (URM), it consists of brick (unit), vertical head joints, horizontal bed joint and brick mortar interface. Figure (2.3) shows the detail of a brick masonry wall.

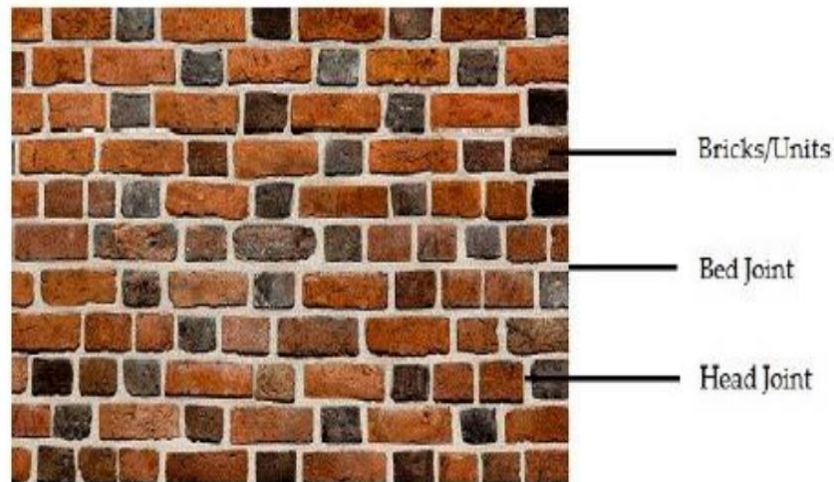


Figure (2.3) Parts of URM wall [3]

### **2.5.1. Failure modes in Unreinforced Masonry Brick (URM)**

#### **1-Bed-joint sliding failure**

Straight or diagonal cracks occur in the bed-joints. This kind of failure is deformation - controlled failure, as shown in Figure (2.4.a).

#### **2-Rocking behavior failure**

This failure is occurs when slender wall has high shear strength and low compressive forces, this failure is deformation - controlled failure, as shown in Figure (2.4.b).

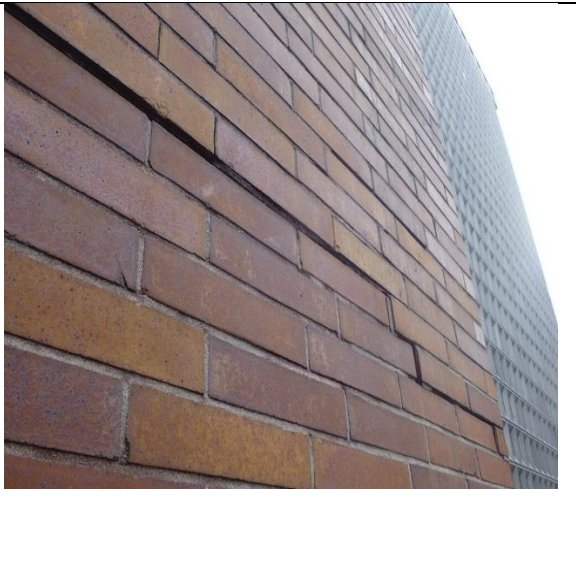
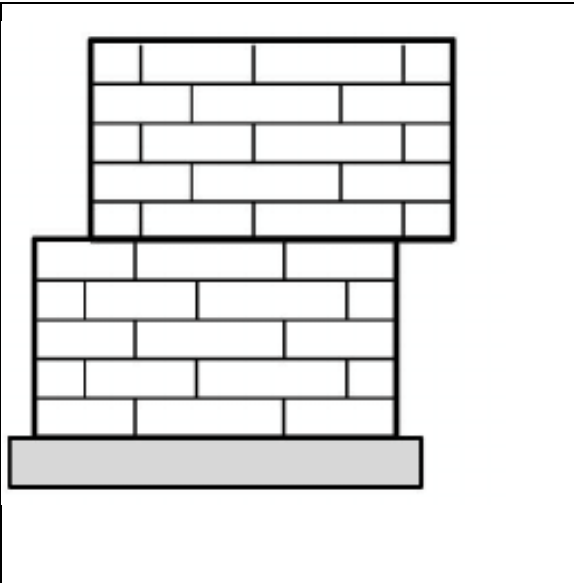
#### **3-Diagonal tension cracking**

This type occurs when units of brick are weak, the mortar is strong and compressive stresses are high. Cracks happen suddenly in most cases and fast

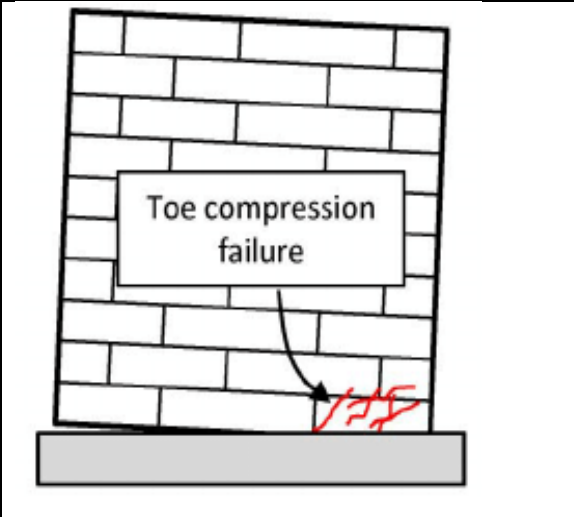
drop in the strength of the wall. This type is force -controlled failure, as shown in Figure (2.4.c).

#### **4-Toe compression failure**

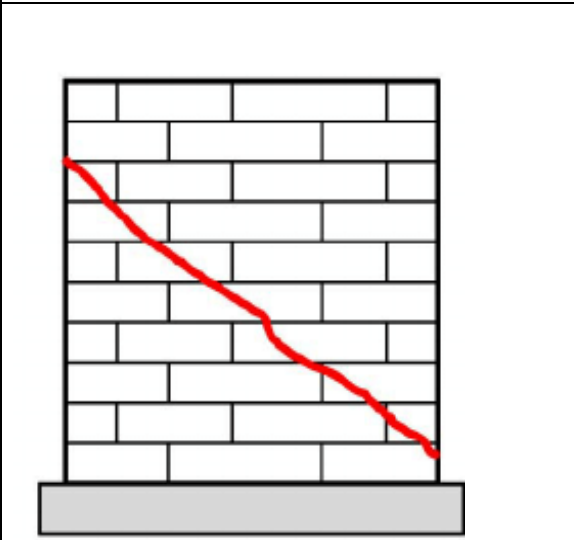
This type occurs after the rocking mode. This type of failure is force - controlled failure.



(a) Bed-joint sliding failure



(b) Rocking behavior



(c) Diagonal tension cracking

Figure (2.4) Failure modes in Unreinforced Masonry Brick (URM)

## 2.6. Previous Studies of Structural Health Monitoring

There are some researchers dealt with performing structural health monitoring technique for civil structure. **Garziera et al** (2007) [9] in this paper a technique of structural health monitoring integrity of historical buildings by a non-destructive and non-contact analysis is presented and discussed. They used the laser Doppler vibrometer (LDV) to detect the damage of a structure, in terms of cracks and overall structural degradation, by the measurement of its dynamic characteristics. The results are computationally determined to identify the response of the structure and to select the evolution of any damaged region through calculating stiffness and mass changes in reverse depending on changes in mode shapes. They made some experiments in laboratory on the square stainless steel plate to validate from measurement by the LDV technique. Figure (2.5) compare the first nine modes of the plate's natural frequencies, which are determined by the number of half-waves in the x and y directions.

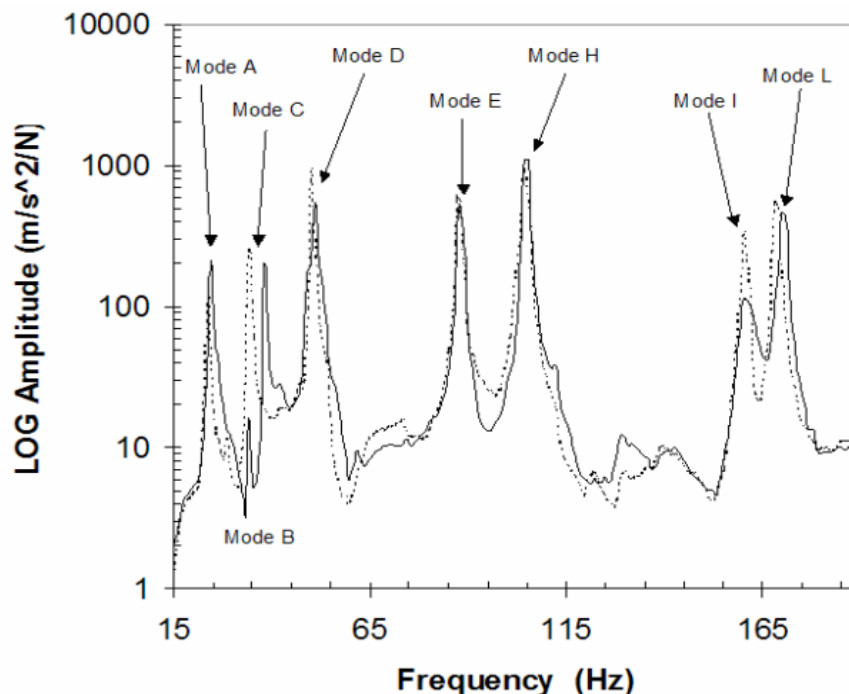
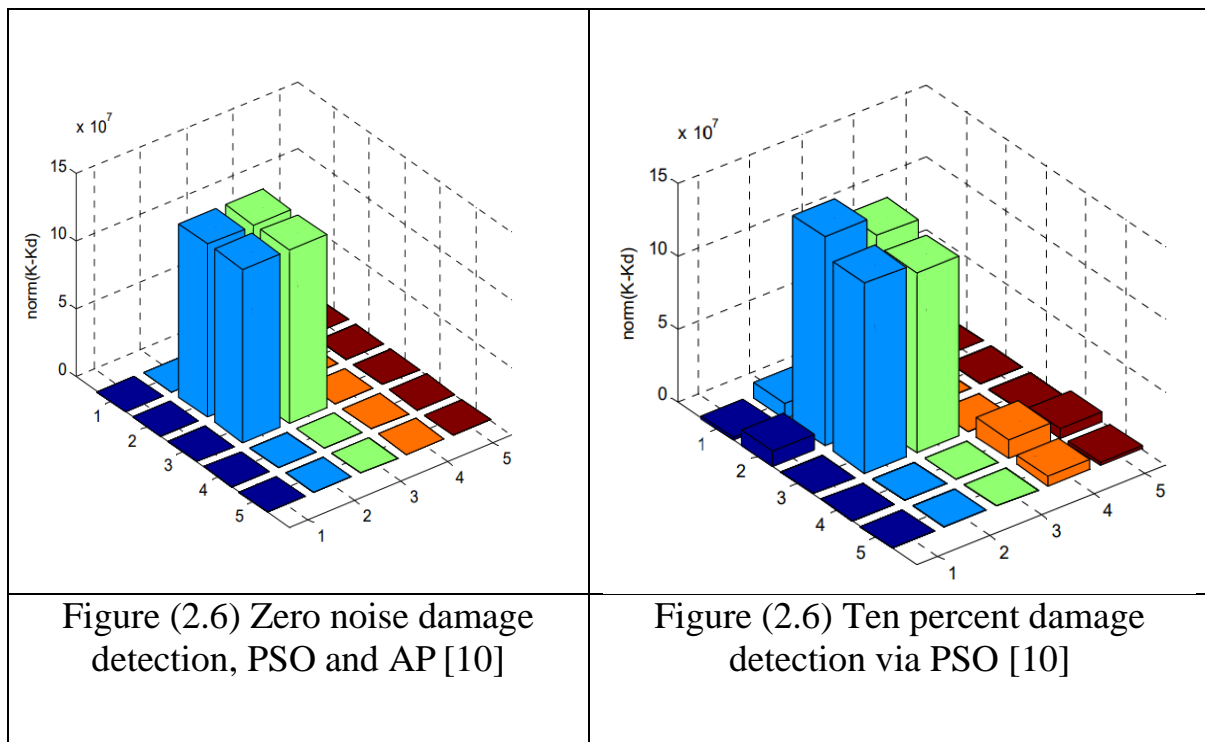


Figure (2.5) Comparison between the experimental (solid line) and the theoretical (dot line) dynamic response of a square plate [9]

**ABDALLA (2009) [10]** in this paper he solved the inverse problem in structural health monitoring is solved by using a Particle Swarm Optimization (PSO) algorithm. Also he compared the PSO technique with Alternating Projection method to estimate damage by using a simulated cantilever beam model.

He used the cantilevered beam as a numerical example, assuming a reduce in stiffness by 25% for that element. The Figures (2.6) and (2.7) show zero noise damage detection PSO and AP



The results show That PSO technique was computationally efficient. Finally, the PSO technique was compared with the famous AP method, but the AP did not implement well with noisy mode shapes because of the conditioning of the projection formulae.

**Bayraktar et al (2011) [11]** illustrated the damages minarets (reinforced concrete and masonry) in town (Erciş) and (Edremit) in Turkey. In this paper response spectrums and Ground accelerations are given. A total of 63 masonry and

reinforced concrete minarets are heavily damaged in the center of city or villages nearby after the earthquakes. They noticed there are several reasons for damages in these minarets such as location and length of the fault, site effect, formation of the discontinuity and reduction in cross section, use of concrete with insufficient strength and use of plain reinforcement steel as shown in Figure (2.8). Also they notice all non-engineering masonry and reinforced concrete minarets completely collapsed or damaged heavily.

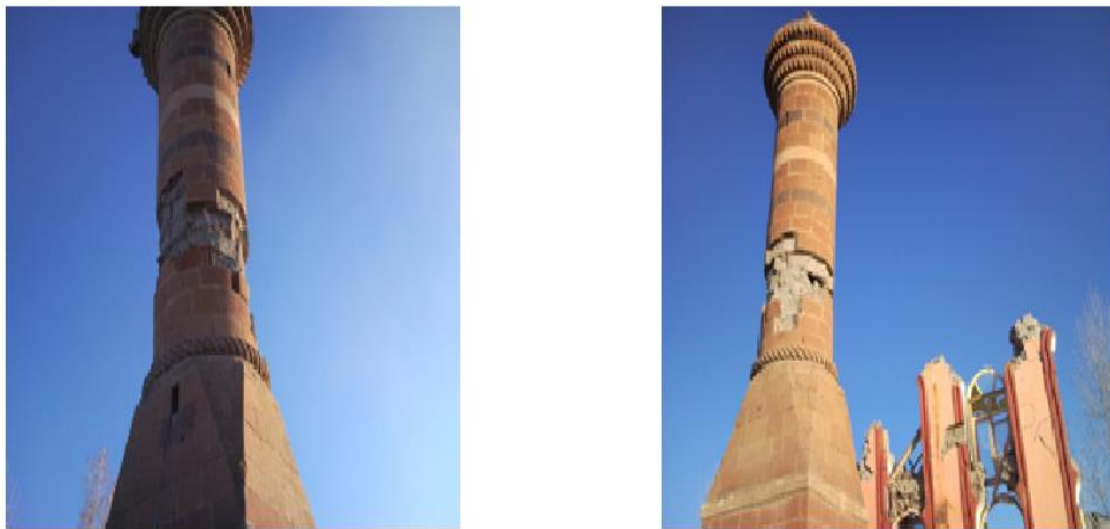


Figure (2.8) Failures occurred at the region between transition segment and cylindrical body [11]

**Kang et al (2012) [12]** "Damage detection based on improved particle swarm optimization using vibration data" in this paper the researchers made a damage detection of structures by using an Immunity Enhanced Particle Swarm Optimization (IEPSO) which combines between the artificial immune system and particle swarm optimization (PSO). The objective function is depending on the vibration data, such as mode shapes and natural frequencies to damage detection. A simply supported beam and truss were used to verify the performance of IEPSO and compare its results with the results of PSO, Differential Evolution (DE) and

RCGA. For beam the control parameters were  $F = 0.5$  and  $Cr = 0.9$ . For RCGA as shown in Figures (2.9), (2.10) and (2.11). The mutation probability is  $pm = 0.02$  and the crossover probability is  $pc = 0.8$ . For all algorithms, population size is 40 and the maximum generation is 200, the first three natural frequencies and mode shapes are adopted. The number of elements and nodes are 20 and 21, respectively. For truss structural the numbers of elements and nodes are 23 and 13, respectively. They concluded that the IEPSO method is quite efficient for damage detection problems.

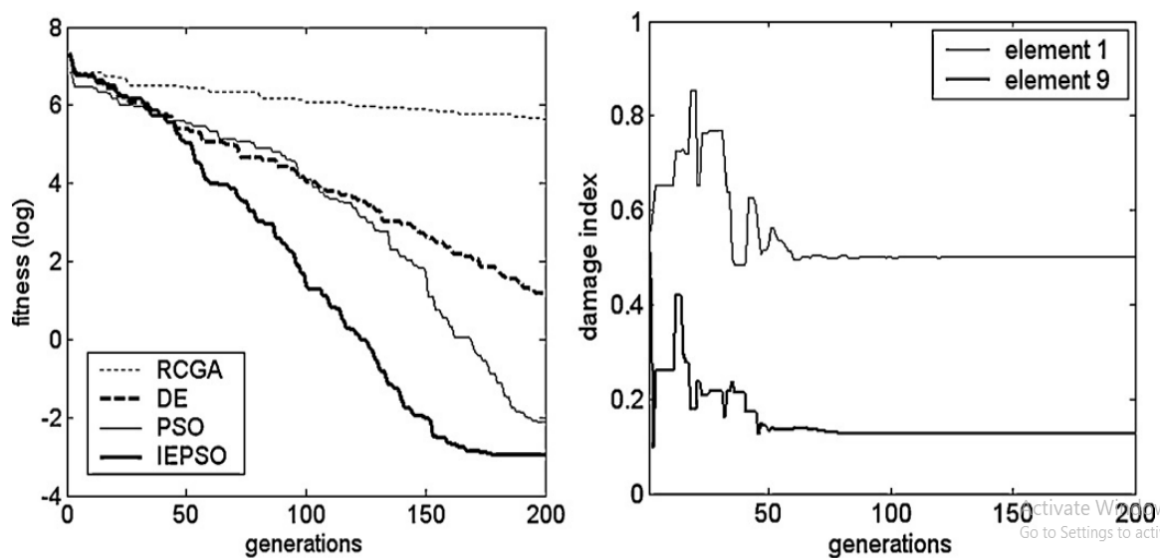


Figure (2.9) Evolutionary processes in case 1 of the beam: (a) the best fitness; (b) damage index [12]

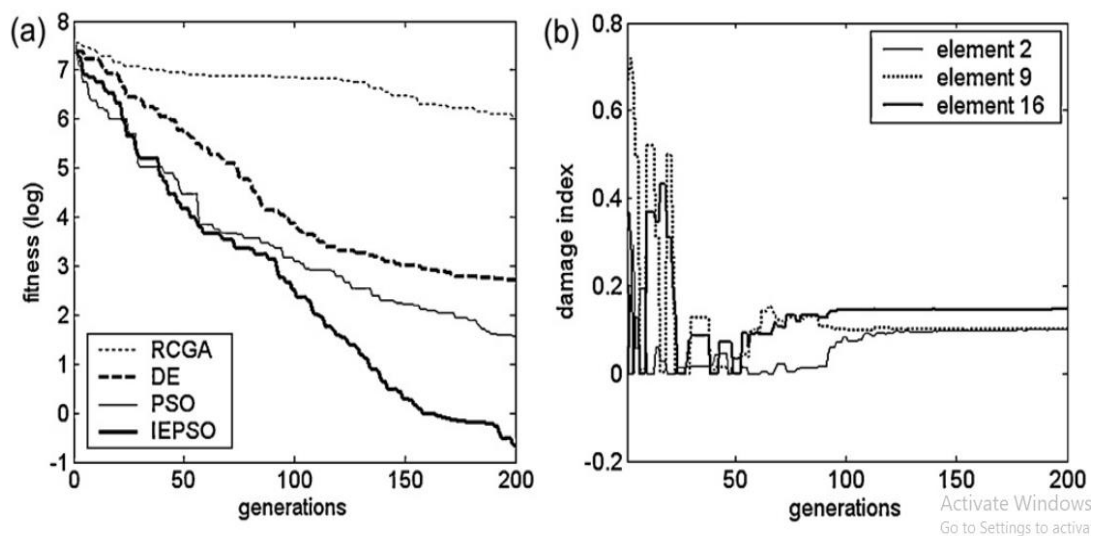


Figure (2.10) Evolutionary processes in case 2 of the beam: (a) the best fitness; (b) damage index [12]

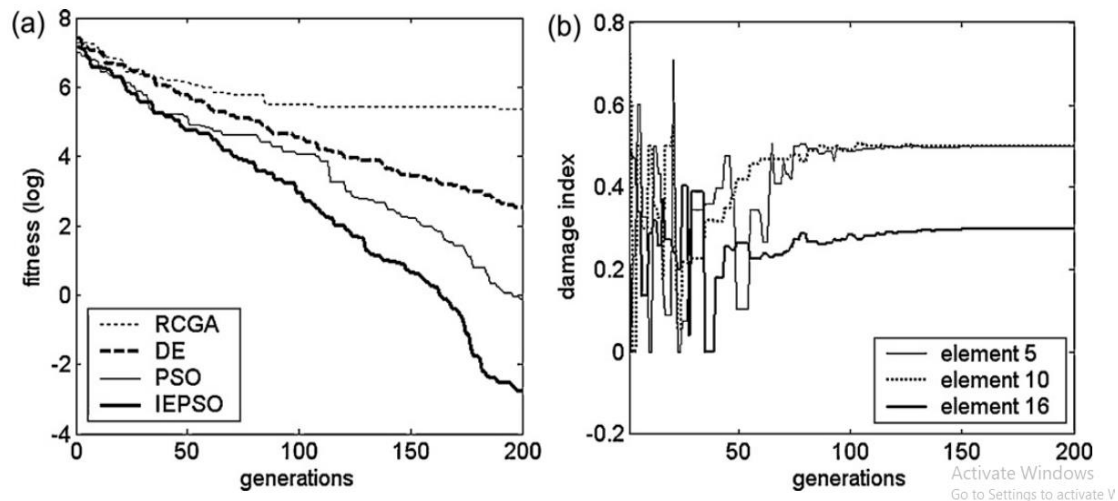


Figure (2.11) Evolutionary processes of example 2: (a) the best fitness; (b) damage index [12]

**Cakti et al (2014) [13]** executed a numerical analyses of two masonry minarets with different heights to reveal their structural behavior. The Mihrimah and Hagia Sophia minarets which are in Turkey. They used 3DEC to create the numerical models of minarets by discrete element method as shown in Figure (2.12) and using a series of sine-wave excitations to perform by progressive changing the frequency and range of input velocity the dimensions of minaret are listed in Table (2.1).

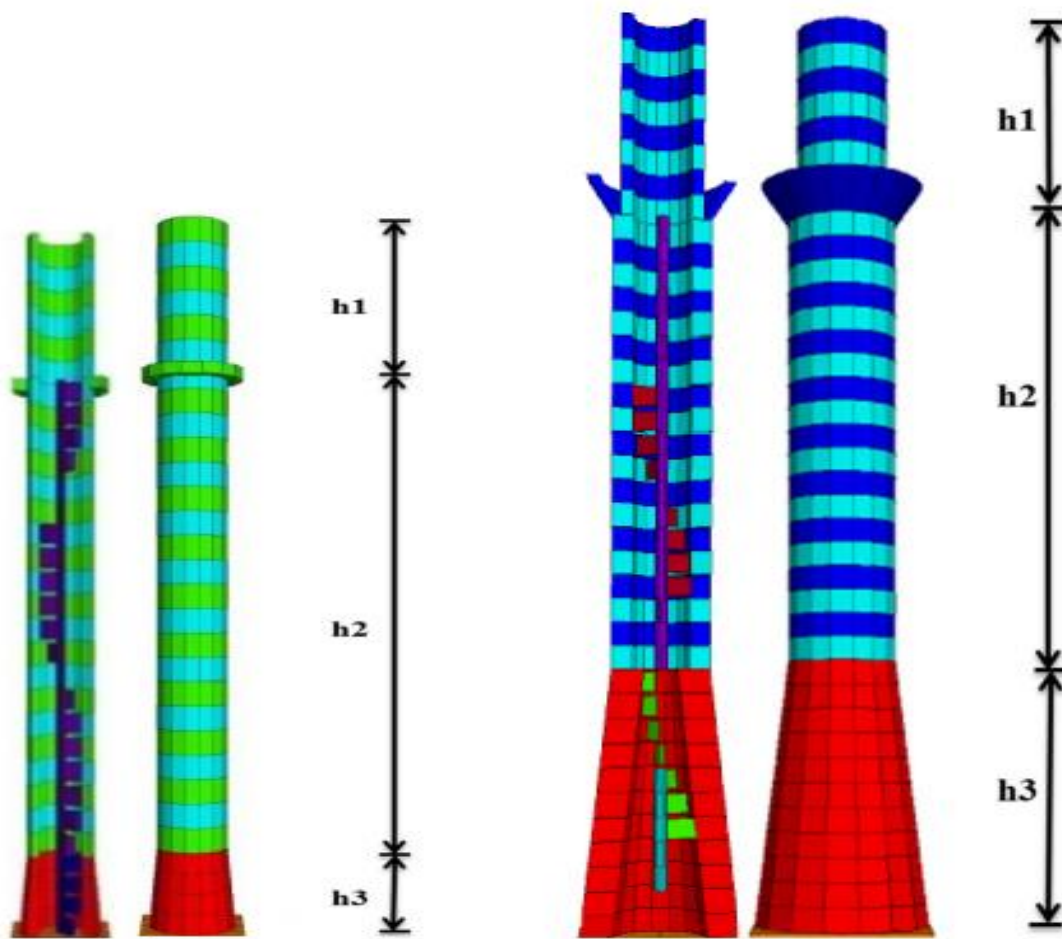


Figure (2.12) Models of Hagia Sophia (right) and the Mihrimah (left) minarets [13]

Table (2.1) Mihrimah minaret model geometrical properties (left), Haiga Sophia minaret model geometrical properties (right) [13]

	Height (m)	Wall thickness (m)		Height (m)	Wall thickness (m)
Transition segment(h3)	3.44	0.30	Transition segment(h3)	11.96	1.60
Body (h2)	21.00	0.30	Body (h2)	19.77	1.00
Top (h1)	6.30	0.30	Top (h1)	8.67	0.60

They recorded the displacement magnitudes, normal, relative and residual displacements. The results are determined and compared with those previously obtained from the analyses determined under synthetic and real earthquake

inputs. The frequencies values of the first minaret was 0.7 Hz and second minaret were 0.94 Hz. They concluded that the frequencies values was height in second minaret compared with first minaret due to larger height and thickness and loading the first minaret has higher maximum displacement in the top as shown in Figure (2.13), (2.14) and (2.15).

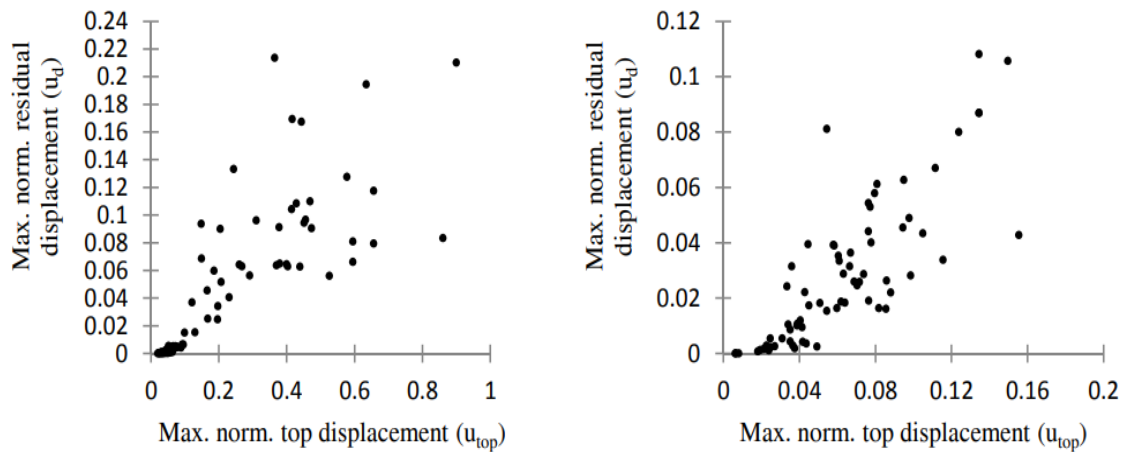


Figure (2.13) Scatter plot of maximum normalized residual displacement versus normalized top displacement for minaret of Mihrimah (left) and Hagia Sophia (right) [13]

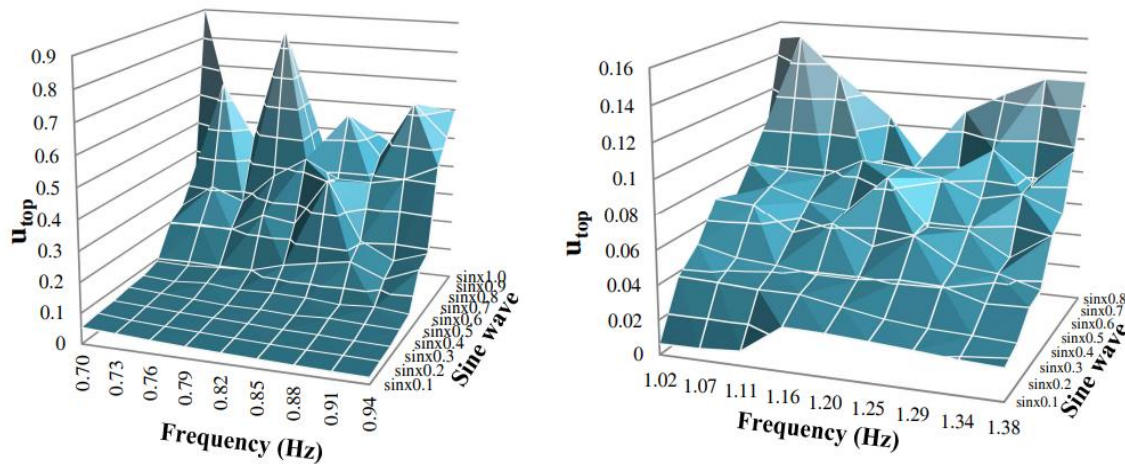


Figure (2.14) Variation of maximum normalized top displacement with the frequency and the amplitude of sine wave for the case of Mihrimah (left) and Hagia Sophia (right) [13]

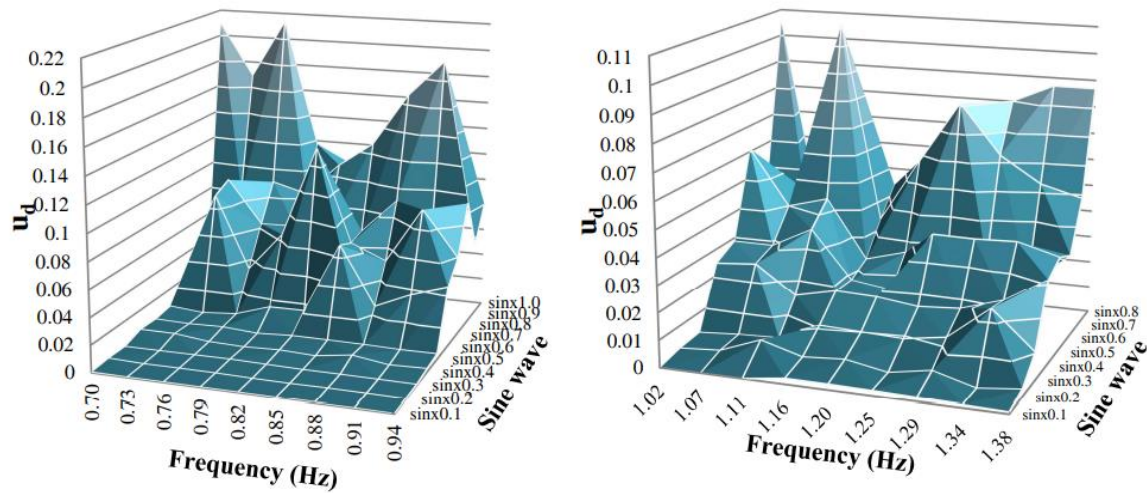


Figure (2.15) Variation of maximum residual displacement with the frequency and the sine wave amplitude for the case of Mihrimah (left) and Hagia Sophia (right) [13]

**DUVNJAK et al (2016) [14]** carried out a structural health monitoring of cultural heritage structures applications on peristyle of Diocletian's palace in Split. In this paper the long-term structural health monitoring system was applied on cultural heritage structures. This monitoring is part of restoration, reconstruction procedures and conservation of Diocletio'n palace in Split. This monitoring system is of two phases: the first phase included the assessment of bearing stone, copper clamps and embedded material, and in the second phase the monitoring system based on strain temperature and continuous static measurement of displacement was installed. Figure (2.16) shows the locations of the strain-gauge.

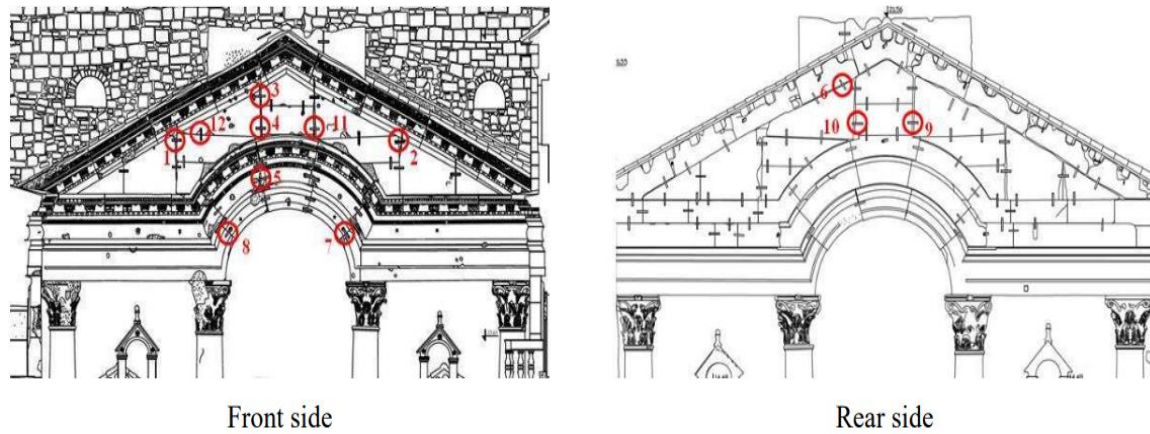


Figure (2.16) Measuring points of Protiron [14]

In this paper the hole-drilling strain-gage method is used to determine the actual force in the clamps in an attempt to find residual strain measurement and used the static compressive test to find mechanical properties of stone. Figure (2.17) shows the hole-drilling strain-gage method for determining the actual force.



Figure (2.17) View on vault of Protiron and copper clamp [14]

The LabVIEW and data acquisition system NICompaqDAQ was used in long-term structural health monitoring system. Seventeen measuring points were selected to monitor relative displacements between the block, stone, strain, temperature and crack openings at discrete nodes of structure. The period of monitoring was three years after measurement results. The state of the structure was stable. Figures (2.18) and (2.19) show the displacement and strain over time

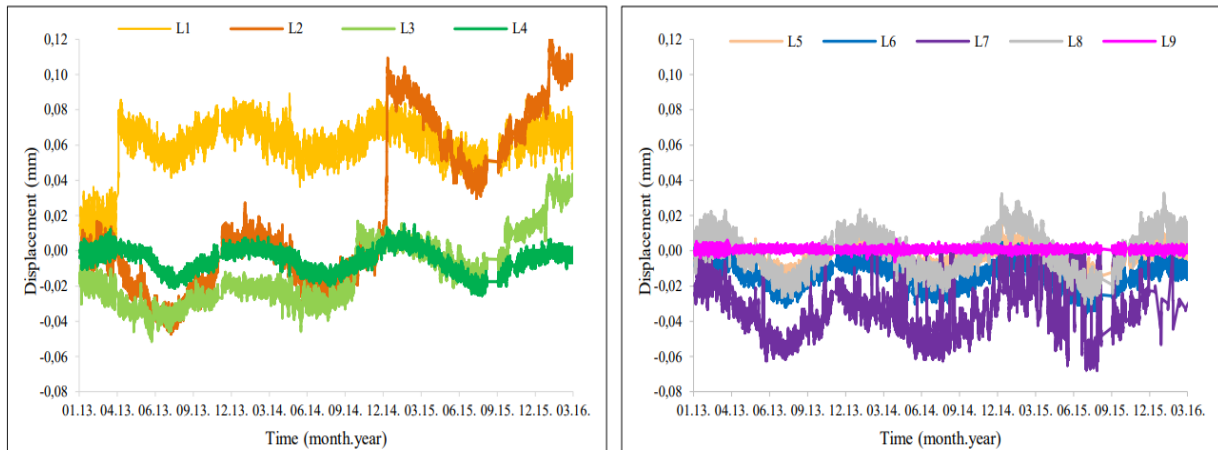


Figure (2.18) Time series of displacements [14]

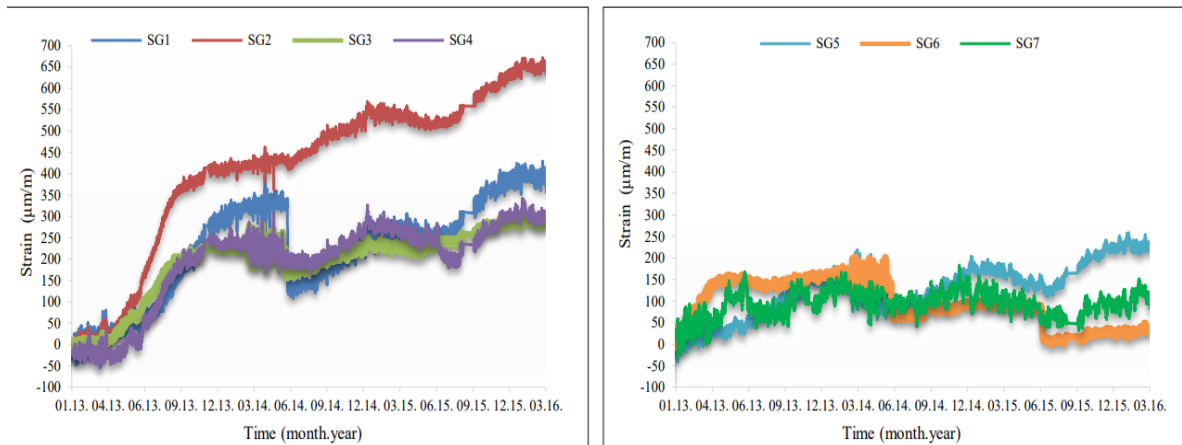


Figure (2.19) Time series of strains [14]

**Mehrian et al (2016) [15]** carried out structural health monitoring using optimising algorithms based on flexibility matrix approach and combination of natural frequencies and mode shapes. In this paper, creating objective function to detect the damage location and its amount they used two methods, combination of natural frequencies, mode shapes and flexibility matrix. The objective function is defined based on differences between the real structure and mathematical model. They reduced the elasticity modulus of the element to represent the damage. The charged system search and particle swarm optimization used to find the best optimization. They used three numerical examples with different scenarios, first a continuous beam with the moment of inertia and cross section area  $22,185 \text{ cm}^4$

and 123.2 cm<sup>2</sup> respectively. Second a two dimensional with 21 elements, and the cross section area for elements is equal to 15 cm<sup>2</sup>. Third a frame with three floors and four spans. 2% and 5% noises are applied to natural frequencies and mode shapes respectively. They used MATLAB to process of damage detection. The damage detection results obtained from PSO and CSS are shown in Figures (2.20), (2.21) and (2.22).

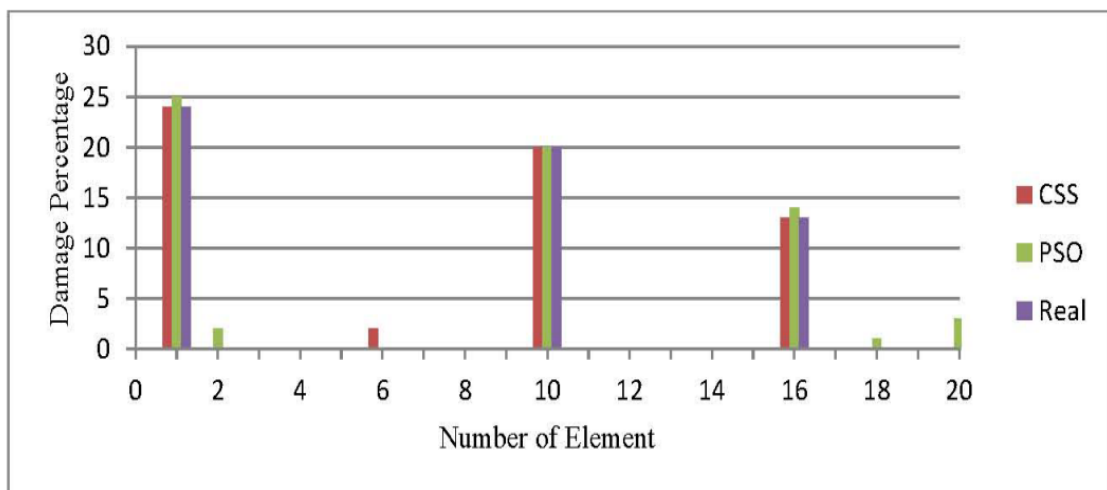


Figure (2.20) Damage detection results obtained from PSO and CSS using combination of natural frequencies and mode shapes for a continuous beam [15]

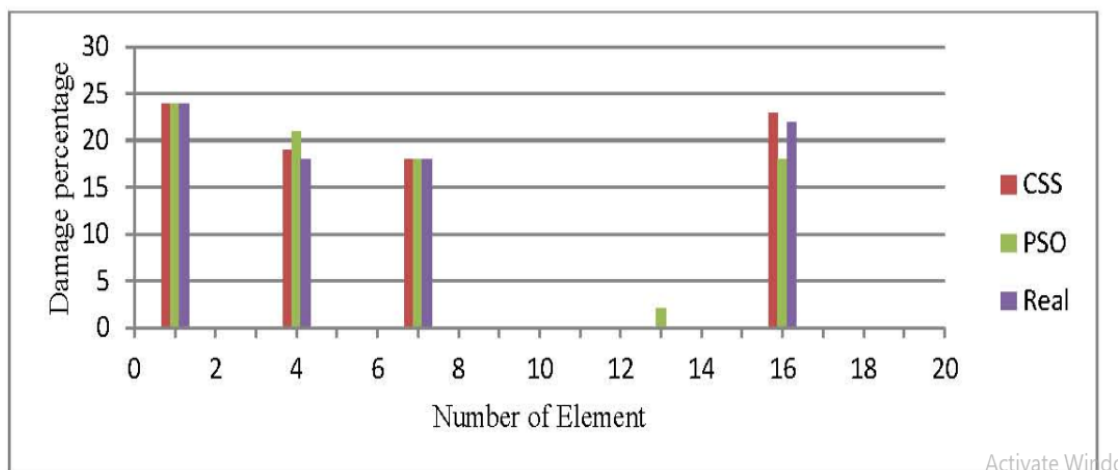


Figure (2.21) Damage detection results obtained from PSO and CSS using combination of natural frequencies and mode shapes for a two dimensional truss [15]

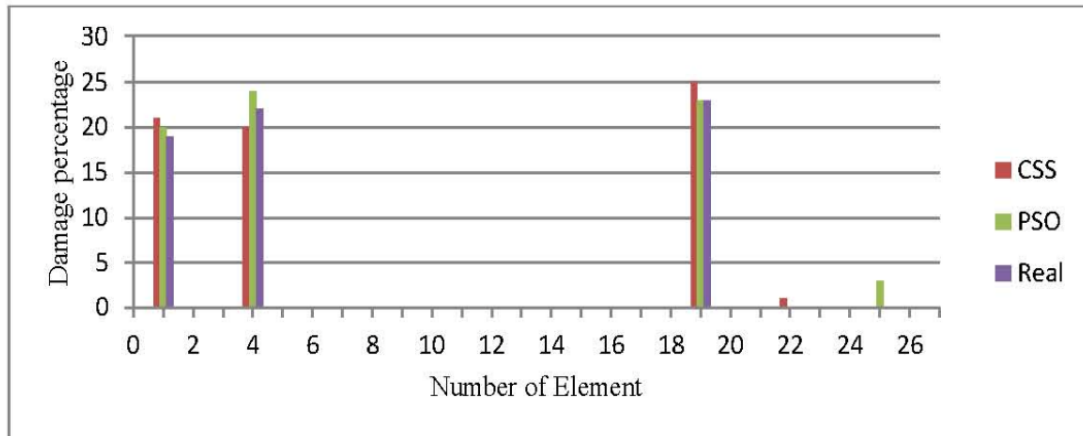


Figure (2.22) Damage detection results obtained from PSO and CSS using combination of natural frequencies and mode shapes for a frame with three floors and four spans [15]

**Livao lu et al (2016) [16]** studied the effect of geometric properties on dynamic behavior of historic masonry minaret in Turkey. They inspected seven historical masonry minarets by investigating effect of geometrical features for this minarets in bursa. They performed ambient vibration test to determine modal parameters of the minarets. The structural behavior of minarets were represented with mathematical models, using the finite element software Abaqus Cae to implemented three dimensional (solid) models. They used relationships between the first mode period and structural properties of minaret such as cross section, height and boundary condition, then they derived the analytical formula from the relationships for rapid estimation of the fundamental period of the typical Ottoman minarets.

**Başaran et al (2016) [17]** investigated the structural behavior of historical masonry minaret of Hacı Mahmut Mosque. They using ABAQUS-software in their finite element model as shown in Figure (2.23), 972851-tetrahedral solid

element type with four nodal points.in the modal analysis the base of minaret was the fixed support type. The frequency values are listed in table (2.2)

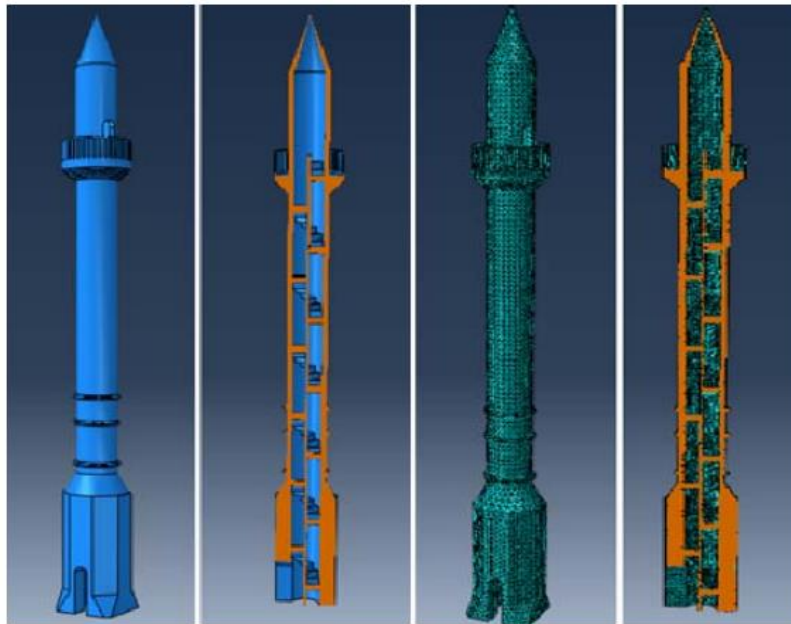


Figure (2.23) Three-dimensional finite elements model of the minaret and meshed state thereof [17]

Table (2.2) Frequency values obtained as a result of numerical analyses [17]

mod	Frequency (Hz)
1	1.21
2	1.22
3	6.891
4	6.972
5	11.958

They used changing in first natural frequency values to extraction of sensitivity analysis and dynamic properties in the finite element analysis of the structure. The optimum mesh size was determine by using the modal analysis to apply the structural modeling. Finite element model of the minaret was updated using dynamic characteristics of the structure and obtained the realistic numerical

model of the structure as shown in Figure (2.24). They concluded that the optimum size of element mesh is 0.6 m.

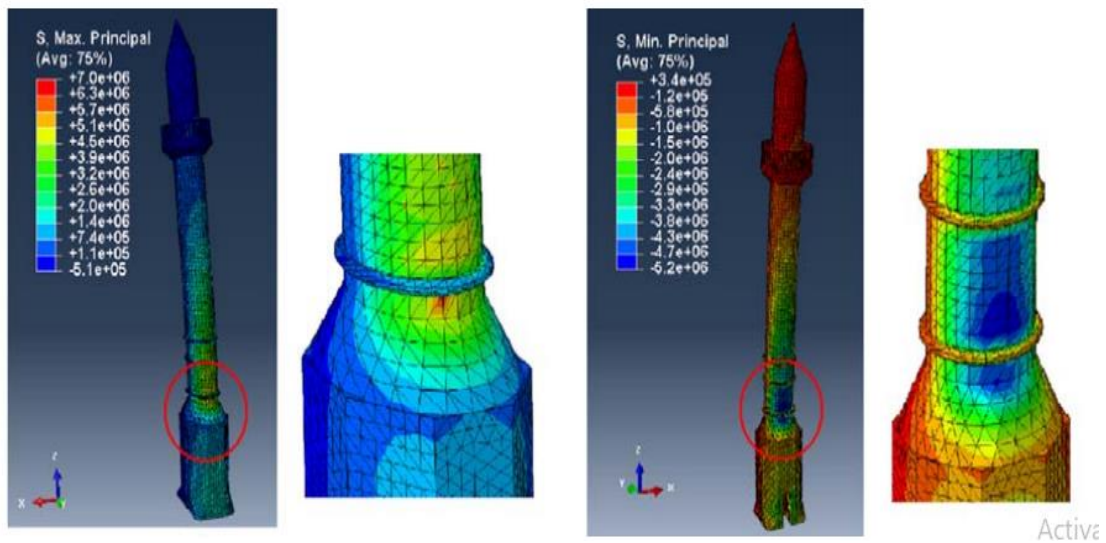


Figure (2.24) Distribution and values of stress occurring in the minaret as a result of analyses [17]

**Nohutcu et al (2017) [18]** estimated seismic damage and the collapse mechanism of the historical stone masonry minaret “Hafsa Sultan”. They obtained the mechanical properties and a 3D solid model of the components of the minaret by material test and surveying measurements. In Linear Time History (LTH) and Nonlinear Time History (NLTH) analyses they used two different ground motions in Akhisar (2016), Düzce (1999) by using the CDP material model. From the results, the tensile stresses were more effective than compression stresses on damage. The stresses from LTH analyses for the minaret subjected to Düzce earthquake exceeded limit stresses. From findings, it was concluded that a severe earthquake could cause strong damages in the historical Hafsa Sultan minaret.

**Nohutcu et al (2019) [19]** In this study, they used Operational Modal Analysis (OMA) method to examined 3 historical mosques, Manisa Muradiye Mosque, Manisa Hafsa Sultan mosque, Bolvadin Imaret Mosque and 3 historical minarets,

Imaret mosque minarets, Bolvadin Alaca and Manisa Hafsa Sultan Mosque minaret. They used Finite Element methods and OMA method to select the dynamic characteristics of these historical structures, damping ratios, natural frequency and mode shapes as shown in Figure (2.23). These structures were evaluated in terms of building material, and they compared the elasticity modules of the whole structures.

They used Stochastic Subspace Identification (SSI) and Enhanced Frequency Domain Decomposition (EFDD) methods to determine the dynamic parameters. They foreseed that the best mesh intervals can be taken as 0.28m for minarets and mosques. The average modulus of elasticity was about 8467 MPa for minarets, 1873 MPa for mosques. In all the studied structures, the 1st and 2nd mode shapes were obtained in the X or Y horizontal directions respectively. The torsional action was determined in the 5th mode for all minarets. The average damping ratio was 0.84 percent for the minarets and 1.8 percent for the mosques.

**Ghannadi et al (2020) [20].** In order to determine the unmeasured mode shapes, the system equivalent reduction and expansion technique are used in this article. The effectiveness of the system equivalent reduction and expansion method in estimating unmeasured mode shapes are demonstrated using two experimental examples, including a cantilever beam and a truss tower. The findings demonstrate the importance of the expansion strategy. The residual force vector based on expanded mode shapes is taken into consideration as the objective function in a damage identification issue that is presented as an optimization problem. Grey wolf optimization and Harris hawks optimization are employed to reduce the objective function. To show the effectiveness of the presented strategy, numerical calculations on a 56-bar dome space truss and experimental validation on a steel frame are carried out. When compared to the results of Harris Hawks optimization, numerical and experimental results show that the combination of

the expanded mode shapes with system equivalent reduction and expansion process and the grey wolf optimization (inspired by the leadership hierarchy and hunting mechanism of grey wolves in nature) can provide a reliable method for determining the severity and locations of damage to skeletal structures.

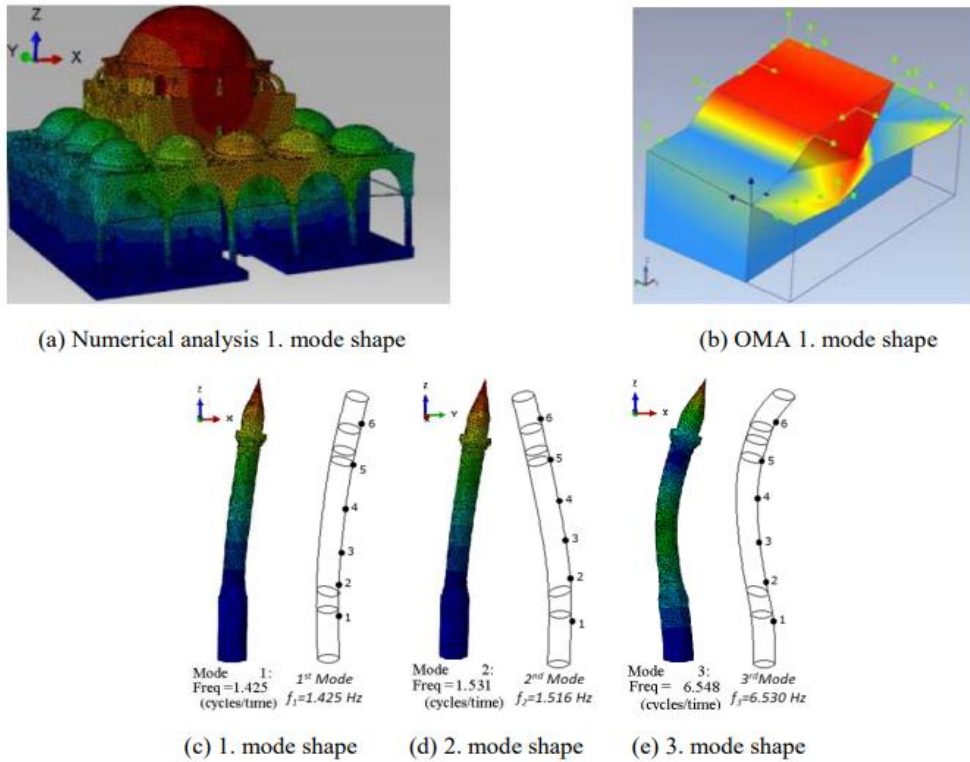


Figure (2.25) Numerical and experimental mode shapes of Hafsa Sultan Mosque and Imaret Mosque minaret as examples [20]

**Nguyen and Livaoglu (2022) [21]** are presented a health monitoring method for detecting damage of minarets. It is specifically intended to identify damage to the Haclar mosque's (24.25 m high) minaret, which was constructed in Bursa, Turkey, in 1467 using stone and brick. There are only four accelerometers installed along with the minaret's height to gather lateral displacements, leaving an insufficient number of degrees of freedom to be measured (DOFs). Because slender minarets and beam-like constructions have comparable bending behavior at low modes, the difficult problem is avoided by transferring the minaret into a

lumped mass system that corresponds to the built sensor network, the result as shown in Figure (2.26).

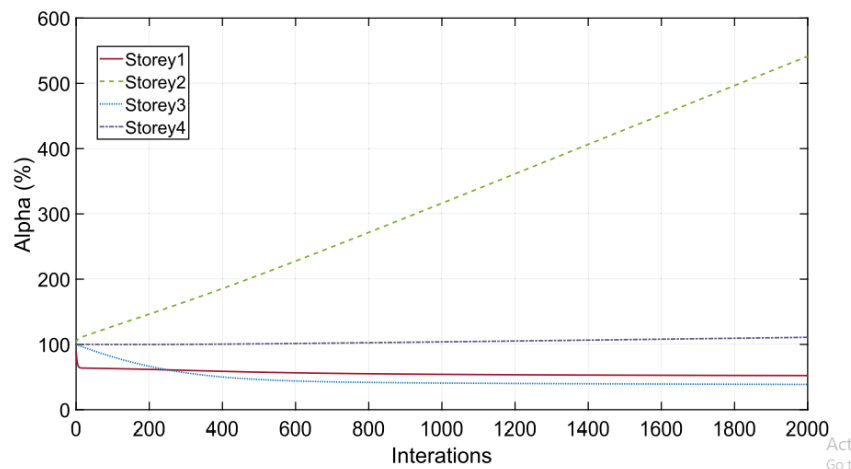


Figure (2.26) Damage detection of S3 using Combo 3–1 with  $h = 3.75$  m [21]

The numerical analysis demonstrates that because the modal data is noise-free, the robustness of the method cannot be questioned. Even though the modal data is noise-contaminated, the approach can nevertheless provide accurate damage detection. Additionally, compared to the higher parts, the lower parts' damage detection is less noise sensitive. Particularly, detect the damage at the bottom parts of the main minaret of the Haclar mosque may be recognized with a noise level of 1% in mode shapes, whereas the parameter is 0.75 % for the upper part.

## 2.7. Summary

1- It is evident from the mentioned studies that the researchers relied on changes in the dynamic characteristics of natural frequencies and mode shapes in damage detection.

2- From the studies mentioned, we note that the PSO method was very effective in detecting damage after comparing it with many other optimization methods such as CSS, AP, DE and etc.

3- In most of the mentioned studies, researchers used analysis programs such as ANSYS, ABAQUS, and SAP2000 to analyze the model and extract the dynamic characteristics.

4- It is also noted that due to the complexity of Islamic forms, researchers used in the analysis the form of a tetrahedral element and a free mesh distribution of the elements.

5- The natural frequencies values of minarets was between 1.2 Hz to 30 Hz for first 7 modes, and in most time the 5th mode was torsion about Z axis.

6- All non-engineering masonry and reinforced concrete minarets completely collapsed or damaged heavily because of earthquakes.

# CHAPTER THREE

## CHAPTER THREE

### Optimization Problems and Heuristics Methods

#### 3.1. Introduction

The optimization theory and its methods are a new subject in computational mathematics, applied mathematics and researches which have wide applications in science, business management, engineering, space technology and military. This subject is used to solve the problems which are defined mathematically, for practical problem can be found the "best" solution from many schemes by means of scientific methods and tools. It includes the study of optimality conditions of the problems, select algorithmic method of solution, the construction of model problems, the establishment of convergence theory of the algorithms, and typical problems with numerical experiments and real life problems [22].

Now there are many modern optimization methods (Heuristics Methods) that can solve difficult and large scale optimization problems, and become an indispensable tool for solving problems in diverse fields [22].

#### 3.2. Optimization Problems

The optimization problem is the problem of finding the best solution from all feasible solutions. In an optimization problem the function is to be maximized or minimized, and this function is referred to as the objective function or the performance index. The function is a quantity such as profit, size, cost, efficiency shape and so on [23]. Table (3.1) shows some optimization problems with its typical objective functions and design variables from different disciplines.

Table (3.1) Typical Optimization Problems [23]

Discipline	Design Variables	Objective Function
Manufacturing	Productivity from different machines	Minimize cost
Corporate	Different capitals from projects	Maximize the net present value
Airline	Different aircrafts, different routes	Maximize the profit
Aerospace	Propellant fraction in different stages	Maximize the payload
Agriculture	Different crops	Maximize the yield
Biology	Gene interaction	Network stability
Electronics	Size of the devices	Minimize the power consumption
Portfolio	Investment in stocks/bonds	Maximize the return
Thermal	Dimensions and material properties	Minimize the heat load

The optimization problem can be mathematically expressed as follows [23].

Minimize

$$f(x)$$

Subject to

$$g_i(x) \leq 0 \quad i = 1, 2, \dots, m < n \quad \dots \quad 3.1$$

$$h_j(x) = 0 \quad j = 1, 2, \dots, r < n \quad \dots \quad 3.2$$

$$x_l \leq x \leq x_u$$

Where  $x$  is a vector of  $n$  design variables given by

$$x = \begin{bmatrix} x_1 \\ x_2 \\ \vdots \\ x_n \end{bmatrix}$$

The functions  $f, g_i$  and  $h_j$  are all differentiable

The design variables are bounded by  $x_l$  and  $x_u$

$g_i$  represent inequality constraints and  $h_j$  represent equality constraints

There are two categories of optimization problems depending on the variables whether continuous or discrete [23]:

1- Discrete optimization (an optimization problem with discrete variables), in this type must be found as an object such as an integer, permutation or graph from a countable set [23].

2- Continuous optimization (A problem with continuous variables), in this type must be found as an optimal value from a continuous optimization. They can include constrained problems and multimodal problems [23].

Many types of optimization method are applied to solve those engineering problems such as; optimization algorithms, iterative methods, global convergence and heuristics methods.

### 3.3. Heuristics Optimization

In the past decades several heuristic tools have evolved to facilitate solving the difficult or impossible optimization problems, such as Simulated Annealing, Evolutionary Computation, Tabu Search, Particle Swarm Optimization, etc. [24]. To solve extremely challenging problems, it needed combining these new heuristic tools with each other and with knowledge elements, and also with more traditional approaches such as statistical analysis. These tools with developing solutions offers two major advantages [25]:

1- In such tool the development time is shorter than when using more traditional approaches [25].

2- The systems are relatively insensitive to noisy and/or missing data, so it is very robust [25].

### **3.3.1. Evolutionary Computation**

Natural evolution is a hypothetical optimization process based on the population. This process when simulating it on a computer, the results in stochastic optimization techniques and these techniques are often best than classic methods of optimization when applied to difficult real-world problems [25].

Evolutionary Computation (EC) includes a class of stochastic optimization algorithms, called Evolutionary Algorithms (EAs) which are optimization algorithm Population-based (evolves a population of candidate solutions), uses probabilistic rules, and it is Bio-inspired (uses principles inspired from biological evolution). It uses a black-box tool for many problems [24].

The Evolutionary Algorithms (EAs) are easy-to-use, it is not need to strict requirements for problems, it widely used for optimization and search problems such as industry engineering, financial and economic systems, transportation and logistics systems and automatic programming, art and music design [24].

### **3.3.2. Genetic Algorithm**

Genetic Algorithm (GA) is one of the search algorithms based on genetics and the conjecture of natural selection. The genetic algorithm is different from other search techniques in several aspects [25]:

1- The algorithm reduces the possibility of local minimum trapping, because the algorithm is a multipath that searches many tops in parallel.

2- The genetic algorithm uses coding of parameters in lieu of the parameters themselves. The coding of parameter help the genetic operator to development the current condition into the next condition with minimum computations.

3- There is no need for computation of derivatives and other auxiliary functions, because the GA evaluates the fitness of each string to guide its search in lieu of the optimization function. It only needs to evaluate objective function (fitness) to guide its search, without derivatives or other auxiliary knowledge.

4- The probability of finding improved performance is high where the strategies employing GA explore the search space [25]. Figure (3.1) shows a typical flowchart of a Genetic Algorithm.

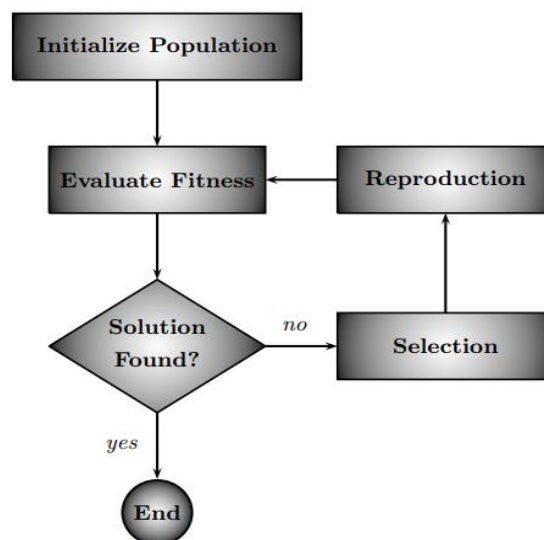


Figure (3.1) Basic genetic algorithm iteration flowchart

### 3.3.3. Evolution Strategies and Evolutionary Programming

Evolution strategies (ES) use real-coded variables, and, in its authentic form, it depends on mutation as the search operator, and a population magnitude of one. The (ES) resemble GA in choosing the best individuals from the population by using selection mechanism, and they both maintain populations of potential solutions. But ES operates on floating-point vectors directly, whereas classic GAs

operate on binary strings. Evolutionary programming (EP) is a stochastic optimization strategy, EP is similar to ES, in spite of that the two approaches developed independently. The Evolutionary programming (EP) is a helpful method of optimization when other techniques such as direct analytical discovery or gradient descent are not possible [25].

### **3.3.4. Differential Evolution**

The Differential Evolution (DE) is developed by Storn and Price in 1995, and it is one of the population-based global optimization techniques for continuous design variables. The DE is the strong global optimization technique and is widely used. The Differential Evolution (DE) mainly focuses on the single objective optimization problems. Many DE versions have been proposed by many researchers [26].

Satoshi Kitayama et al [26] used Differential Evolution as the Global Optimization Technique and its Application to Structural Optimization. They applied DE for eleven benchmark problems, and to two structural optimization problems. They used the standard deviation of objective for measuring robustness of the algorithm, and the function call was used for measuring the efficiency. Compared with the PSO, the DE can find the global minimum of the benchmark problems with smaller function calls. They revealed that the DE is a stronger algorithm than optimization techniques under the parameter settings used in this paper.

### **3.3.5. Ant Colony Search Algorithm**

This algorithm simulates the behavior of real ants. Real ants are able to find the shortest path from the nest to the food source they discover without the need for visual cues. As soon as the old path becomes unsuitable due to a new obstacle, they quickly find a new shortest path. Studies reveal that these abilities are due to the so-called “pheromone pathways,” which ants use to communicate information

to other individuals. Where ants deposit a certain amount of pheromone while walking, and each ant follows the direction rich in pheromone [25].

### **3.3.6. Tabu Search**

This method depend on search in memory, where the memory preserves previously that visited states along and states that might be considered unwanted. If no convergence is found in the Tabu Search the search will be reset randomly [25].

### **3.3.7. Simulated Annealing**

The Simulated Annealing (SA) method is a simulation of annealing physical of particle system to find the global optimum solutions. The research on global optimum solution depend on using a temperature parameter where temperature is slowly lowered, the system cools down, and by the annealing function a new point is generated [25].

### **3.3.8. Particle Swarm Optimization**

Particle Swarm Optimization (PSO) is a new methodology in evolutionary computation that is similar to a genetic algorithm where the system starts with a population of random solutions [25].

This method depends on swarm intelligence to search for food such as fish schooling and bird flocking, where search for food is done by sharing the information among the individuals of the swarm. This way of searching for food inspired the researchers Kennedy and Eberhart suggest a method for function optimization, they called it particle swarm optimization (PSO) (Kennedy and Eberhart, 1995) [32].

The particle swarm algorithm keeps a set of particles and each particle has a location in a multi-dimensional space (the problem space). Initially, the particles take random locations and then search for the lowest (or upper) value for a

particular function by navigating through the search space. The function measures the quantity and quality of food everywhere in the search space, and the swarm of particles searches for the location that contains the best and most food. This motion of particles depends on its velocity and the best position found by the particle itself or neighboring particles [27]. The particle swarm optimization PSO does not use gradient information, unlike many deterministic methods.

Below is a scheme for a PSO algorithm [27]:

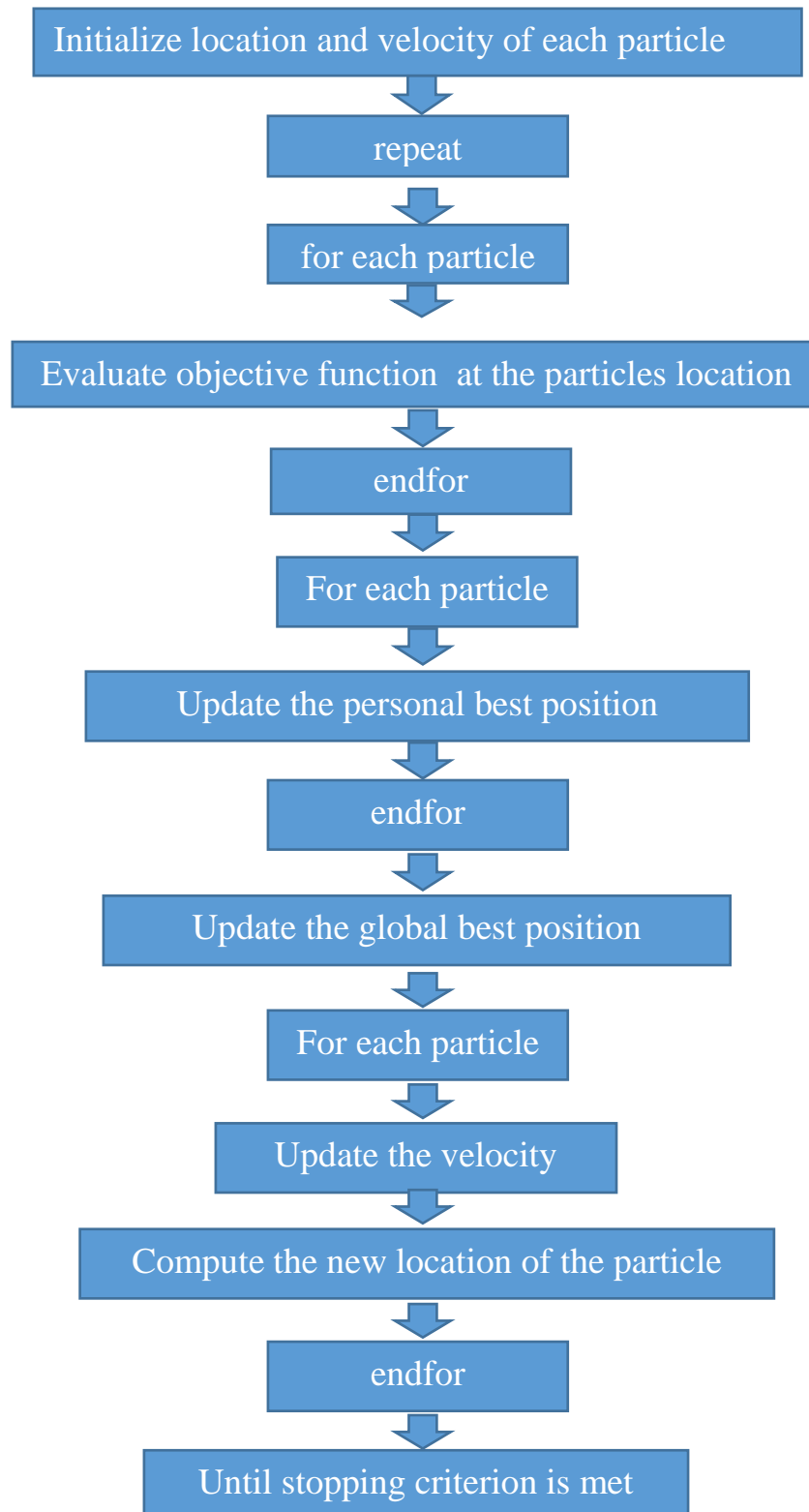


Figure (3.2) Scheme for solving problem by PSO method

## Background of Particle Swarm Optimization

By few simple rules the Swarm behavior can be modeled. But the behavior of the swarm can be complicated even if the behavior rules of each particle (agent) are simple. Reynolds used the following three vectors as simple rules for the research [25].

1-Get far from the nearest particle.

2-Go to the destination.

3-Go toward the center of the swarm.

This mean that each particle moves by two vectors, the first toward the local best position and the second to the global best position of the entire swarm. The Figure (3.3) shows these two vectors of the particle [25].

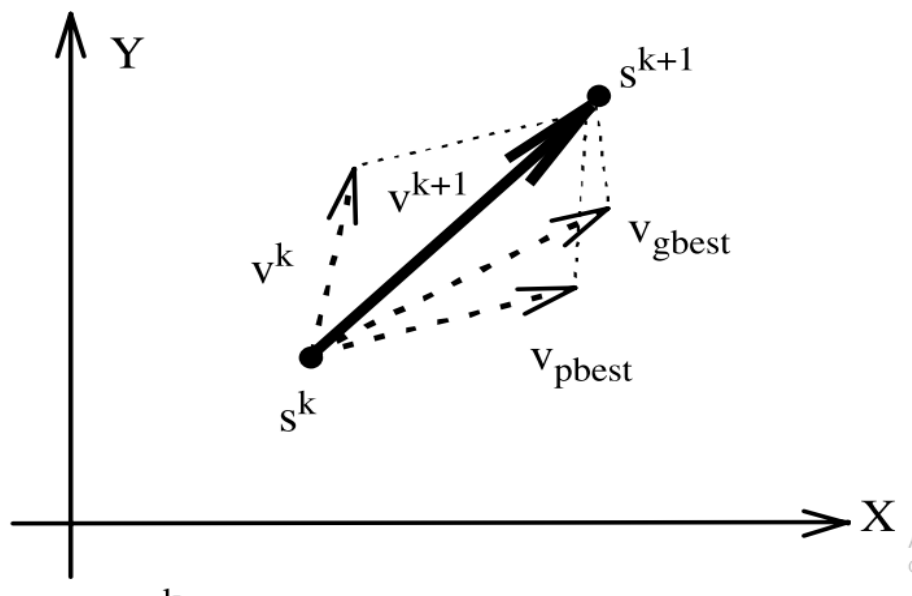


Figure (3.3) Modification of a searching point via PSO concept [25]

$s^k$  : Current searching point

$s^{k+1}$  : modified searching point

$v^k$  : Current velocity

$v^{k+1}$  : modified velocity

$v_{pbest}$  : Velocity based on pbest

$v_{gbest}$  : Velocity based on gbest

Velocity of each particle can be modified by the following equation:

$$v_i^{k+1} = wv_i^k + c_1rand_1 * (pbest_i - s_i^k) + c_2rand_2 * (gbest_i - s_i^k) \quad \dots 3.3$$

Where  $v_i^k$  is velocity of particle  $i$  at iteration  $k$ ,  $c_j$  is weighting coefficients,  $w$  is weighting function,  $s_i^k$  is current position of particle  $i$  at iteration  $k$ , (rand) is random number between 1 and 0,  $gbest_i$  is gbest of the group, and  $pbest_i$  is pbest of agent  $i$  [25].

The weighting function is usually following in:

$$w = w_{max} - \frac{w_{max} - w_{min}}{iter_{max}} * iter \quad \dots 3.4$$

Where  $w_{max}$  and  $w_{min}$  are initial weight and final weight respectively,  $iter_{max}$  and  $iter$  are maximum iteration number and current iteration number respectively.

The current position can be modified by the following equation:

$$s_i^{k+1} = s_i^k + v_i^{k+1} \quad \dots 3.5$$

The Figure (3.4) shows a general flowchart of PSO

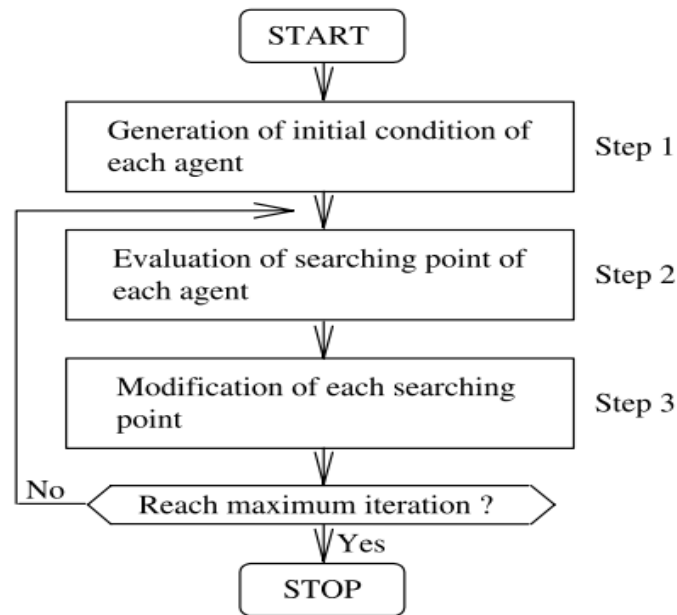


Figure (3.4) Flowchart of PSO method in general [25]

There are many researches which have used the method of particle swarm optimization in many areas, especially in structural engineering, where it is used in the design, damage detection or structural health monitoring of structures. For instances, Al-Wazni and Zainul-abideen (2019) [28] carried out intelligent non-destructive technique for crack existence inspection in a structure using Particle Swarm Optimization (PSO). They included the natural frequency, mode shapes and vibration properties in the non-destructive proposed technique.

They adopted steel clamped beam model with length 600 mm, and the section dimension 24 mm width and 10 mm depth. The material properties, modulus of elasticity and mass density, are 200 GPa and 7800 kg/m<sup>3</sup>, respectively. The number of elements in the structural model are 20 elements.

The numerical analysis was done by ANSYS-APDL software to find the vibration properties, this study included six natural frequency values. They used two scenarios for simulating the crack by reducing the depth of elements by 10%, the first element no.3 at 75 mm from the support and the second element no.8 at 225 mm from the support.

From the results, this technique displays robust and satisfactory performance for detecting the size and location of damage (crack) in the structural model.

Wei et al. (2018) [29] used particle swarm optimization to Structural damage detection. They used three different structures, a beam, a truss and a plate. A simply supported beam with 120 cm length, with 20 elements and 21 nodes and they utilized the first three natural frequencies and modes shapes. They used two cases, first the element 1 and 9 has 50 and 87.5% reduction in stiffness, respectively, and in the second case, they assumed that element 2 and 9 have both 10% reduction in stiffness and element 16 has 15%. A truss includes 31-bar, the length of each exterior and interior bar 1 and 1.41, respectively. The number of elements is 31 and nodes are 14, six local damages are adopted at the (2, 10, 17, 18, 23, 28) elements with reduction in stiffness (30, 40, 20, 25, 35, 23) %, respectively. And a plate with dimension of 3m 4m 0.1m, the plate is divided into (6\*8) 4-nodes plate elements, seven local damage are adopted in this study at (1, 12, 19, 24, 27, 38, 45) element with reduction in stiffness (15, 30, 16, 23, 30, 15, 28)%, respectively as listed in Table (3.2). They used a disturbance process to help particles escape from local minimum. From the results, the proposed method is very effective and efficiency.

Table (3.2) damaged elements and damage percentages for different structures

structures	elements	nodes	Damaged elements	Damage percentage
beam	20	21	1, 9	50%, 87.5%
			2, 9, 16	10%, 10%, 15%
truss	31	14	2, 10, 17, 18, 23, 28	(30, 40, 20, 25, 35, 23) %
plate	48		1, 12, 19, 24, 27, 38, 45	(15, 30, 16, 23, 30, 15, 28)%

# CHAPTER FOUR

## CHAPTER FOUR

### Finite Element Modeling and Structural Analysis of Masonry Minaret

#### 4.1. Introduction

The shrine of Imam Ali is one of the historical, cultural and religious buildings. The two minarets are important parts of this religious edifice as shown in Figure (4.1). In this research, one of the two minarets was selected as a model adopted. In this chapter, it will be explained how to take real measurements of the minaret, create a FE model for minaret and make a nonlinear (static) and linear (dynamic) analysis in the ANSYS program to extract high stresses location, frequencies and mode shapes. Finally, in this study investigation and parametric study of adopted minaret is carried out.



Figure (4.1) The structure of Imam Ali shrine

#### 4.2. Description and Geometry of Minaret Structure

The minaret's geometry were real measured by measuring machines on site, such as the height, diameter, interior shape, stairs and the places where the minaret is

connected to the shrine following a research [4] who carried out seismic behavior of Imam Ali holy shrine structure, he measures all dimensions on site by measuring machines, as shown in Figure (4.2).

The minaret contains a base of 2.38m height and 3.56 m diameter. The body of the minaret is of 17.38 m height starts with (3.56 m, 1.8 m) outer and inner diameter, respectively, but on top of the minaret's body it is narrower by 2.6 m and 1.3m. The body of the minaret connects with the walls of the shrine by 135 degrees as shown in Figure (4.2). The balcony of the minaret starts 2.6 m to 4.12 m diameter. The upper body of the minaret has a cylindrical shape with 6.2 m height and an outer diameter of 2m and inner diameter 1.3m. At the end of the minaret there is a dome with 1.57m height, as shown in Table (4.1).

Table (4.1). Dimensions of minaret (m)

	base	body	balcony	Upper body	dome
Height	2.38	17.38	1.25	6.2	1.57
Outer radius in bottom	1.78	1.78	1.3	1	1
Inner radius in bottom		0.9	0.65	0.65	0.65
Outer radius in top	1.78	1.3	2.06	1	
Inner radius in top		0.65	0.65	0.65	

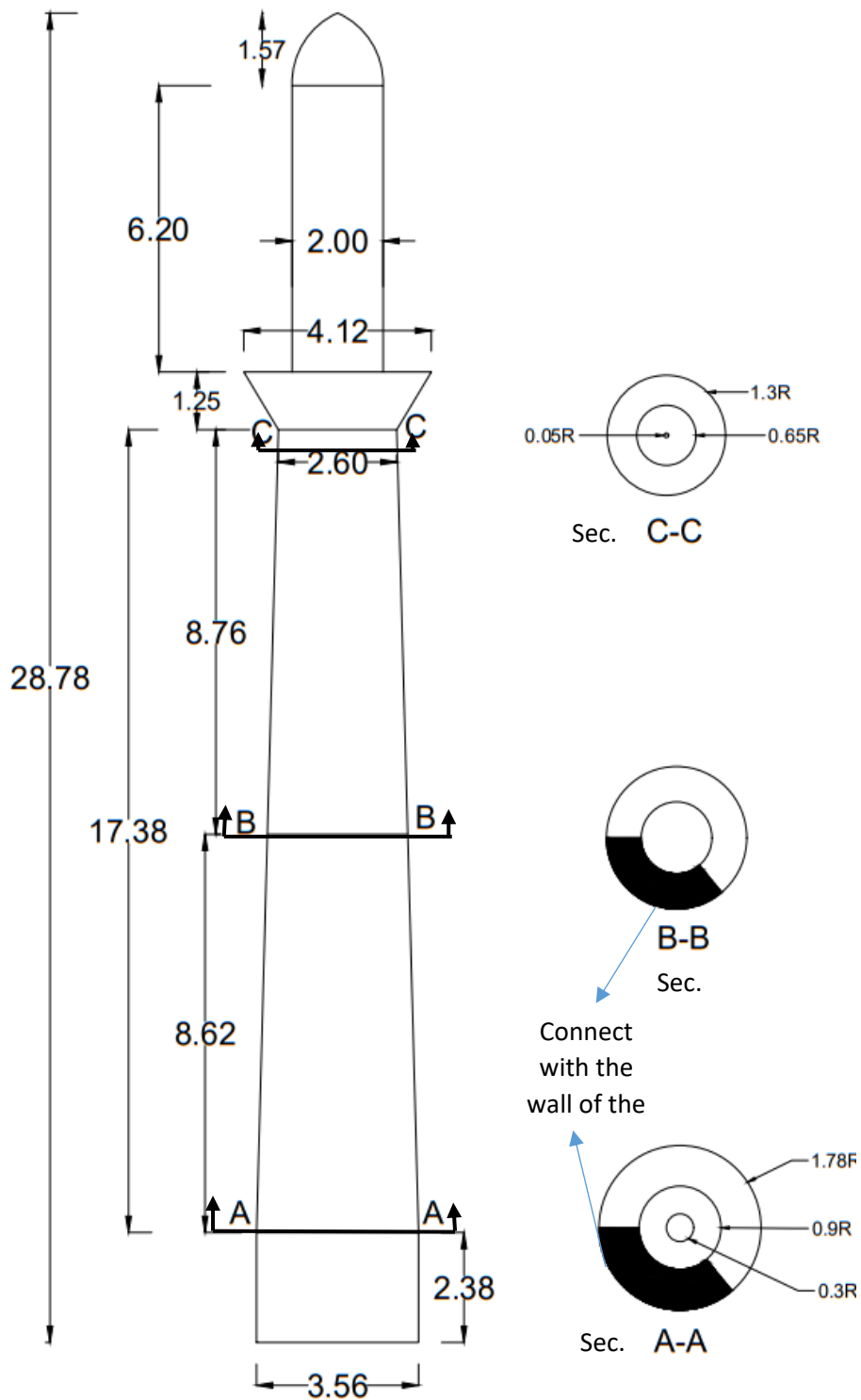


Figure (4.2) Dimensions of minaret (m)

The minaret has a stair inside from the base to the balcony, the stair is connected with the walls of the minaret's body and is connected from inner side by cone shape starting with 30 cm radius to and 5 cm near the balcony. This stair is made

from masonry bricks like the minaret. Each step is 0.6 m in length, 0.5 m in height and the width of each step is 0.15 m near the center and 0.4 m far of center and at the end of stairs it becomes 0.1 m near center and 0.3 m far of center.

### 4.3. Material Properties of Minaret Structure

The minaret is a historical building that was built of bricks and gypsum, and it contains from the inner side a stair supported from the bottom by wood structural elements. As for the outer side, it is covered with beautiful pieces of gold as shown in Figure (4.3).

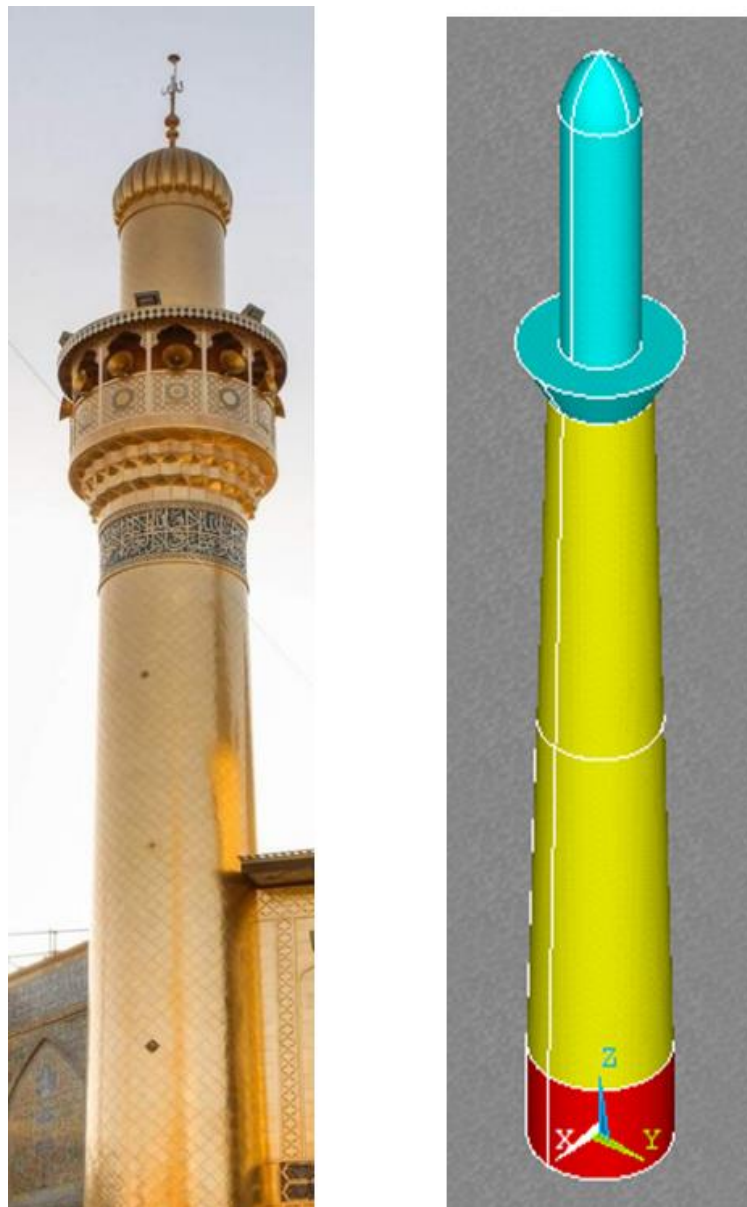


Figure (4.3) Real and ANSYS finite element model of minaret structure

The Modulus of Elasticity of the minaret were taken from a research conducted by **Khalifa and Al-Wazni (2021) [30]** and Poisson's Ratio assumed from [30] who carried out Experimental testing and made a comparison between historical and traditional masonry brick, where they tested masonry brick specimens. The mass density from [4]. They took it on site during the repairing of the structure and compared them with the properties of the materials currently available which were used using to fix damages. The values of the material properties for the historical brick prism model are adopted as listed in the Table (4.2).

Table (4.2) Material properties of adopted brick minaret model.

<b>Material properties</b>	<b>Values</b>
Modulus of Elasticity (MPa) [30]	$3.4 \times 10e3$
Mass Density (kg/m <sup>3</sup> ) [4]	$1.2 \times 10e3$
Poisson's Ratio [30]	0.2

#### **4.4. Finite Element Model Using ANSYS Software for Minaret Structure**

##### **4.4.1. Creating the model**

The finite element model of the minaret was done using the ANSYS program using the APDL method, where the model was drawn by using commands of ANSYS in an external file [31].

The CONE command was used to draw the cone shapes of the minaret (the body of the minaret, the balcony, the upper body and the base of the minaret) as shown in Figures (4.4) and (4.5).

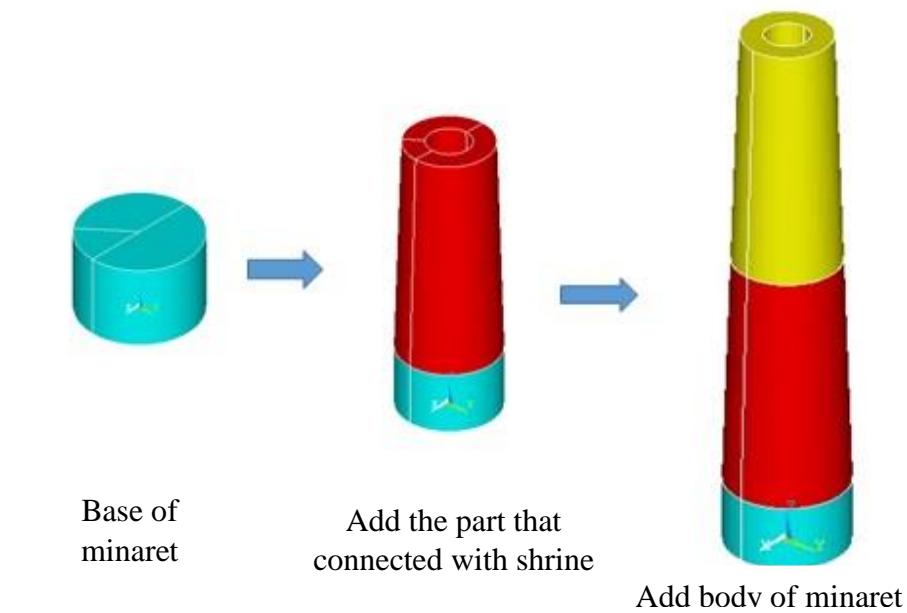


Figure (4.4) Finite element of the body of minaret structure

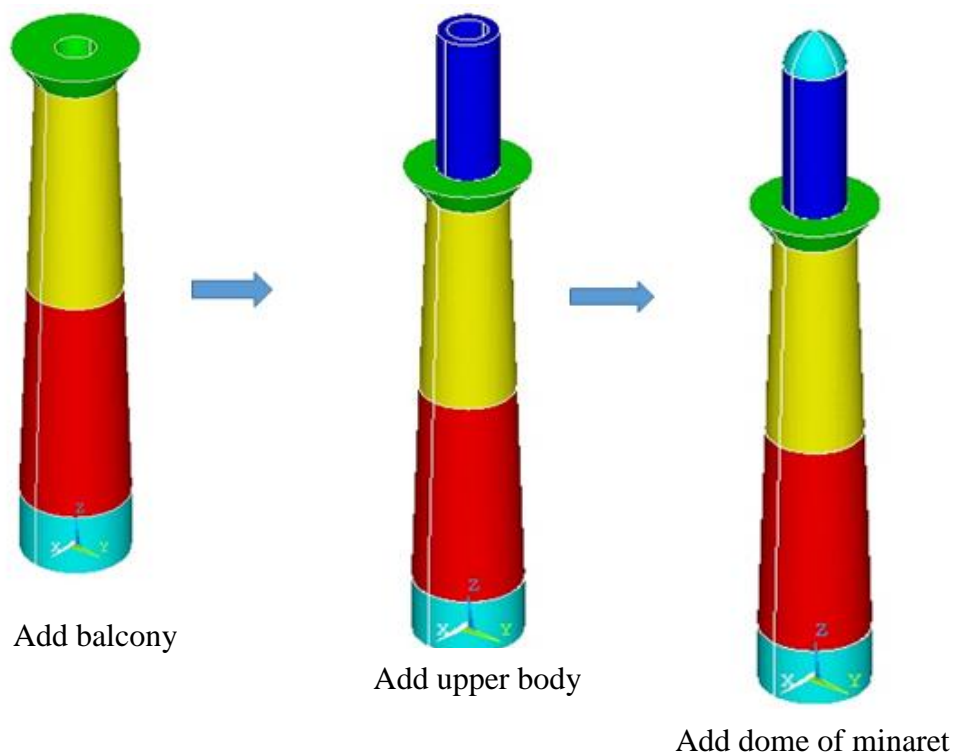


Figure (4.5) Finite element of the balcony and upper body of minaret structure

The dome was drawn by drawing key points and connecting them to draw an area shape for the dome's section and rotate it by using VROTAT command to depict the dome and attached to the minaret, as shown in Figure (4.6).

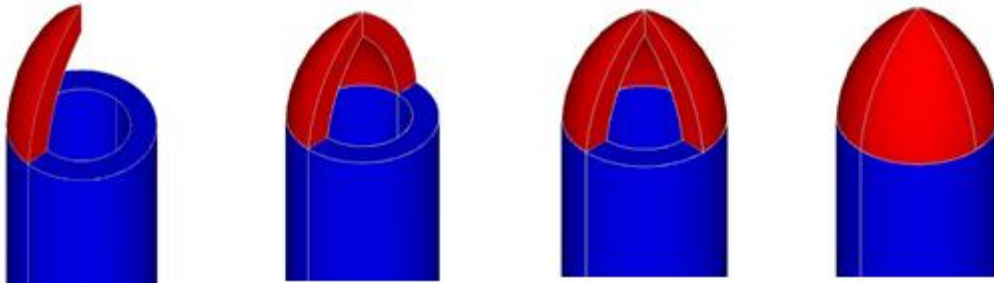


Figure (4.6) Steps to drawing parts dome

The stair were drawn by CYLIND command and in the form of graduated cylinder parts as close as possible to the real shape and connected to the minaret by using the Volumes Add (VADD) command, as shown in Figure (4.7).

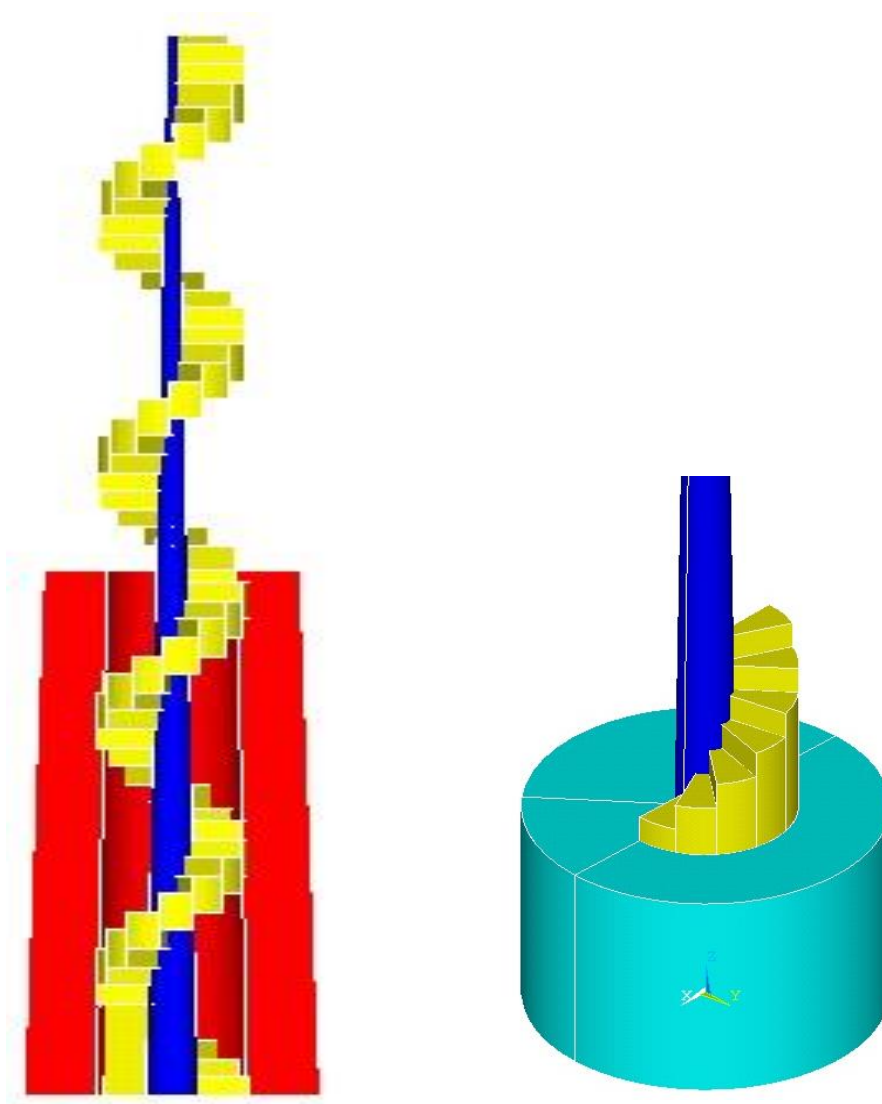


Figure (4.7) Steps to drawing stair of minaret

After completing drawing all the parts of the minaret, the parts were connected to each other and merged by using the VADD and Volumes Glue (VGLU) commands. The minaret is fixed from the bottom and connected to the base of the shrine, and the body of the minaret is fixed with the walls of the shrine, as shown in Figure (4.8). The boundary condition is simulated by fixed the area of that elements

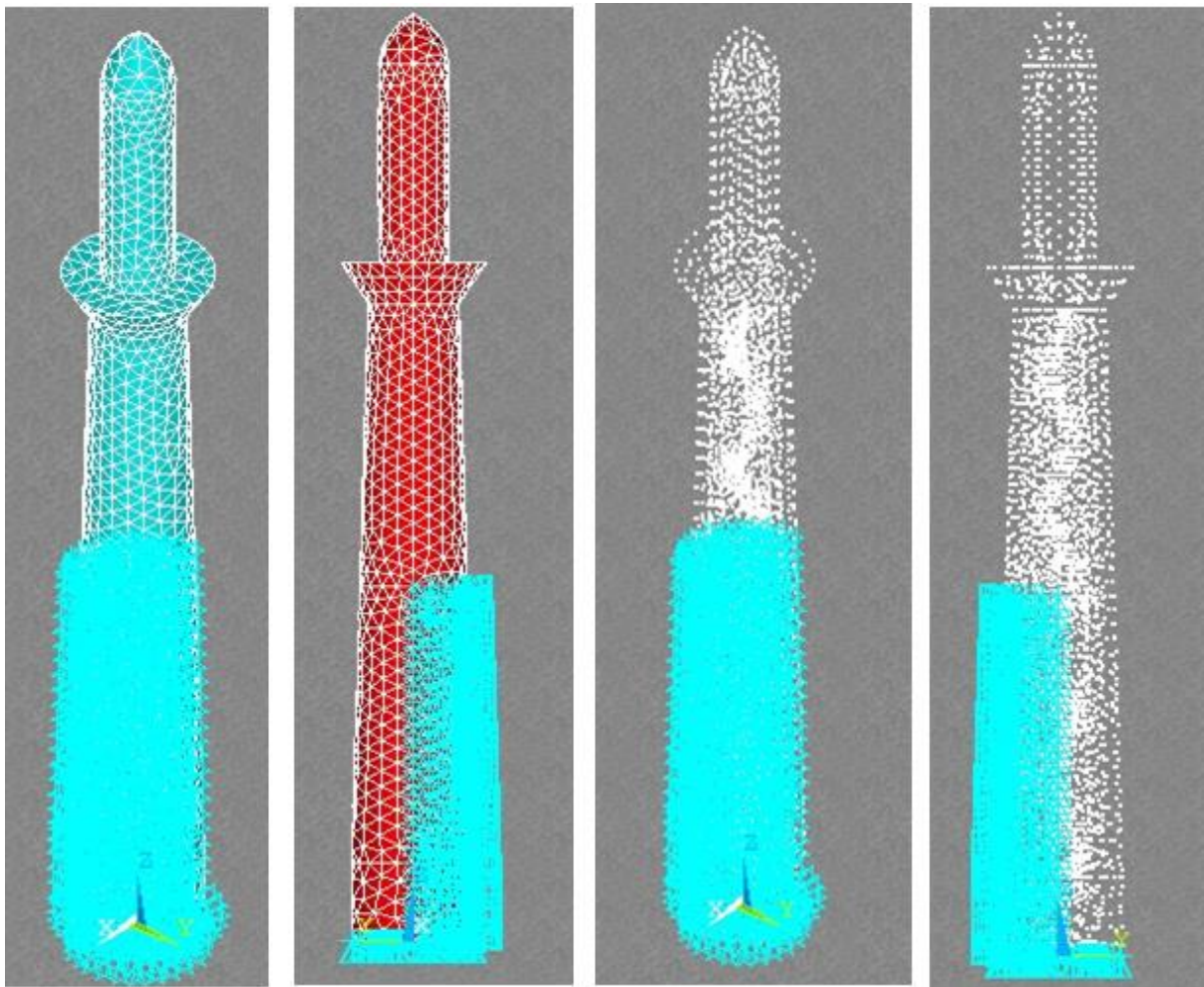


Figure (4.8) Fixed areas in minaret model

#### 4.4.2. Meshing of model

A free mesh has no specified pattern applied to it, and has no restrictions in terms of element shapes, but the mapped mesh is restricted in terms of the pattern of the mesh and the element shape it contains, for a mapped area mesh has only triangular or only quadrilateral elements as shown in Figure (4.9), for a mapped

volume it has only hexahedron elements. Also a mapped mesh typically has a regular pattern [32].

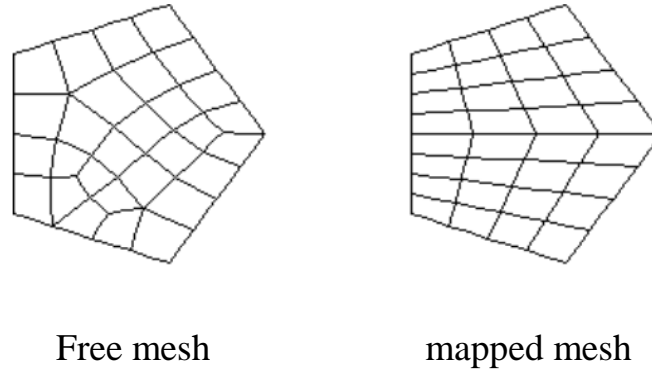


Figure (4.9) Difference between mapped mesh and free mesh [32]

There are more than one shape, for instance, area elements can be triangular and quadrilateral shaped within the same meshed area as shown in Figure (4.10). Volume elements can be hexahedral (brick) or tetrahedral shaped, but mixing them is not recommended [32].

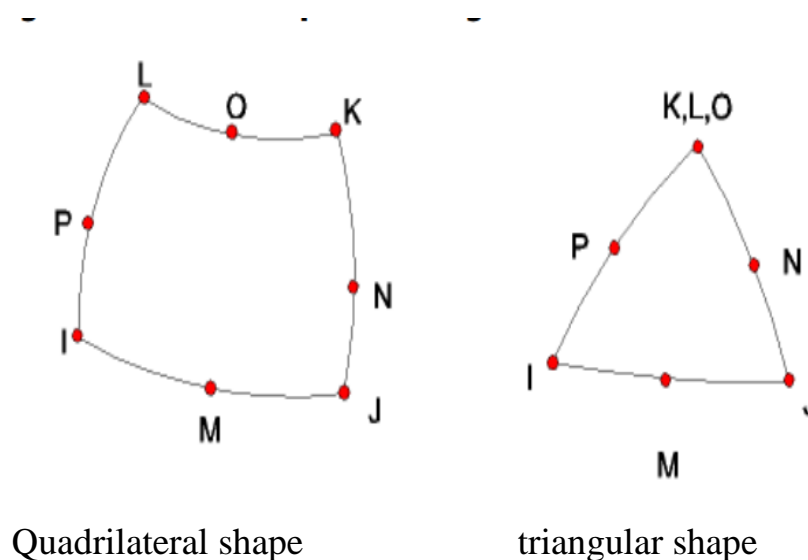


Figure (4.10) two type elements of mesh area [32]

There are many types of elements (**SOLID 200**, **SOLID 185**, **SOLID 45**, **SOLID 65** and etc.) in this study using element type **SOLID65** this type use for 3-D

modeling of solids with or without reinforcing bars (rebar). The solid is capable of cracking under tension and crushing in compression [33], Figure (4.11) shows types and geometry of element **SOLID65**.

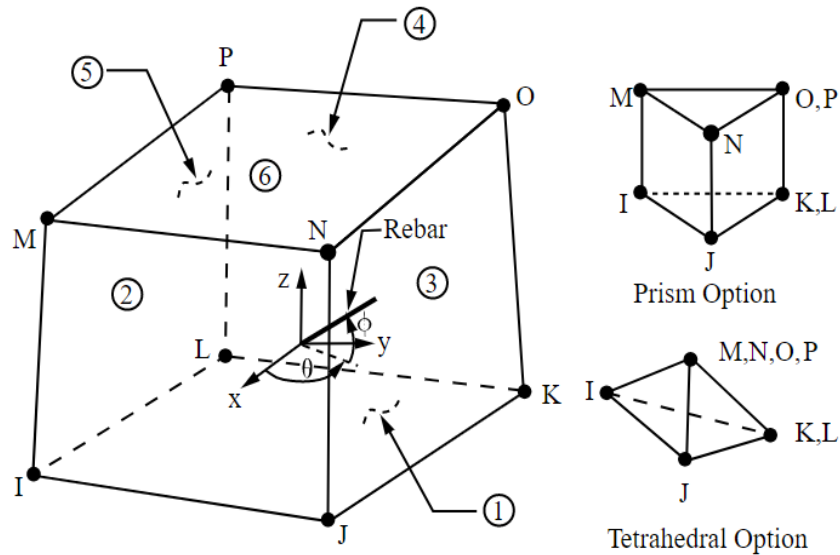


Figure (4.11) Types and geometry of element solid65 [33]

Since the minaret contains complex volumes such as (dome, balcony and round stair), hexahedral or prism elements cannot be used. Therefore, tetrahedral elements were used in the meshing process. Also, because of the complex shapes, it is difficult to use mapped mesh, the free mesh method was used. Figure (4.12) shows tetrahedral element in ANSYS software and its geometry.

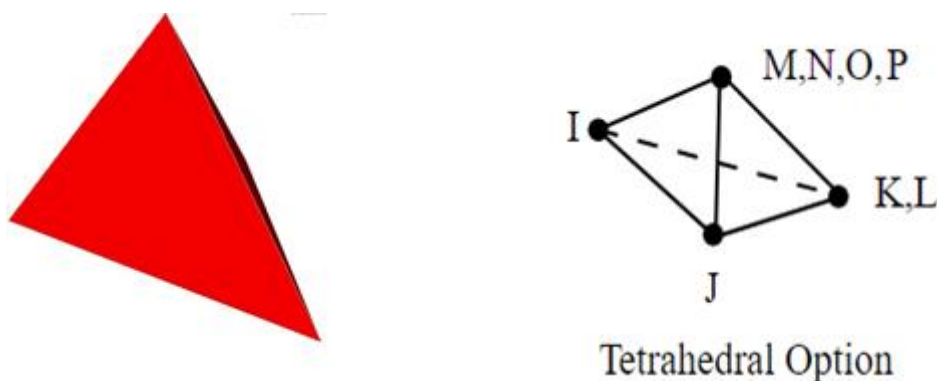


Figure (4.12) Geometry of tetrahedral element

After completing the selection of the type of element, a free mesh was made for the minaret, and the mesh size selected is 500 mm. The results were as in the Figure (4.13), which shows the elements of the minaret and the minaret nodes.

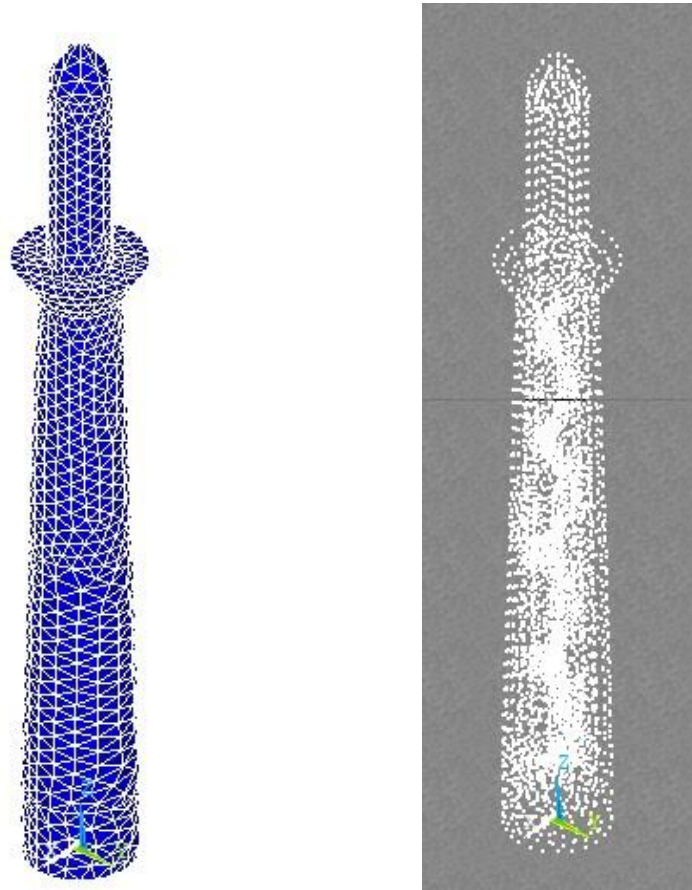


Figure (4.13) Elements and nodes of minaret

Table (4.3) shows the type, shape, number of elements and number of nodes for this study.

Table (4.3). Finite element properties of adopted brick minaret model

Type of Element	Solied65
Shape of Element	Tetrahedral
Number of Elements	21685
Number of Nodes	5425

In this research, two types of analysis for the FE structural minaret model, static and modal (dynamic) analysis were taken. Static analysis was conducted to investigate the structural static behavior of the model. Modal analysis was implemented to extract the dynamic properties of the model, natural frequency and mode shape, which are used in the proposed SHM technique in this study.

#### 4.5. Static analysis of FE minaret model

The nonlinear static analysis for the FE minaret model was done by using ANSYS software, the details of the model, geometry, element type, material properties, material modeling, meshing size and boundary conditions were fed by importing external text file using APDL technique in ANSYS analyzer. The results of the FE analysis were displayed using the GUI technique to evaluate the model. The static analysis was done to investigate the distribution of internal forces and stresses under structural loads, also the cracks and maximum displacement locations. The adopted nonlinear material modeling of the FE model in ANSYS is Multilinear Isotropic Hardening (MISO) and the compressive stress-strain curve for MISO material modeling of prism masonry is extracted experimentally from a research conducted by **Khalifa and Al-Wazni (2021) [30]**, as shown in Figure (4.14) and listed in Table (4.4).

Table (4.4) stress-strain points

Strain (mm/mm)	Stress (MPa)
5.88235E-05	0.2
0.0001183	0.4
0.0001845	0.6
0.0002535	0.8
0.0003576	1.1

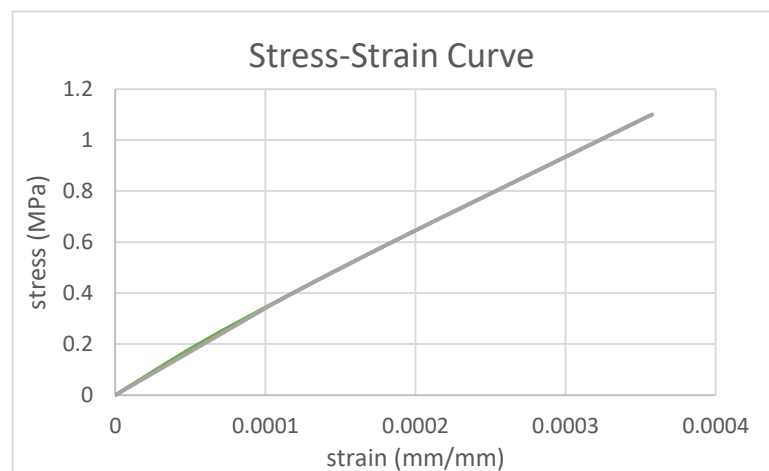


Figure (4.14) Compressive stress-strain curve for prism masonry extracted experimentally [30]

The material properties of the model, mass density, modulus of elasticity and Poisson's ratio, are  $1200 \text{ kg/m}^3$ ,  $3400 \text{ MPa}$  and  $0.2$ , respectively. In the nonlinear static analysis, gravity load was calculated automatically in ANSYS procedures using gravitational acceleration of  $9.81 \text{ m/sec}^2$  and the data necessary for the analysis were adopted from the previous researches [4] as listed in Table (4.5). The load divided as loading steps with the input data, each loading step consists of smaller increment to represent the nonlinear solution path. The increment size required to be assumed as much as small percent of the applied load through the steps to ensure that the elastic limit has not been overstepped. In this research the initial used increment size was 5% of the maximum applied load then ANSYS analyzer automatically increases increment.

Table (4.5) inputs for nonlinear static analysis for the FE minaret model

Discription	Value
Nonlinear material modeling	(MISO)
Modulus of elasticity (MPa)	3400
Mass density ( $\text{kg/m}^3$ )	1200
Poisson's ratio	0.2
Gravitational acceleration ( $\text{m/sec}^2$ )	9.81
The increment size required	5%
Applied load ( $\text{kN/m}^2$ )	2
Location of applied load [4]	On balcony
Open shear transfer coefficient (N/A) [4]	0.25
Closed shear transfer coefficient (N/A) [4]	0.75
Uniaxial cracking (tensile) stress (MPa) [4]	0.22
Uniaxial crushing (compressive) stress (MPa) [4]	5.8
Tensile cracking factor (N/A) [4]	0.6

The boundary condition of FE model of the minaret used in the analysis was mentioned in **paragraph (4.4.1)** where the base of the minaret is fixed with the base of the shrine and part of the body of the minaret is fixed with the walls of the shrine. The results for maximum displacement in the minaret model after executing the FE nonlinear static analysis are displayed in Figure (4.15). From Figure (4.15) the maximum transverse displacement in x and y direction are 0.538

mm and 1.097 mm, respectively, at the top of the minaret. The maximum vertical displacement in z direction is -0.525 mm at the top. While, the displacement vector at the top of the minaret is 1.306 mm, as shown in the Figure (4.15).

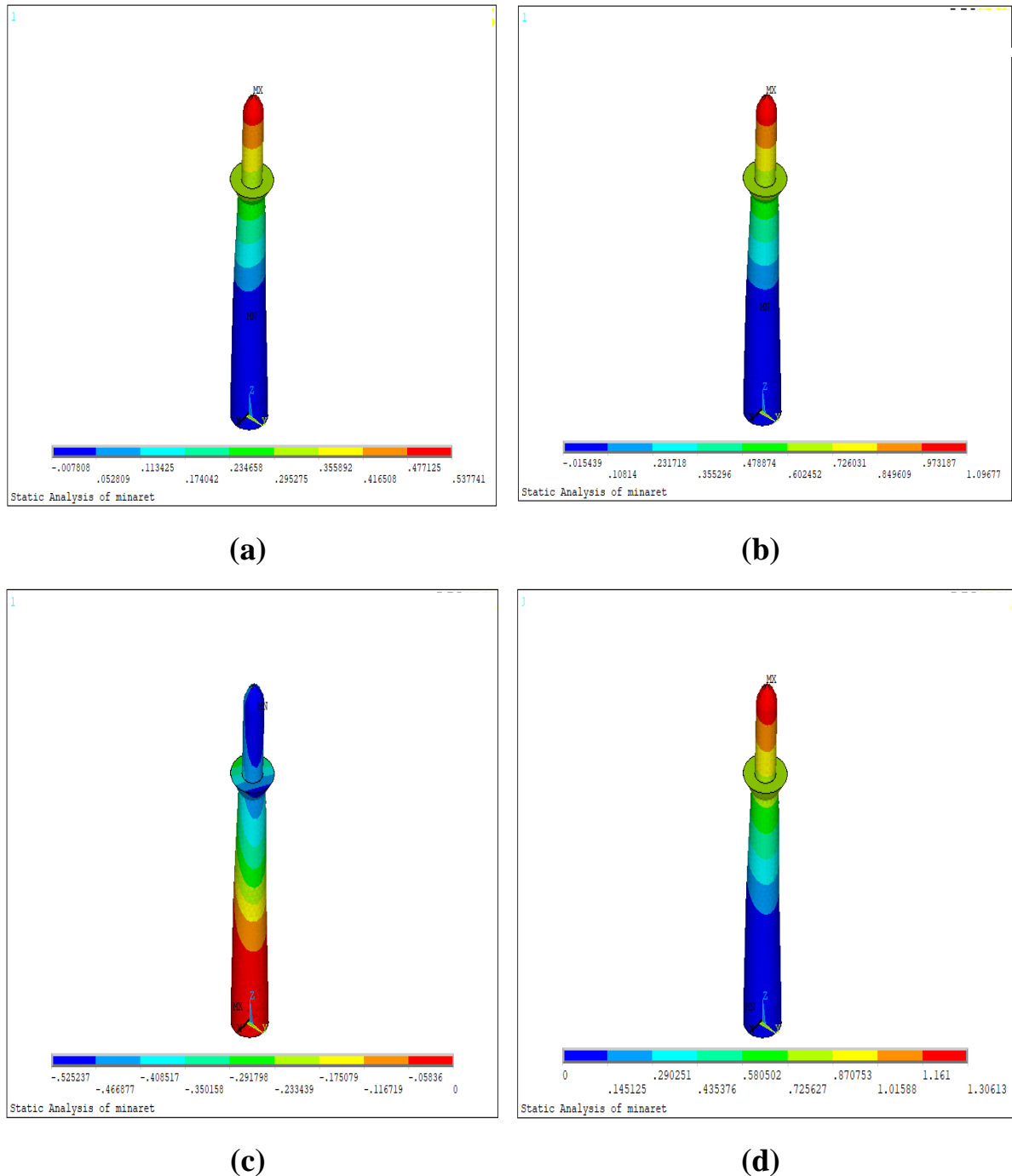


Figure (4.15) (a) and (b) transverse displacement in x and y direction, respectively, (c) vertical displacement in z direction and (d) displacement vector of the minaret model

The results of the von Mises stresses is shown in Figure (4.16). The maximum von Mises stress is 0.336 MPa in the middle area of the minaret between fixed walls and the free part of the minaret.

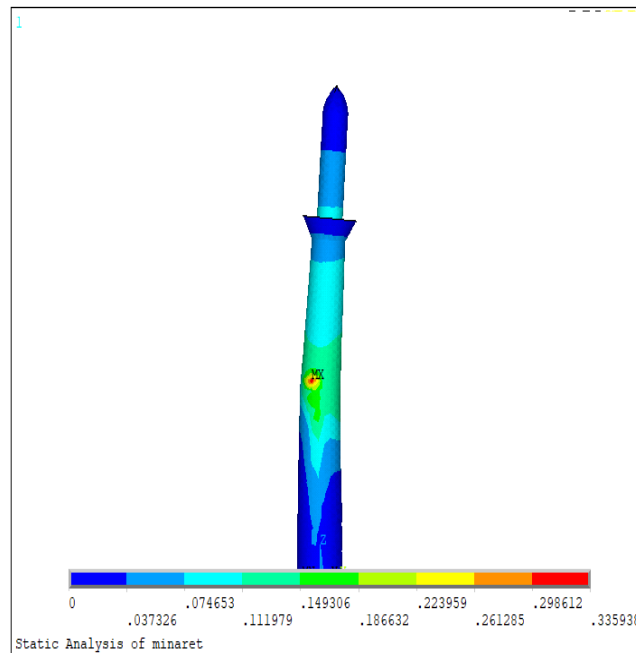


Figure (4.16) Von Mises stress of minaret

The location of cracks in the FE minaret model is shown in the Figure (4.17). The figure displays the cracks pattern in tension face at the same region of maximum stresses.

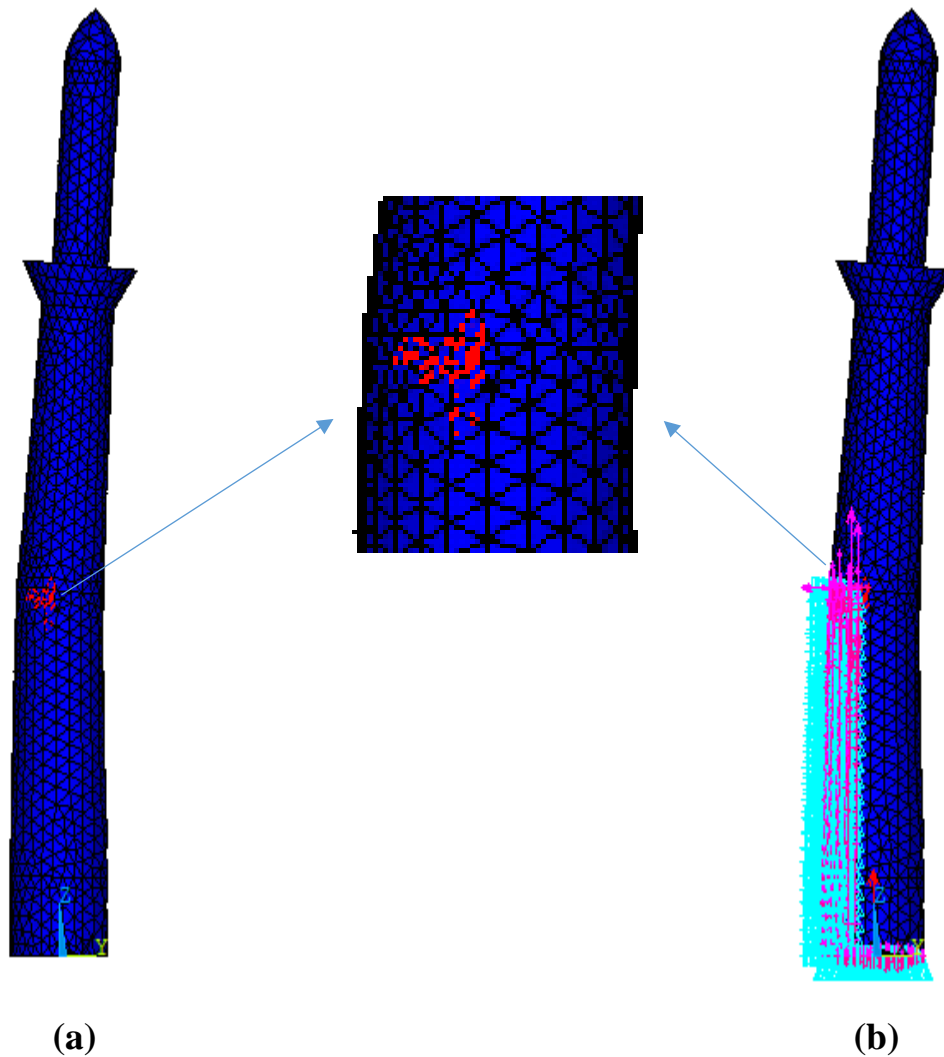


Figure (4.17) Location of cracks in FE minaret model under maximum load

From the nonlinear static analysis, it could be noticed that was acceptable agreement between the FE model and real structure of the minaret. Also, it was observed during loading steps that the places where cracks appeared were the same as structural behavior of the minaret model.

#### 4.6. Modal analysis of FE minaret model

The modal analysis is a linear dynamic analysis that extracts the dynamic properties for structures, natural frequencies and mode shapes. The modal analysis for the minaret model was done by ANSYS software [34], block Lanczos

method, where the block Lanczos method uses the sparse matrix solver. When looking for eigenfrequencies in a specific region of the eigenvalue spectrum of a given system, the block Lanczos approach is particularly effective. When modes at the midrange and higher end of the spectrum are extracted, the eigenfrequencies will converge at roughly the same pace as when the lowest modes are extracted [35].

The boundary condition of FE model of the minaret used in the analysis was mentioned in **paragraph (4.4.1)** where the base of the minaret is fixed with the base of the shrine and part of the body of the minaret is fixed with the walls of the shrine.

The modal analysis method using block lanczos method does not require applied loads on the structure, only the loads of structure itself defined by modulus of elasticity and mass density.

To select the number of modes that have more effect and Investigation and Parametric Study of adopted minaret under vibration loading to determine the effect changing modulus of elasticity and mass density and geometry on modal properties of minaret ( natural frequencies and mode shapes). The element type was SOLID65 with tetrahedral element shape.

#### **4.6.1. Selection the size of mesh**

Convergence analysis is used to mesh the structural model of the minaret with the proper mesh size, providing precise interpretation of the FE model data. Due of this, five different mesh sizes of 100 mm, 200 mm, 300 mm, 400 mm, and 500 mm each were chosen to represent fine, moderate, and coarse mesh. The convergence study uses the initial natural frequency value that was retrieved for each type of mesh, and the outcomes are shown in Table (4.6).

Table (4.6). Effect of mesh size on elements number and first natural frequency value

Mesh Size (mm)	1st Natural Frequency Value (Hz)	Number of Elements
100	3.32601	1272065
200	3.35496	185946
300	3.37756	76919
400	3.42158	30747
500	3.44881	21685

Figure (4.18) shows the mesh size of the FE model's convergence results, and Figure (4.19) shows the natural frequency value of the first mode with the number of elements according to mesh size. The chart clearly shows that the natural frequency value gradually grew as the mesh size increased with little influence. In order to produce more precise results, the FE model of the minaret is employed in this parametric study and for determine the effective modes with a mesh size of 200 mm. but for SHM technique in this study was used size mesh is 500 mm because the small size is need long time and strong computers to give result when connected with PSO method in MATLAB software.

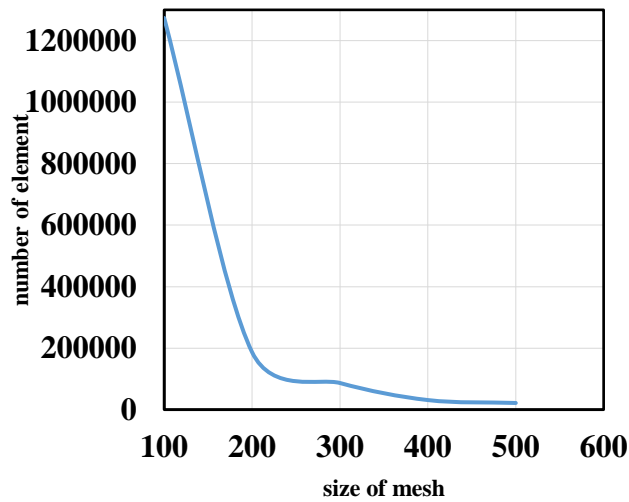


Figure (4.18) Convergence of mesh size

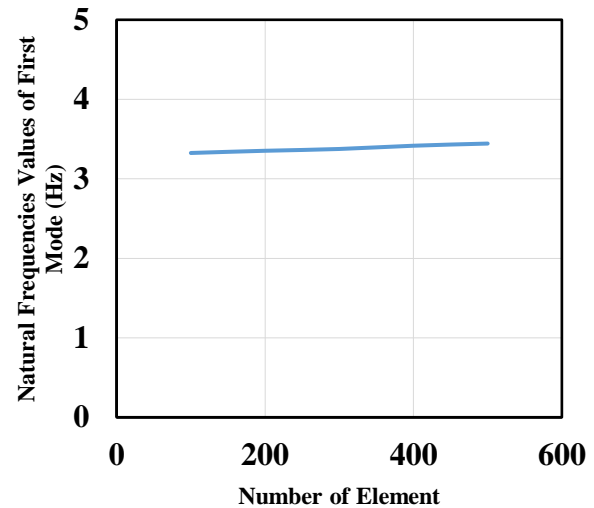


Figure (4.19) Natural frequency value of first mode with different mesh size

#### 4.6.2. Selection the effective modes

The cumulative mass fraction for modes shown in Table (4.7) and (4.8) the difference between modes under the 7th mode is very small and the values is near and less effect so first seven modes adopted in this study.

Table (4.7) mass participation of modes in x direction

Mode number	Frequenc y (Hz)	Period (s)	Ratio	Cumulative mass fraction
1	3.35271	0.29827	0.002329	3.21E-06
2	3.48842	0.28666	1	0.591575
3	11.5877	8.63E-02	0.00132	0.591576
4	11.9033	8.40E-02	0.649449	0.841092
5	21.0542	4.75E-02	0.032293	0.841709
6	27.4137	3.65E-02	0.002025	0.841711
7	29.1597	3.43E-02	0.517275	1

Table (4.8) mass participation of modes in y direction

<b>Mode number</b>	<b>Frequenc y (Hz)</b>	<b>Period (s)</b>	<b>Ratio</b>	<b>Cumulative mass fraction</b>
1	3.35271	0.29827	1	0.651413
2	3.48842	0.28666	0.002313	0.651416
3	11.5877	8.63E-02	0.632758	0.912231
4	11.9033	8.40E-02	0.001337	0.912232
5	21.0542	4.75E-02	0.000033	0.912232
6	27.4137	3.65E-02	0.367029	0.999984
7	29.1597	3.43E-02	0.004927	1

The Table (4.9) show the natural frequencies and modes characteristic for first seven mode.

Table (4.9) Natural frequencies values and modes characteristic with size of mesh (200)

<b>Mode No.</b>	<b>Natural Frequency (Hz)</b>	<b>Mode characteristic</b>
1	3.35271	1st bending in X direction
2	3.48842	1st bending in Y direction
3	11.58770	2nd bending in X direction
4	11.90330	2nd bending in Y direction
5	21.05420	Torsion about Z direction
6	27.41370	3rd bending in Y direction
7	29.15970	3rd bending in X direction

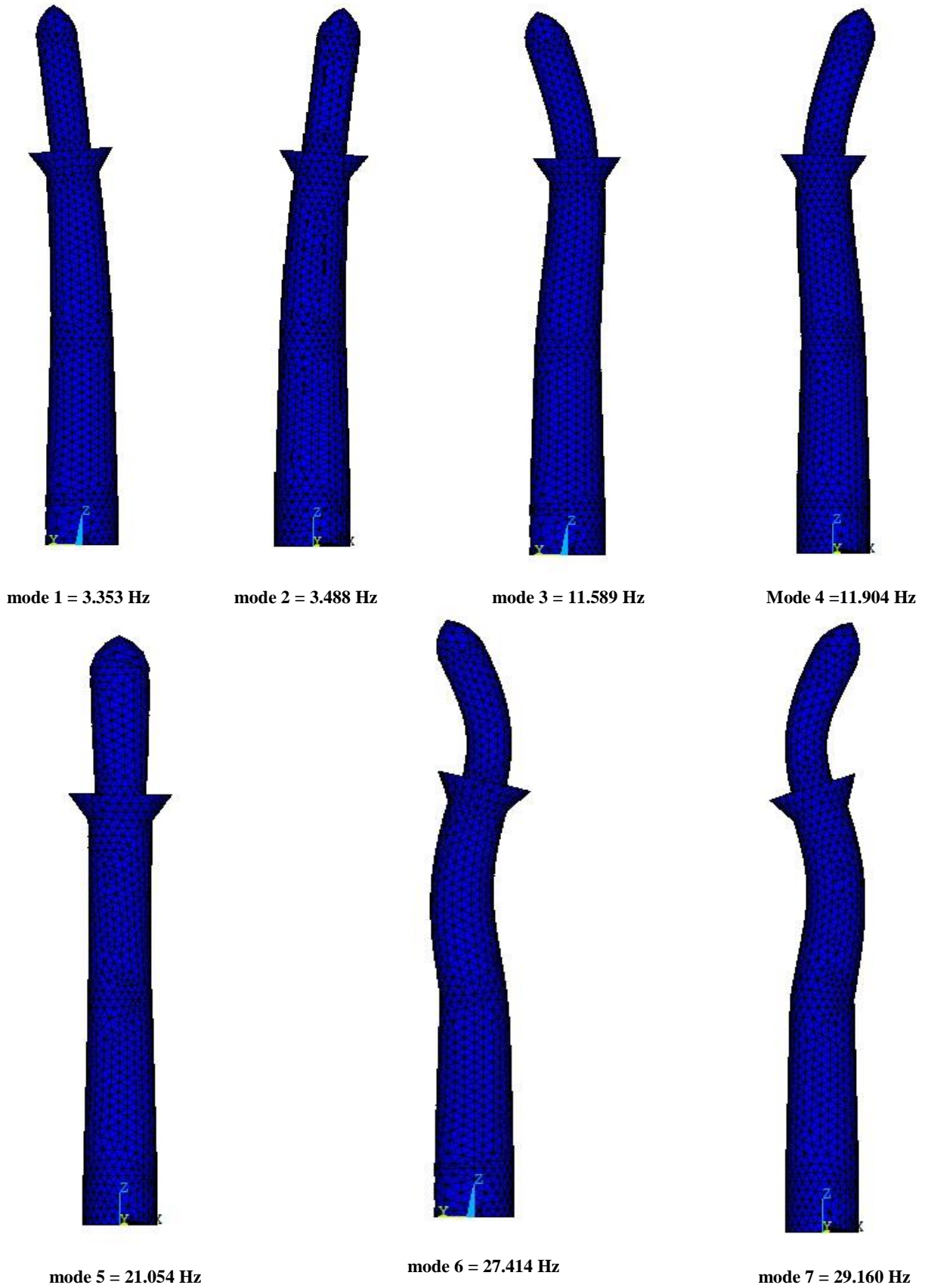


Figure (4.20) Extracted mode shapes of adopted brick minaret structure

#### **4.7. Parametric Study of FE Minaret Model Under Modal Analysis**

In this work, four parameters representing material qualities, including modules of elasticity and mass density, were investigated. Additionally, the impact of geometry properties, such minaret height and radius, was considered. Where, the presence of cracks in a structure will reduce the structural stiffness. So, the reducing value of modules of elasticity or mass density for elements can represent the reduction in stiffness of the structure [36]. Therefore, this paper adopts parametric study to investigate the parameters which have high sensitivity on changing of the dynamic properties of structure.

Two parameters are modulus of elasticity and mass density were taken with a change rate of  $\pm 5\%$ . Parametric study was made for the change of parameters to determine which of the two parameters has the most effect on the natural frequencies values. The geometric parameters of the minaret structural model, the height and diameter, are also studied to get information about the structural behavior which is very important for dynamic analysis and design for future projects. The change of parameters are 2 m in height and 5% of diameter. The extracted results are the effects of those four parameters on the first, third, fifth and sixth natural frequencies values [36].

##### **4.7.1. Changing Modules of Elasticity**

Five values for Modulus of Elasticity (E) were selected to study the effect on the natural frequency. The extracted natural frequencies values of first, third, fifth and sixth modes for each value for Modules of Elasticity are listed in Table (4.10).

Table (4.10) Natural frequencies values with changing Modules of Elasticity

E (MPa)	Reference				
	3.06E+03	3.23E+03	3.4E+03	3.57E+03	3.74E+03
Set	Natural Frequency (Hz)				
1	3.181	3.268	3.353	3.436	3.516
3	10.993	11.295	11.589	11.875	12.154
5	19.974	20.521	21.054	21.574	22.082
6	26.007	26.720	27.414	28.091	28.752

All values of natural frequencies for the four modes are plotted in Figure (4.21), the positive relationship between natural frequencies values and Modulus of Elasticity of all modes. The first mode was little affected with increasing Modulus of Elasticity which has difference in natural frequency value 0.335 Hz. In the third mode the effect is increased, and the difference was 1.161 Hz, while the difference in the fifth and sixth modes was significant high of 2.108 Hz and 2.745 Hz respectively.

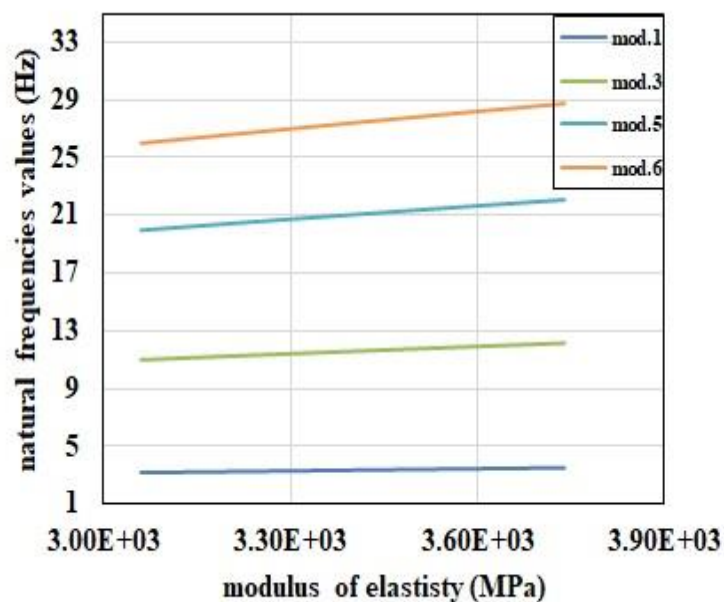


Figure (4.21) Natural frequency value versus Modulus of Elasticity

### 4.7.2. Changing Mass Density

In this parameter, five values of Mass Density (MD) was selected by range of  $(1.08-1.32) \times 10^3 \text{ kg/m}^3$  with percent of change value of 5%. Also, the four natural frequencies values (first, third, fifth and sixth) are adopted to investigate the effect of mass density value on the natural frequency, as listed in Table (4.11).

Table (4.11) Natural frequency values with changing mass density

MD (kg/m <sup>3</sup> )	Reference				
	1.08E+03	1.14E+03	1.2E+03	1.26E+03	1.32E+03
Set	Natural Frequency (Hz)				
1	3.534	3.44	3.353	3.272	3.197
3	12.216	11.89	11.589	11.309	11.049
5	22.193	21.601	21.054	20.547	20.075
6	28.897	28.126	27.414	26.753	26.138

From Figure (4.22) the relationship is decreasing between them. The four modes have decreasing ratio percent of 9.5% with change mass density.

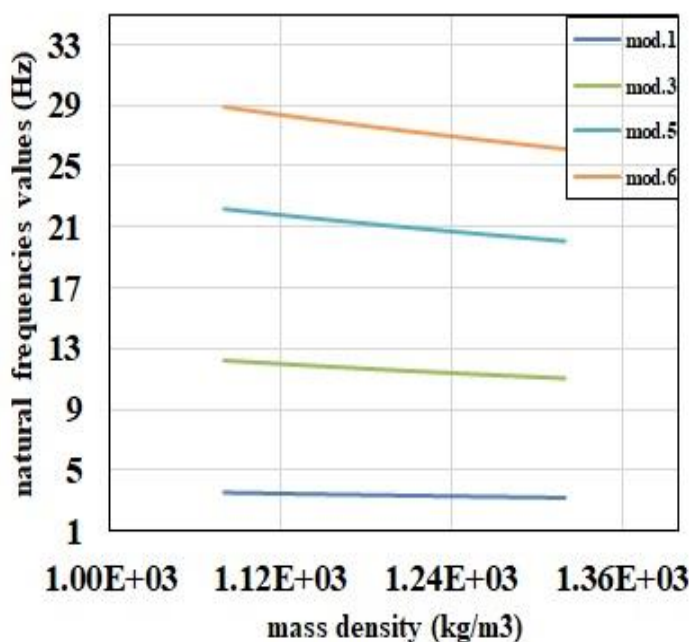


Figure (4.22) Natural frequency value versus mass density

### 4.7.3. Changing Height of Minaret

Four different value of minaret height were adopted in the parametric study with the real minaret height of 28.78m. The changing rate value was  $\pm 2$ m in each step increasing and decreasing of the real height. The natural frequencies values of first, third, fifth and sixth modes are listed in Table (4.12).

Table (4.12) Natural frequencies values with changing height of minaret

Height (m)	Reference				
	24.78	26.78	28.78	30.78	32.78
Set	Natural Frequency (Hz)				
1	4.426	3.836	3.353	2.953	2.623
3	14.923	13.109	11.589	10.309	9.23
5	24.482	22.645	21.054	19.676	18.475
6	32.602	29.977	27.414	24.938	22.663

The natural frequencies values of first, third, fifth and sixth mode with different minaret heights plotted in Figure (4.23). The x-axis represents the ratio of minaret height to the outer radius of minaret which is 1.78 m. The relationship is decreasing between them and the decrease in natural frequencies values has nonlinear behavior. The effect of height on natural frequency value of first mode has difference of 1.803 Hz, while in third mode the effect on natural frequency value is increased in difference of 5.693 Hz, whereas in fifth and sixth mode the effect is higher and the difference in natural frequency value is 6 Hz and 9.9 Hz respectively. As a difference ratio percent, the first natural frequency has significant effect during change the minaret height.

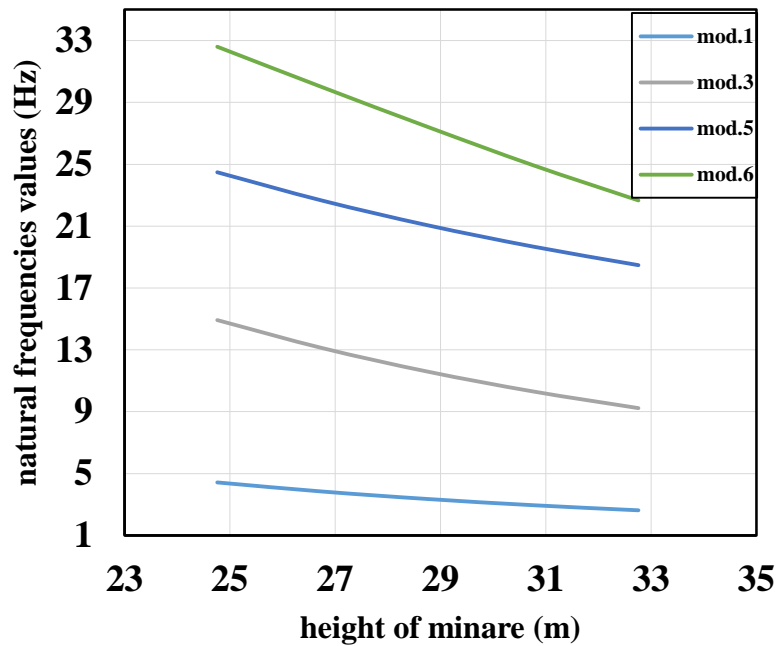


Figure (4.23) Changing natural frequency with height of minaret

#### 4.7.4. Changing Radius of Minaret

Four values of minaret outer base radius were selected in this study with a real outer base radius of 1.78 m with change value of 5%. The natural frequencies values of first, third, fifth and sixth modes with outer base radius of minaret are listed in Table (4.13).

Table (4.13) Natural frequencies values versus minaret radius

<b>Outer Radius / Inner Radius</b>	1.602/0.9	1.691/0.9	1.78/0.9	1.869/0.9	1.958/0.9
<b>Set</b>	<b>Natural Frequency (Hz)</b>				
1	3.42	3.592	3.353	3.3735	3.413
3	9.902	11.056	11.589	12.241	12.852

5	21.724	22.498	21.054	20.755	20.487
6	25.711	27.194	27.414	27.468	27.213

The natural frequency value of first, third, fifth and sixth modes with changing the ratio ( outer radius to inner radius) is shown in figure 10. It is obvious from figure 10, there is inverse behavior for natural frequencies value during changing thickness of minaret for four selected modes. The first natural frequency has slowly difference ratio percent of 4.79% to quarter value of minaret thickness and then it decreases to -6.6% and in end increases to 1.7%. However, the third natural frequency has difference ratio percent of 22.9%. For the fifth natural frequency, the difference ratio percent is 3.44% and then it decreases significantly to -8.93%. For sixth natural frequency the difference ratio percent is 6.4% and then it decreases significantly to -0.93%

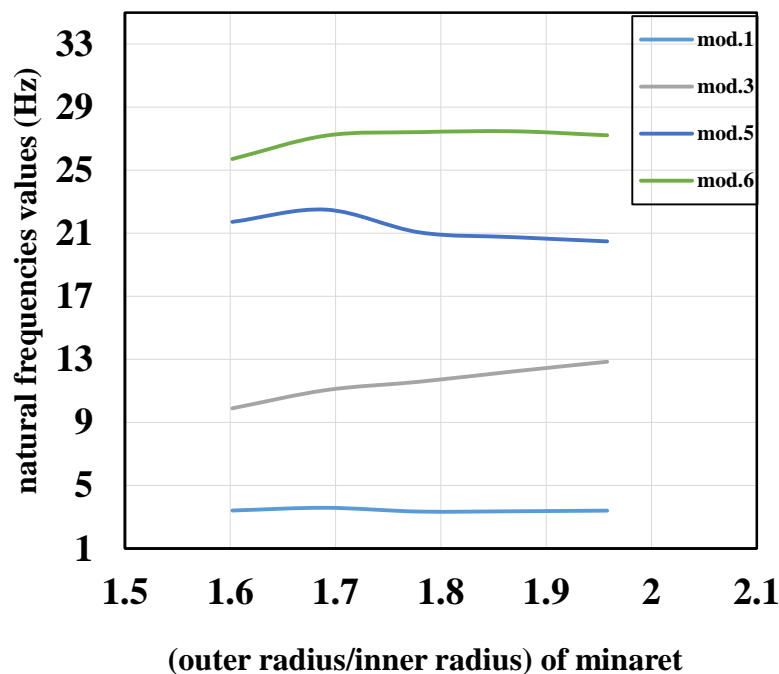


Figure (4.24) Changing natural frequency with base outer radius of minaret

From Figure (4.24) and (4.23), the effect of changing in height is more than changing in outer radius and thickness of wall. As the natural frequency is decreased with increased in ratio (height/outer radius) of minaret. Since, the natural frequency of a structure depends on geometry, mass and material properties. The variation of natural frequency values of a structure is very important in the analysis and design to not be coincide with excitation force frequency and causes resonance phenomena in the structure. The resonance causes to magnify the displacement in the structure then yields the failure.

After determine the size of mesh, effective modes and parametric study, the effective modulus of elasticity was adopted to present the damage in SHM technique. The Table (4.14) show Natural frequencies values and modes characteristic with size of mesh (500 mm) to use in SHM technique.

Table (4.14) Natural frequencies values and modes characteristic with size of mesh (500 mm)

Mode No.	Natural Frequency (Hz)	Mode characteristic
1	3.393412268913	1st bending in X direction
2	3.479856104073	1st bending in Y direction
3	11.91664111322	2nd bending in X direction
4	12.16794926303	2nd bending in Y direction
5	21.34992632022	Torsion about Z direction
6	27.17613329720	3rd bending in Y direction
7	29.13207558374	3rd bending in X direction

As shown in Table (4.14), the first seven modes of character are: torsion for mode 5, first bending for modes 1 and 2 in x and y-direction, second bending for modes

3 and 4 in x and y-direction, and third bending for modes 6 and 7 in x and y-direction. The Figure (4.25) show natural frequencies periods for first seven mode

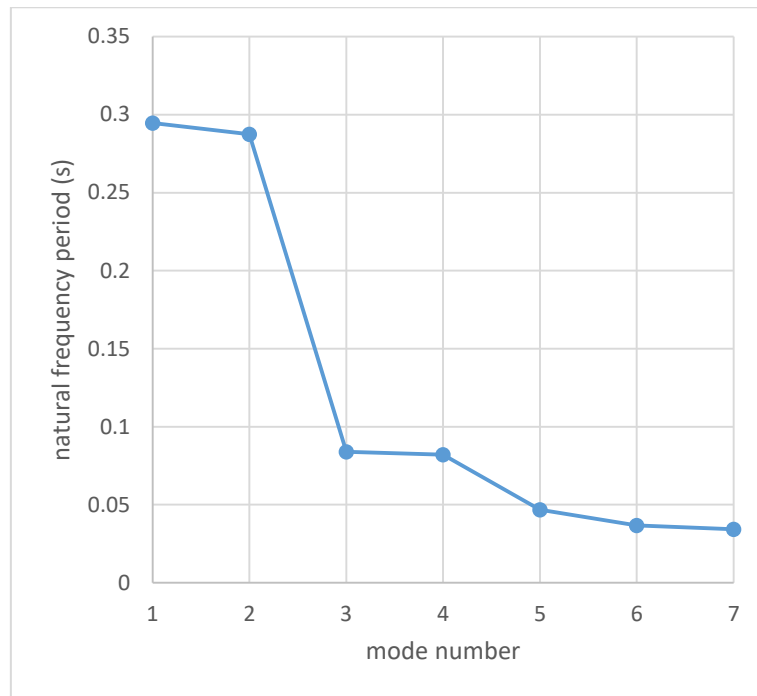


Figure (4.25) Natural frequency period of each mode

# CHAPTER FIVE

## CHAPTER FIVE

### Proposed Structural Health Monitoring Technique of Imam Ali Structure and Verifications

#### 5.1. General

It has been mentioned that structural health monitoring is one of the important techniques for nondestructive testing of structures and for giving a periodic report on their integrity. In this chapter, it is clarified how to do structural health monitoring of the minaret of the Imam Ali shrine structure. Otherwise, it was not possible to carry out experimental modal analysis using sensors techniques with data collection device on the real structure due to administrative and security reasons related to the shrine of Imam Ali and for lack of capabilities of conducting such testing at the present time for this structure. Therefore, this technique has been adopted from a numerical representation of the minaret by depicting a scenario damage of the minaret using ANSYS and MATLAB software, as well as using one of the modern optimization methods, which is the particle swarm method to detect the damage.

#### 5.2. Adopted Proposed Technique for SHM

The structural health monitoring demands comparing between two stages of the system (as explained in **paragraph 2.2.**). First dynamic properties (natural frequency and mode shapes) have been extracted for experimental analysis (in this study was using Scenario) by ANSYS software and compared with the dynamic properties suggested by numerical analysis for finite element model by using PSO method in MATLAB software [37]. When there is convergence, it continues and extracts the optimum location and optimum percentage of damage, and if not, it re-updates the value of the modulus of elasticity and creates a new damage location and new damage percentage, and the process continues until there is a convergence of damage location and damage percentage updated with

the location of damage and the percentage of damage in Scenario the Figure (5.1) shows general chart of SHM technique.

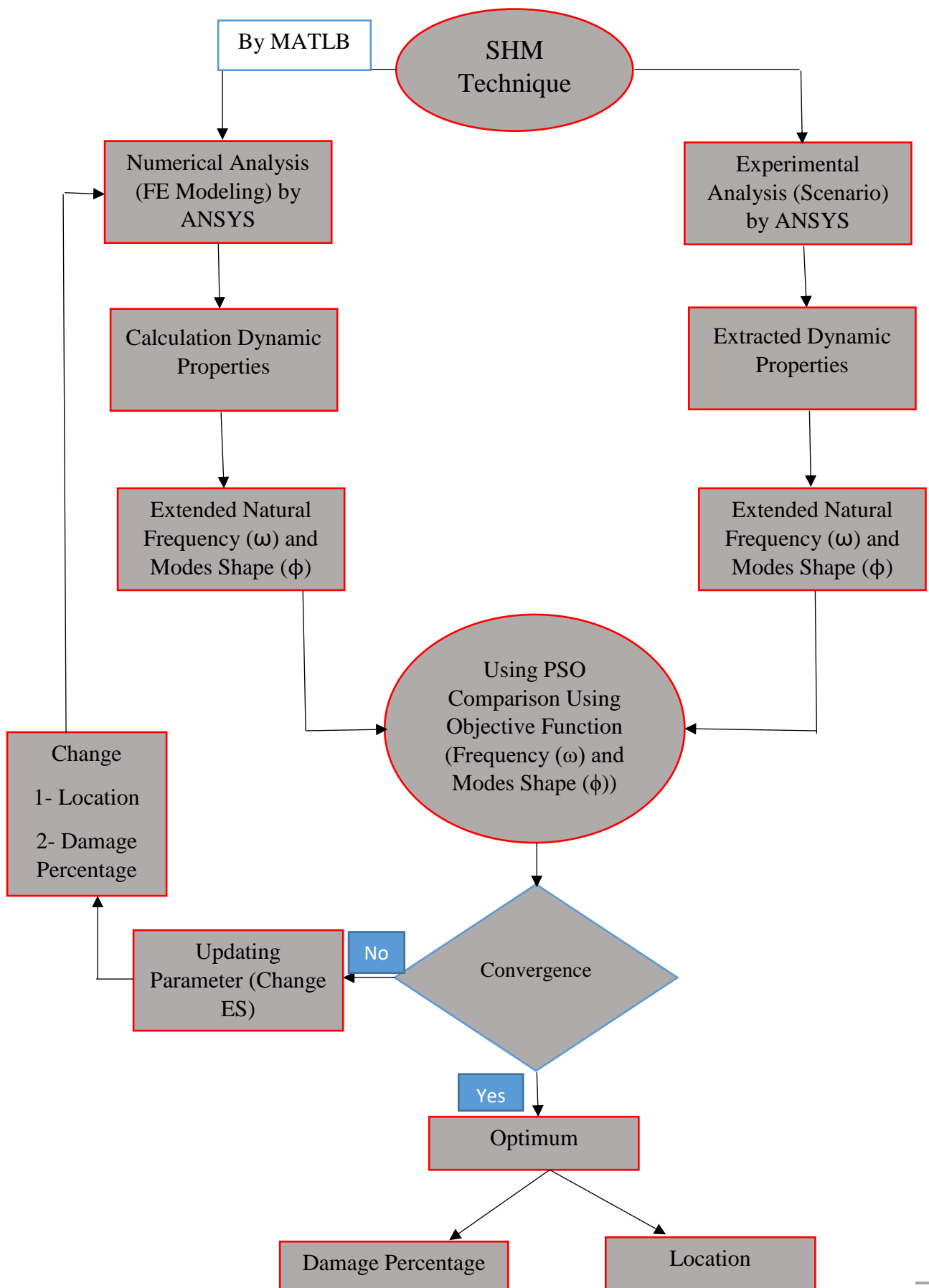


Figure (5.1) General chart of SHM technique

### 5.3. Representing Damage in Proposed SHM technique

A scenario file has been created using APDL commands, where when a crack occurs in a specific part of the minaret it causes a decrease in the stiffness of this part, so this decrease can be represented by reducing the modulus of elasticity by a certain percentage in the element in which the crack occurred. Where the paragraph (4.5.2.3. Parametric study of structural model under modal analysis ) explained the effect of changing the modulus of elasticity, mass density, height and radius on the dynamic characteristics (natural frequency and mode shapes) on the FE minaret model behaviour.

This study depends only on a change in modulus of elasticity because of the limited is time not enough for using all of them. Six damage scenario were depicted, in the first scenario, the damage element is near the base with a damage percentage of 0.9, in the second scenario, the damage element is in the middle of the body of the minaret with a damage percentage of 0.9, in the third scenario, the damage element is in the balcony with a damage percentage of 0.9 and in the fourth, fifth and sixth scenarios are in dome of the minaret with different damage percentages (0.9 – 0.5 – 0.1), respectively, as shown in Table (5.1) and figures (5.2) (5.3).

Table (5.1) damage element and percentage and location for damage scenarios

No. of scenarios	Sc.1	Sc. 2	Sc. 4	Sc. 3	Sc. 5	Sc. 6
Damaged element	3055	14697	445	1000	1000	1000
Damage percentage	0.9	0.9	0.9	0.9	0.5	0.1
Modulus of elasticity	340	340	340	340	1700	3060
Damage location	base	body	balcony	dome	dome	dome

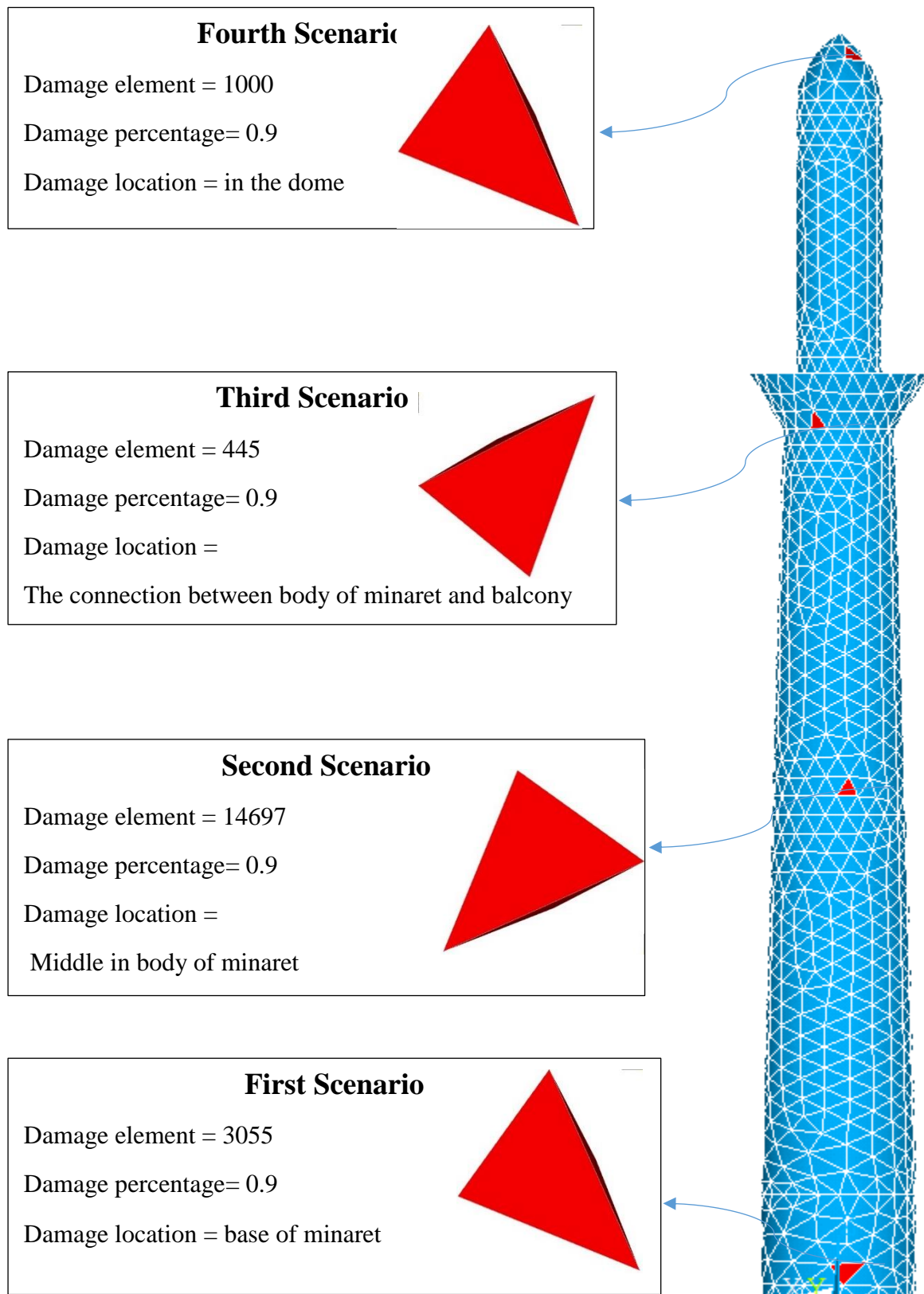


Figure (5.2) Damaged element and percentage and location for first, second, third and fourth scenario

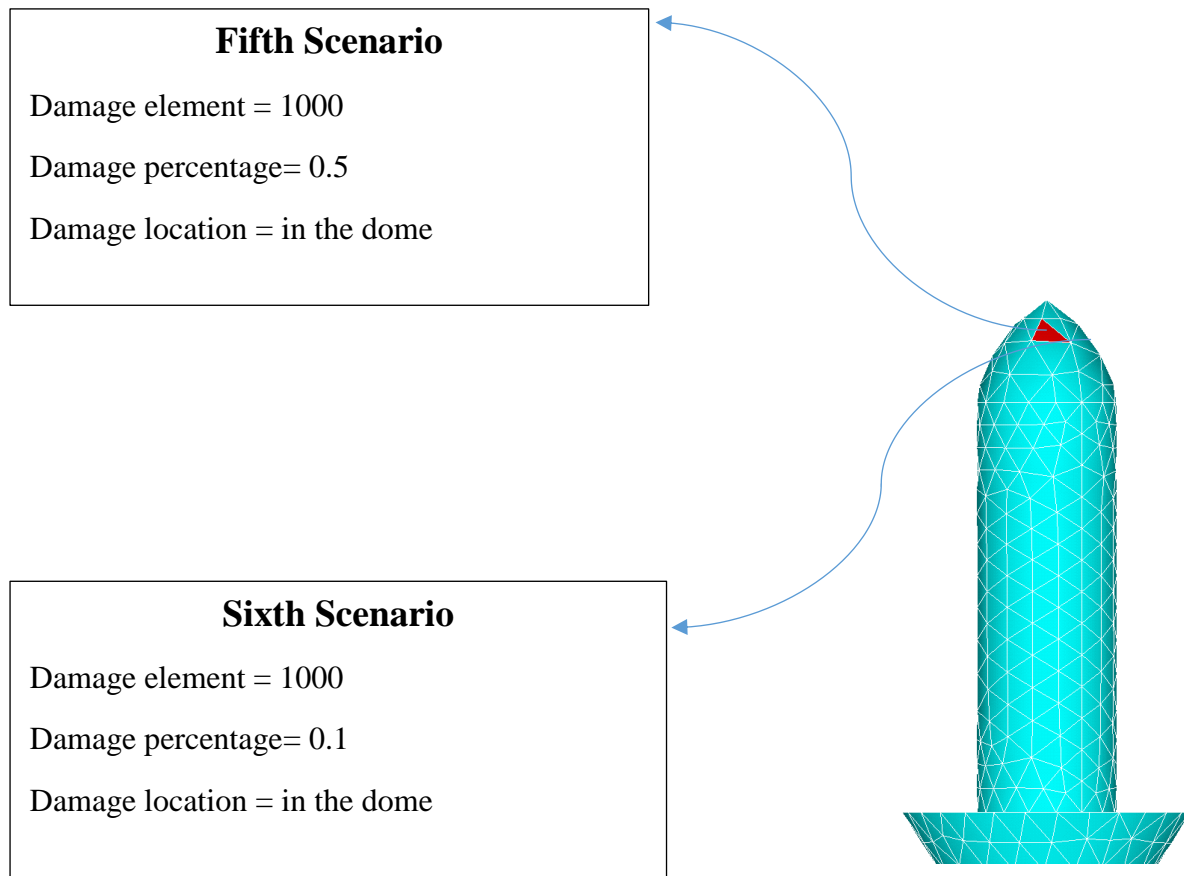


Figure (5.3) Damaged element and percentage and location for fifth and sixth scenario

#### **5.4. Creating of the Subroutine for Proposed SHM Using PSO Method**

The PSO method is one of the modern optimization methods (heuristics methods) that simulates flocks of birds in search of food as explained in chapter three in section (3.3.8. **Particle Swarm Optimization**). This method has been programmed using MATLAB software, where at first, the PSO coefficients (C1, C2, W) have been used, also the number of elements and nodes that were extracted from the model analysis using the ANSYS software. In the beginning, random elements and random damage percentages are created, then these random

elements and damage percentages are transferred in the update file and they are analyzed using the ANSYS software for extracting the results, if the results are identical with the results from scenario of damage model, then this is the element (location) that contains the damage with the ratio damage. If the results are not equal, the random elements and damage percentages are updated using the PSO equations by entering a speed for these values to bring them closer to the element that contains the damage. The analysis and comparison process is repeated and thus continues with a certain number of iteration until the results are compatible equal with the scenario results then the damage location and percentage are determined as shown in the Figure (5.4) of Scheme of PSO method in MATLAB.

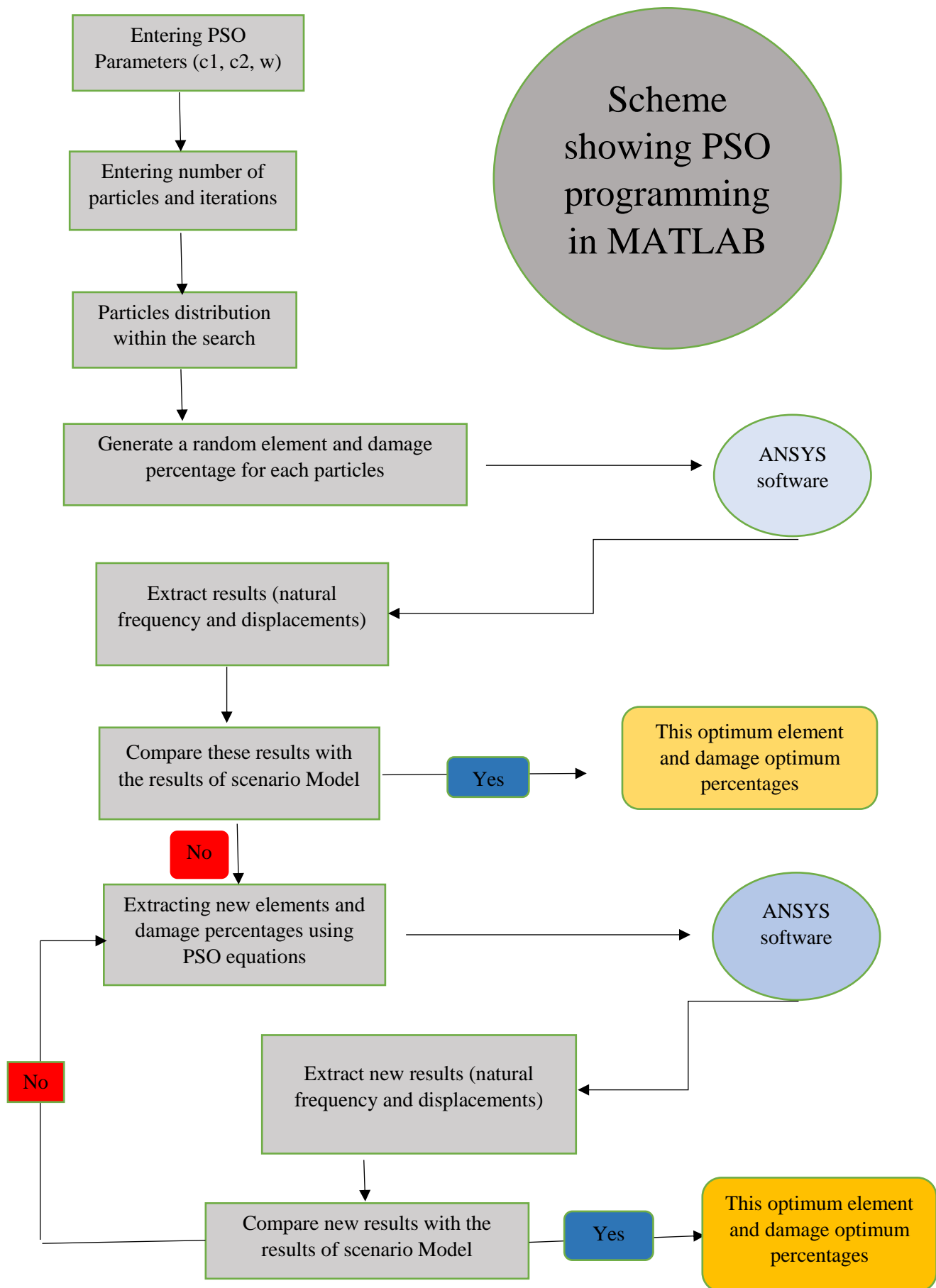


Figure (5.4) Scheme showing PSO programming in MATLAB

#### 5.4.1. Adopted objective function for PSO method

In this study, the adopted objective function for the application of the proposed PSO optimization procedure is adopted for structural health monitoring for damage detection. In this study the objective function includes two parameters: the first is the difference in natural frequencies between the damage scenario and the numerical updated model. The second is the differences in displacement points of mode shape between the damage scenario and numerically updated model. Those parameters are chosen due to their significant effect on the structure. The adopted objective function is defined by Eq (5.1) [8].

$$Obj\_fun = W_f \times Freq + W_d \times Disp \quad \dots 5.1$$

$W_f$  and  $W_d$  are weighting factors of two parts of objective function, difference in natural frequencies and difference in displacement points of mode shape, respectively.

$Freq$  is the differences in the natural frequencies between extracted from damage scenario model and numerically estimated from updated FE model, as given in Eq. (5.2).

$$Freq = \sum_{i=1}^n \left( \frac{f_i^{scenario-dam} - f_i^{updated-dam}}{f_i^{scenario-dam}} \right)^2 \quad \dots 5.2$$

where:

$f_i^{scenario-dam}$  :- The natural frequencies that was extracted from damaged scenario model

$f_i^{updated-dam}$  :- The natural frequency that was numerically estimate from updated FE model

$n$  :- The number of included modes in the computations.

In the second part of objective function ( $Disp$ ) the precise mathematically defined norm is adopted as a measure of difference between nodes displacement of each mode shape, as given in Eq. (5.3).

$$Disp = \sum_{i=1}^n \left[ \sqrt{\sum_{j=1}^m \left( \phi_{ij}^{scenario-dam} - \phi_{ij}^{updated-dam} \right)^2} \right] \quad \dots 5.3$$

$\phi_{ij}^{scenario-dam}$  and  $\phi_{ij}^{updated-dam}$  the nodes displacement of each mode shape divided by maximum displacement are extracted from damage scenario model and estimated numerically from updated damage FE model, respectively.

$m$  :- the total number of nodes of all modes

#### 5.4.2. Adopted coefficients for PSO method

The PSO method need coefficients (C1, C2 and W) as shown in chapter three in section (3.3.8. Particle Swarm Optimization) in this study the weighting function is following in Eq (5.4).

$$w = w_{max} - \frac{w_{max} - w_{min}}{iter_{max}} * iter \quad \dots 5.4$$

Where  $w_{max}$  and  $w_{min}$  are initial weight and final weight (0.9 – 0.4) respectively,  $iter_{max}$  and  $iter$  are maximum iteration number and current iteration number respectively.

(C1 and C2) are weighting coefficients, in this study the weighting coefficients for detect the damage element is (0.5) and for detect the damage percentage was depend on Eq (3.5).

$$C1 = C_{max} - \left( \frac{(C_{max} - C_{min}) * iter}{iter_{max}} \right)^1 \quad \dots 5.5$$

$$C2 = C_{max} - \left( \frac{(C_{max} - C_{min}) * iter}{iter_{max}} \right)^2 \quad \dots 5.6$$

Where  $(C_{max} - C_{min})$  are maximum and minimum weighting coefficients (2.5 – 0.5) respectively.

## 5.5. Verification of Proposed SHM Technique Using PSO Method

After completing the PSO method programming using MATLAB software, the program was tested on a steel beam with 600 mm length and the results were compared with the research carried out by **Al-Wazni and Zainul-abideen (2019)** [28] using the Particle Swarm Optimization (PSO) method [28]. Second, it is applied on a brick wall.

### 5.5.1. Test on steel clamped beam model

The study on a beam is adopted by **Al-Wazni and Zainul-abideen (2019)** [28] which was carried out depending on experimental results published by **Nanda et al. (2012)** [38] structural model, the beam was a steel clamped beam with 600 mm length, 200 GPA modulus of elasticity, and 7800 kg/m<sup>3</sup> mass density. The model was divided into 20 elements, as shown in Figure (5.5).

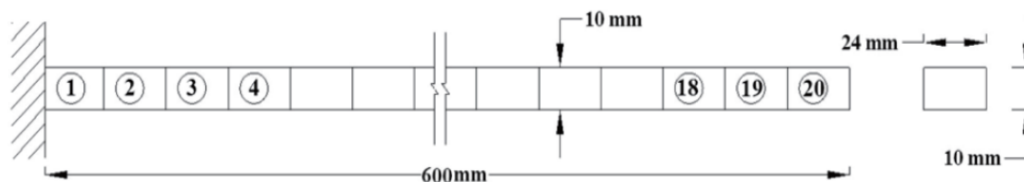


Figure (5.5) Steel clamped beam model [28].

Two scenarios of crack were adopted for this study by reducing the height of the cross section 10%, as shown in the Table (5.2).

Table (5.2) Crack scenarios of the steel clamed beam

Crack Scenario	Element No.	Distance from support (mm)	Crack Size (%)
1	3	75	10
2	8	225	10

The occurrence of crack in the element causes a decrease in the stiffness of this element and therefore a decrease in the stiffness of the structure. Table (5.3) shows the difference in the natural frequencies for both scenarios and compares it with intact frequencies.

The results of the modal analysis (natural frequency and mode shapes) in this study is compatible with the results extracted by **Nanda et al. (2012) [38]**.

Table (5.3) Modal frequencies for intact, first and second crack scenario for the clamped beam

Mode Intact	Intact Freq. (Hz)	Cr.Sc.-1 Freq. (Hz)	Cr.Sc.-2 Freq. (Hz)
1	22.721	22.162	22.527
2	142.343	141.520	141.503
3	398.363	398.613	395.586
4	863.141	849.996	855.127
5	1288.396	1283.372	1273.994
6	1922.711	1908.959	1915.230

### 5.5.1.1. First crack scenario of steel clamped beam

The (PSO) technique was applied via MATLAB for the first scenario on element 3 with a distance, from support, of 75 (mm). Figure (5.6) shows the values of the objective function for the number of 20 iterations, while Figure (5.7) shows the (PSO) technique ability to detect element 3 as the damaged element with 0.1 damage percentage.

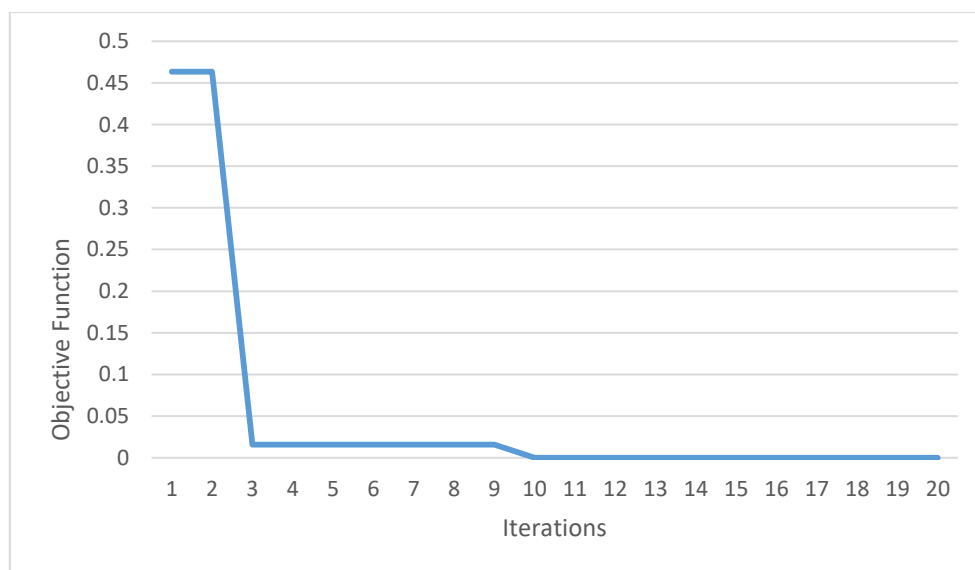


Figure (5.6) Convergence of objective function for first crack scenario of steel clamped beam

From Figure (5.6) the SHM technique detected the damage in iteration 10 this consider very good compared with result by **Al-Wazni and Zainul-abideen [28]**.

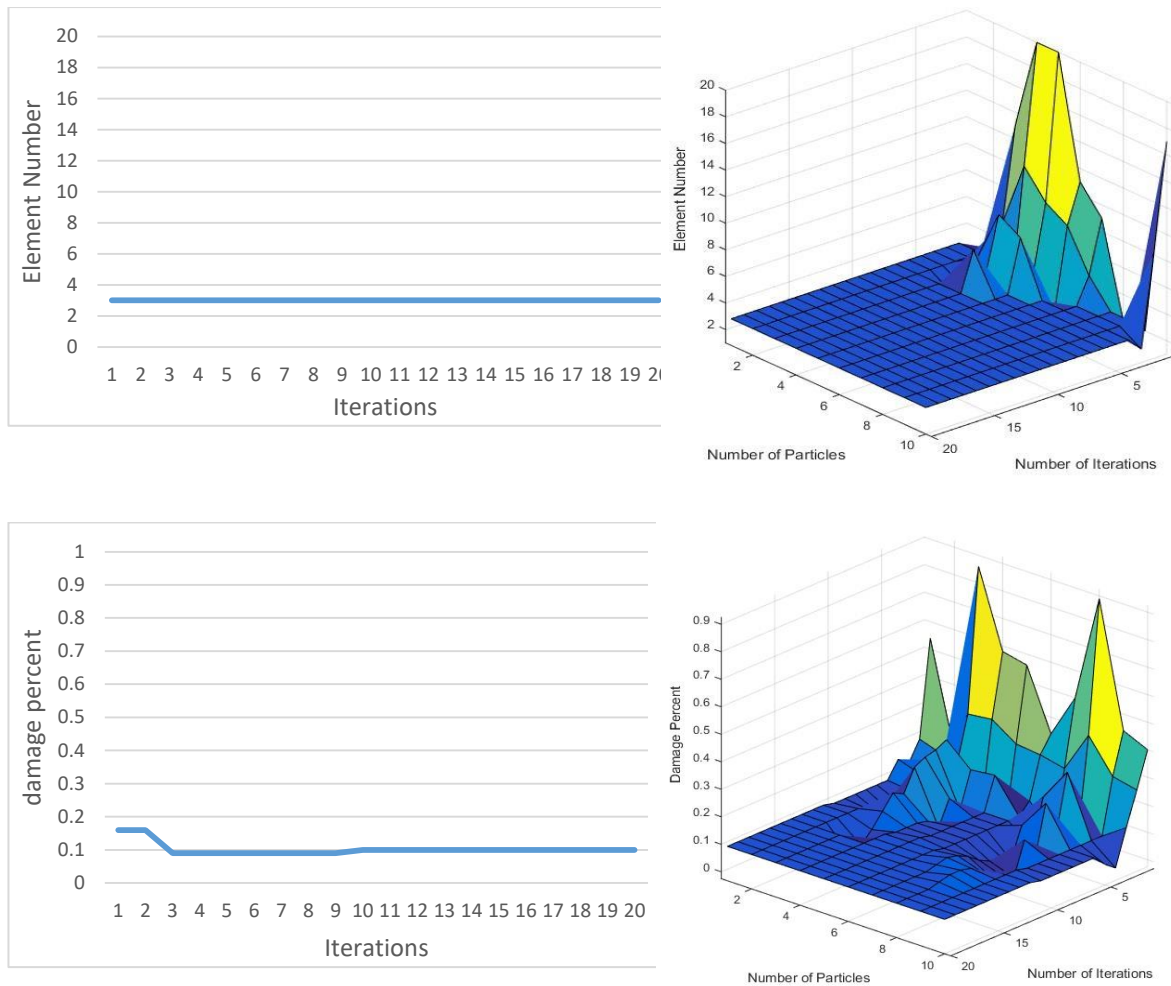


Figure (5.7) History of damaged element number and damage percentage for first crack scenario of steel clamped beam

### 5.5.1.2. Second crack scenario of steel clamped beam

The second scenario on element 8 with a distance from support 225 mm. Figure (5.8) shows the values of the objective function for the number of 20 iterations where the SHM technique detected the damage in iteration 9, while Figure (5.9) shows the (PSO) technique ability to detect element 8 as the damaged with 0.1 amount of damage.

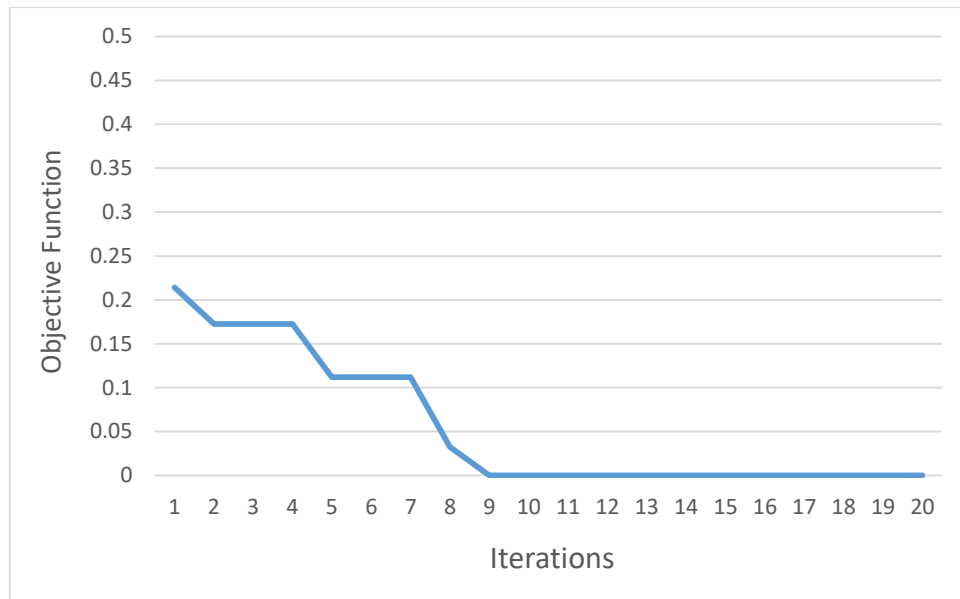


Figure (5.8) Convergence of objective function for second crack scenario of steel clamped beam

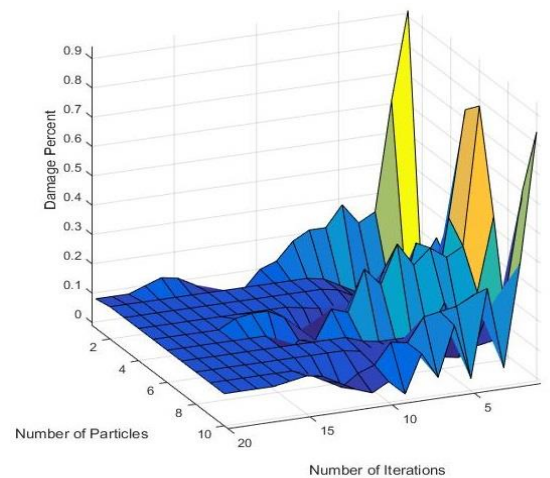
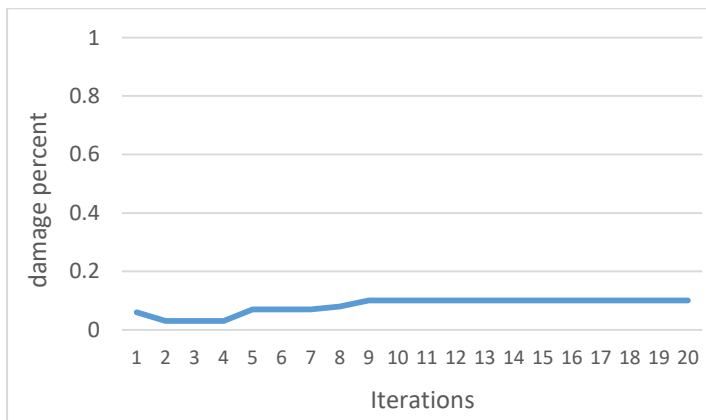
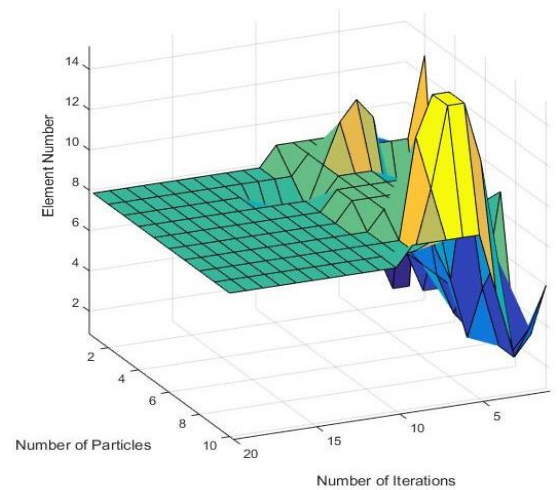
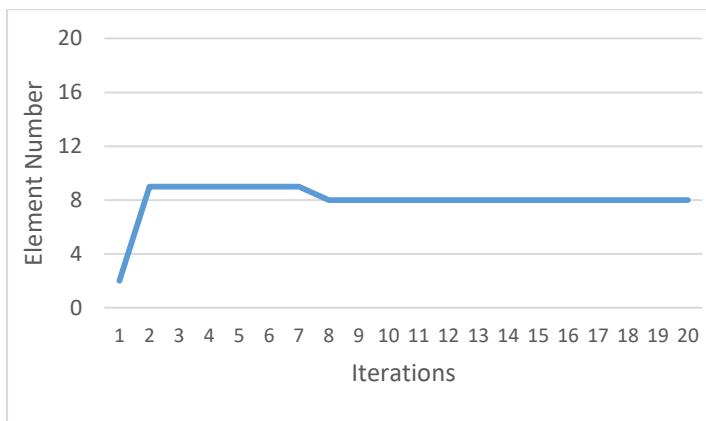


Figure (5.9) History of damaged element number and damage percentage for second crack scenario of steel clamped beam

By comparing the current study with Nanda et al [40] study and Al-Wazni and Zainul-abideen [28] study, the objective function value improved and converged more quickly. The results demonstrate how effective and reliable the new technique is.

### 5.5.2. Test on brick masonry wall

The second test was done on a masonry wall with dimensions (1 m width, 1 m height and 0.25 m wall thickness) as shown in Figure (5.10).

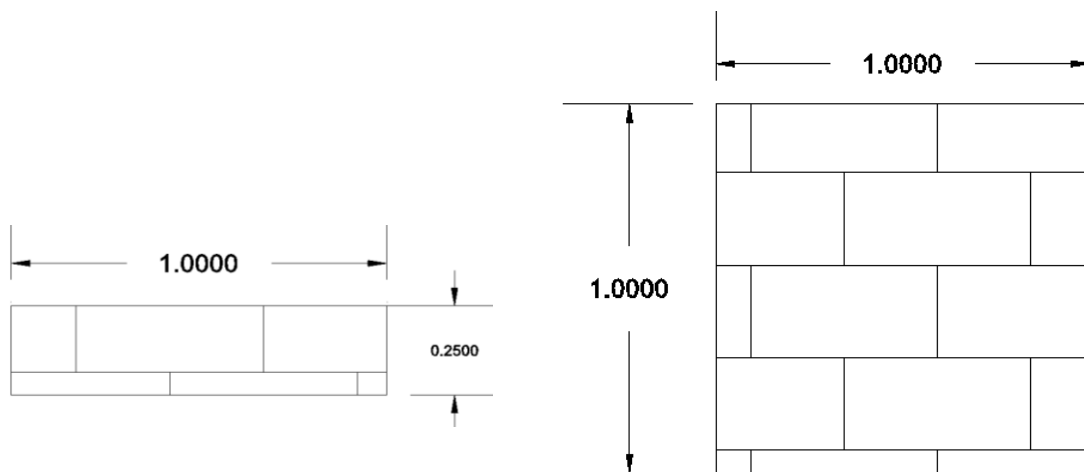


Figure (5.10) Dimension of brick masonry wall

The materials properties of the wall were taken from a research by **Khalifa and Al-Wazani [30]**, where they extracted the material properties of masonry wall made from brick and gypsum mortar. The finite element model was divided into 96 elements. The support is the area base was fixed.

Table (5.4). Material properties of adopted brick minaret model

<b>Material properties</b>	<b>Values</b>
Modulus of Elasticity (MPa) [30]	$3.4 \times 10e3$
Mass Density (kg/m <sup>3</sup> ) [4]	$1.2 \times 10e3$
Poisson's Ratio [30]	0.2

Four crack scenario were adopted for this study, the crack was represented by reducing modulus of elasticity by 10 and 50 percent, as shown in Table (5.5) and Figure (5.11).

Table (5.5) Crack scenarios of the structural model

Crack Scenario	Element No.	Distance from support (mm)	Damage percentage %
1	1	41.66	10
2	50	541.66	10
3	1	41.66	50
4	50	541.66	50

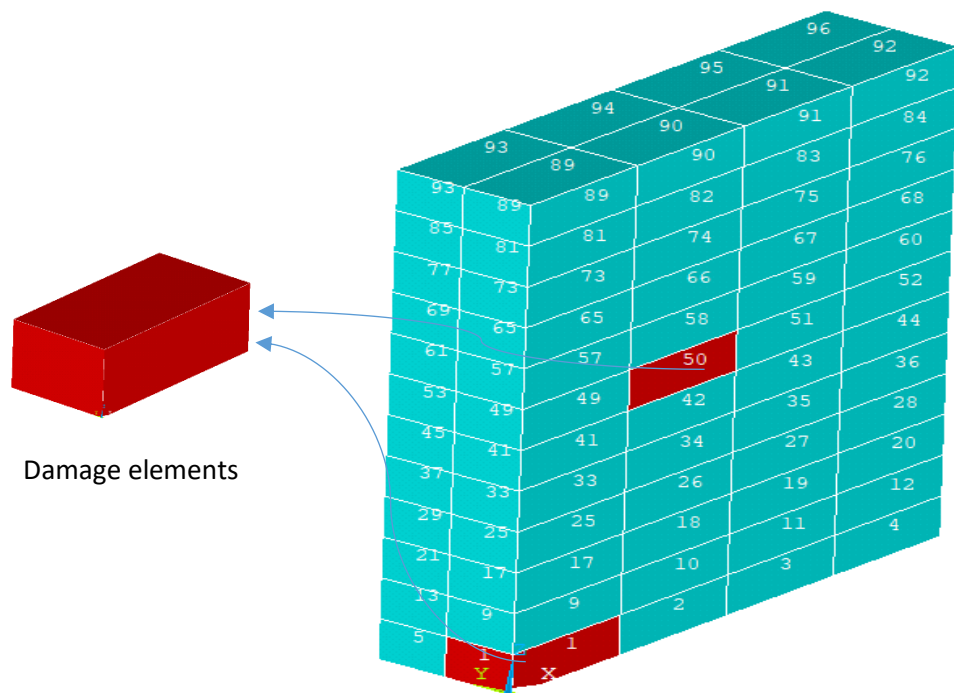


Figure (5.11) Damaged elements of brick masonry wall

When there is a decrease in the modulus of elasticity for element, it causes a decrease in the stiffness of the structure and a difference in frequencies from the intact frequencies of the structure. Table (5.6) shows the difference in the natural frequencies of damage scenarios compared with intact frequencies.

Table (5.6) Modal frequencies of the masonry wall for intact, first, second, third and fourth crack scenario.

Mode	Intact	Cr.Sc.-1	Cr.Sc.-2	Cr.Sc.-3	Cr.Sc.-4
Intact	Freq. (Hz)				
1	66.357	66.239	66.343	65.542	66.267
2	151.074	150.831	150.98	149.353	150.42
3	181.691	181.257	181.6	178.867	181.19
4	346.080	345.585	345.80	342.783	344.24
5	423.425	422.934	423.2	420.196	422.03
6	460.019	459.923	459.64	459.277	457.75

### 5.5.2.1. First crack scenario of brick masonry wall

In this scenario the damaged element is (1) with (41.66 mm) distance from support, the damage percent in this scenario is (0.1). Figure (5.12) shows the values of the objective function for the number of (50) iterations, while Figure (5.13) shows damage detection in element number (1) and the percent of damage is (0.1).

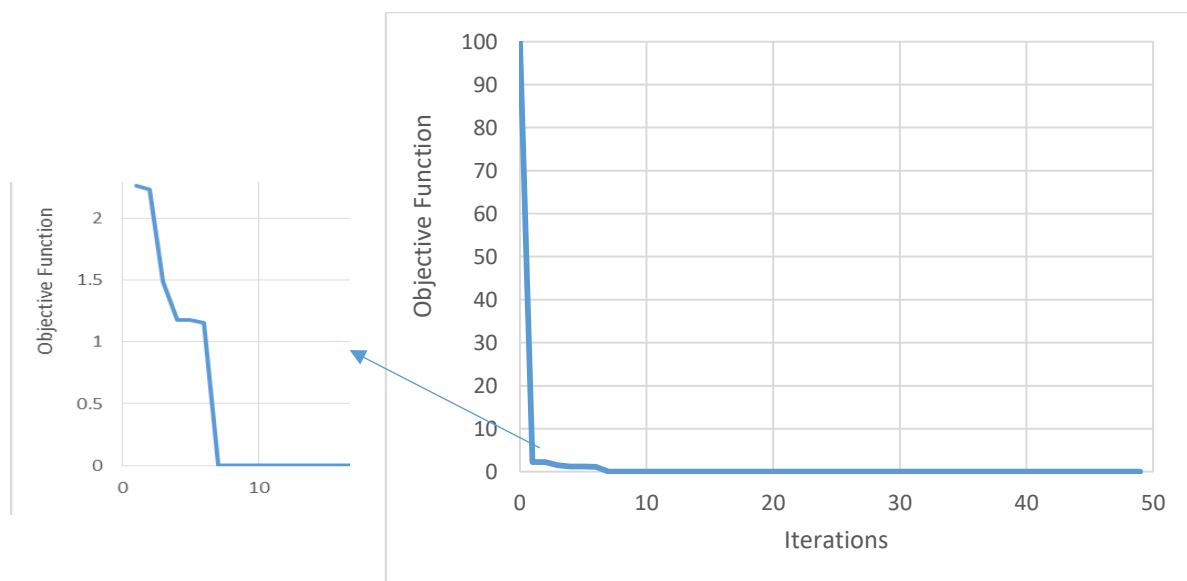


Figure (5.12) Convergence of objective function for first crack scenario of brick masonry wall

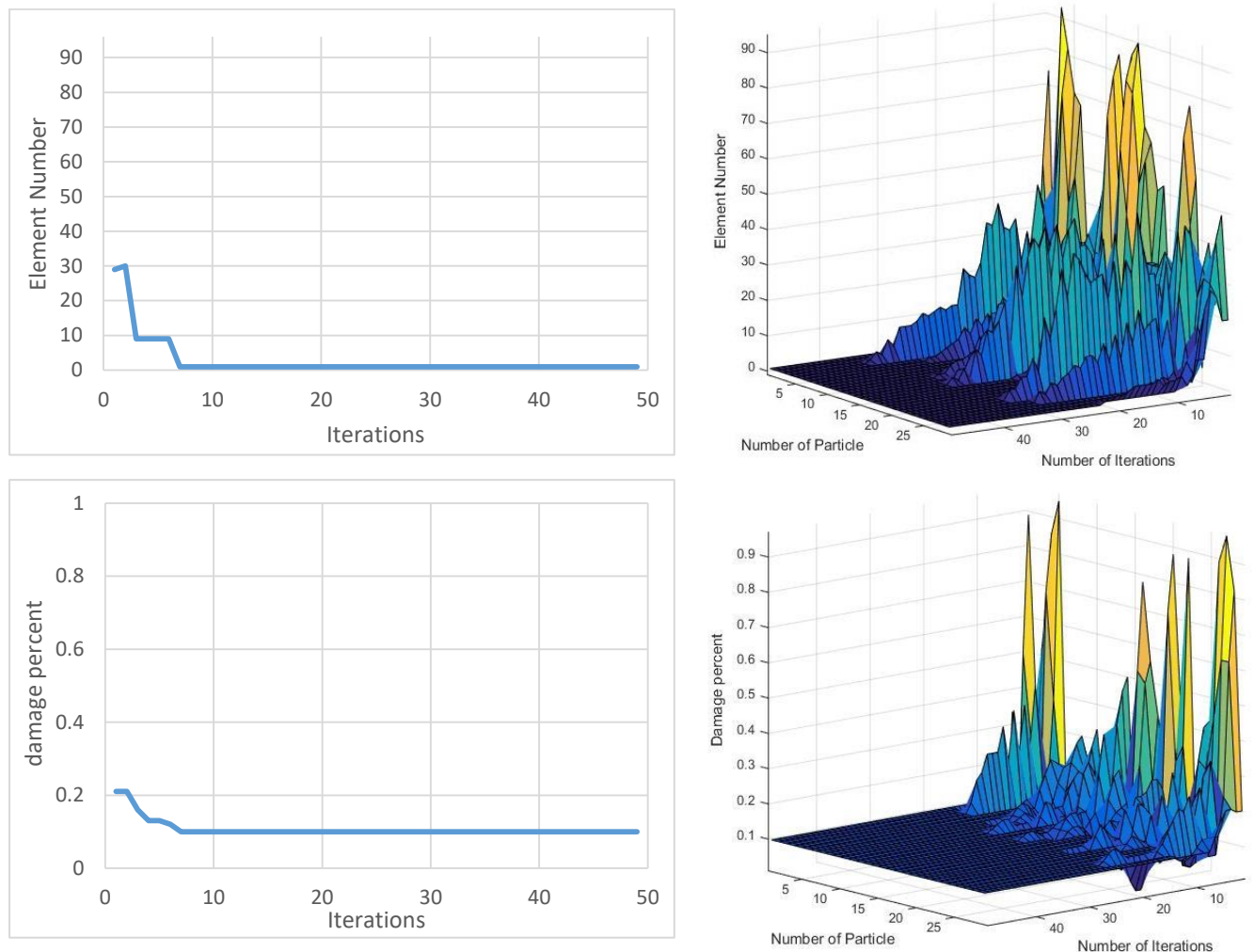


Figure (5.13) History of damaged element number and damage percentage for first crack scenario of brick masonry wall

The SHM technique was very efficiency where it detected the damaged element and damage percentage in iteration number 8 and in iteration 36 all particles convergence toward the damaged element and damage percentage. The SHM technique used about 6.208333 % from search space 9600 to convergence all particles.

### 5.5.2.2. Second crack scenario of brick masonry wall

In this scenario the crack was in element 50 with (541.66 mm) distance from the support, the damage percentage decreased by 10 percent from the modulus of

elasticity. The objective function as shown in Figure (5.14), while Figure (5.15) shows the discovery of the damage location and its percentage.

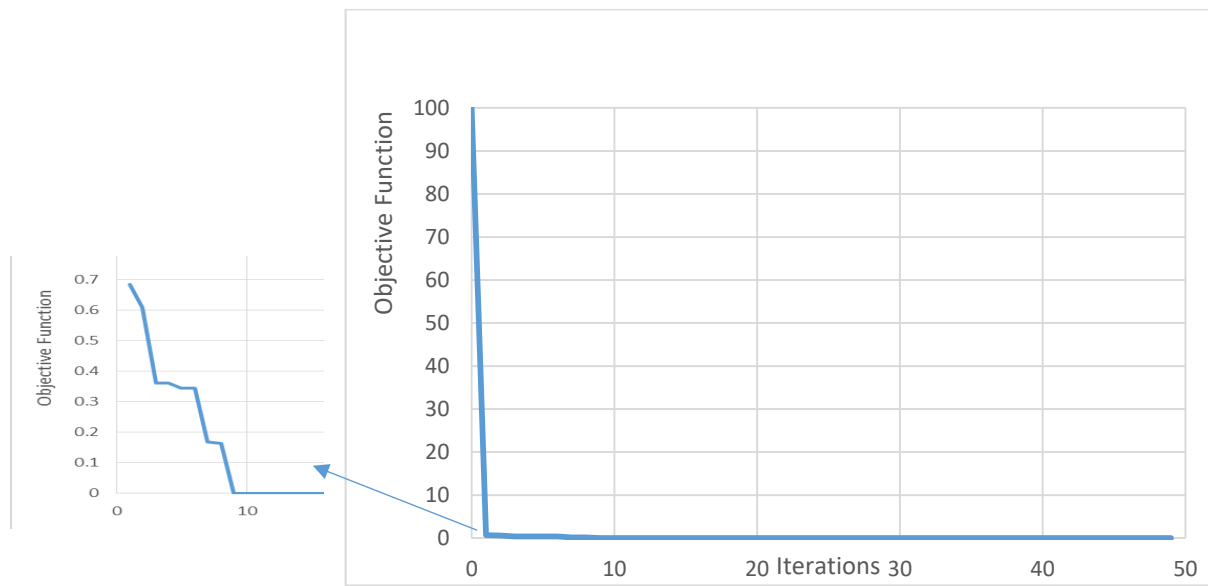


Figure (5.14) Convergence of objective function for second crack scenario of brick masonry wall.

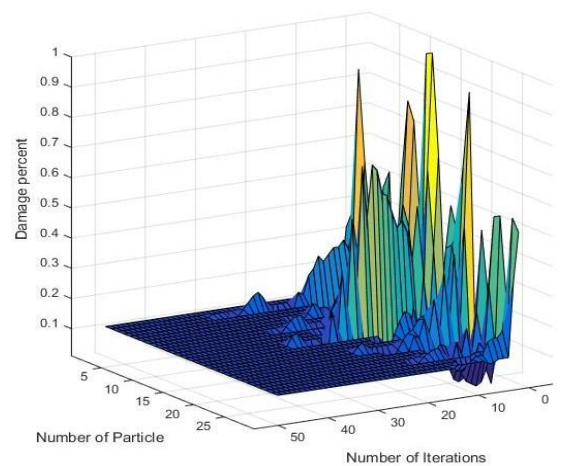
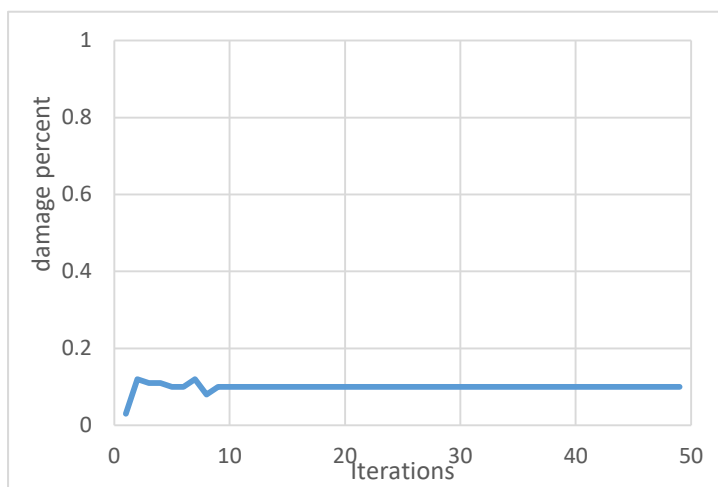
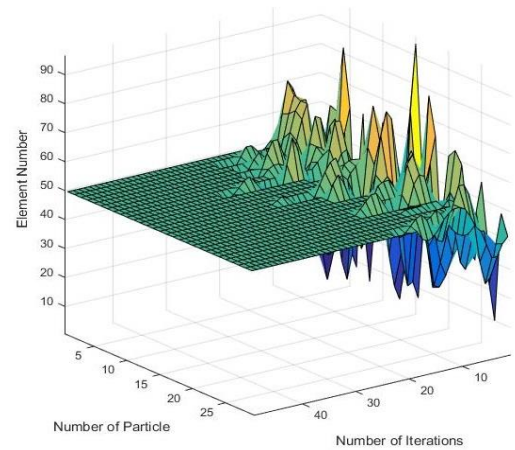
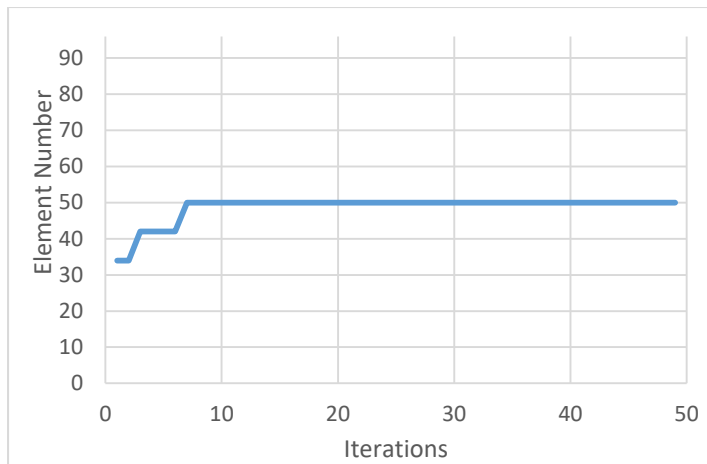


Figure (5.15) History of damaged element number and damage percentage for second crack scenario of brick masonry wall

The SHM technique was efficiency where it detected the damaged element and damage percentage in iteration number 9 and in iteration 32 all particles convergence toward the damaged element and damage percentage. The SHM technique used about 5.291667% from search space to convergence all particles.

### 5.5.2.3. Third crack scenario of brick masonry wall

The third scenario of element 1 with a reduction in modulus of elasticity to the half. Figure (5.16) shows the values of the objective function with 50 iterations, while Figure (5.17) shows the (PSO) technique ability to detect element 1 as the damaged element with an amount of damage of 0.1.

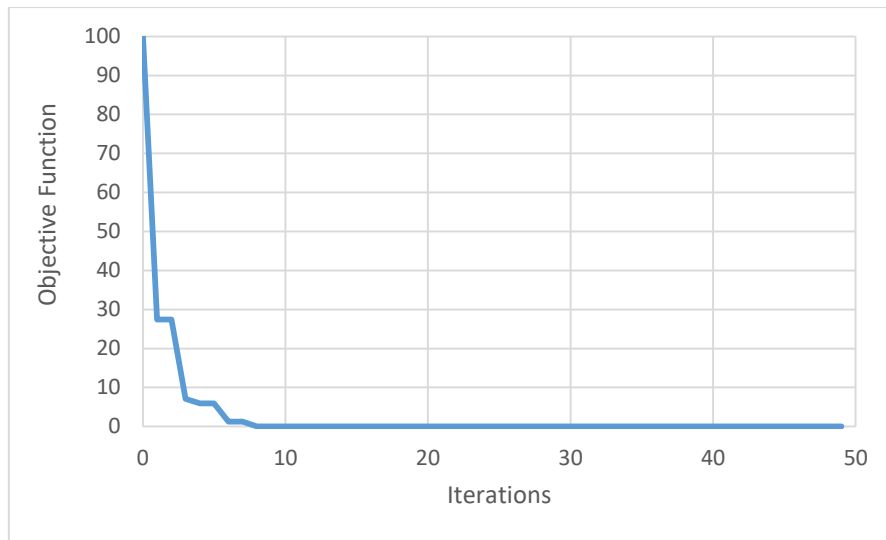


Figure (5.16) Convergence of objective function for third crack scenario of brick masonry wall

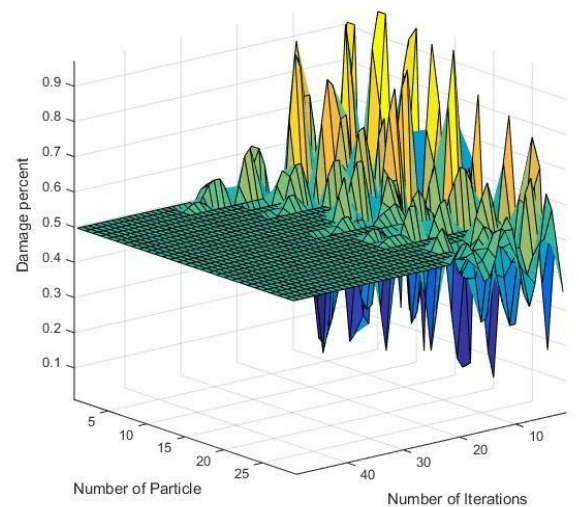
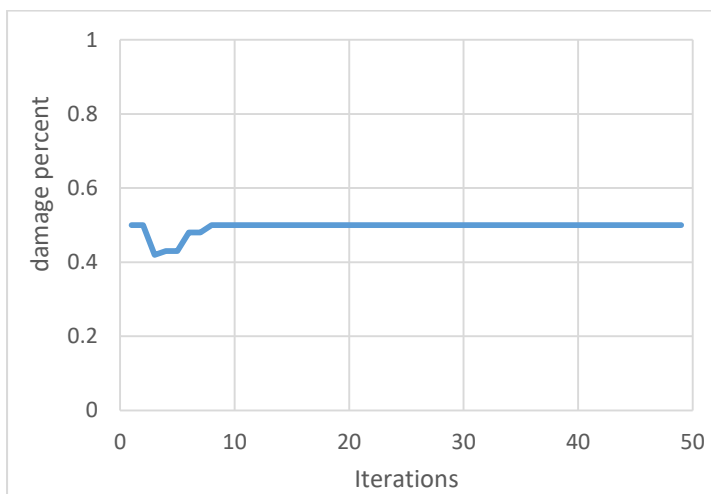
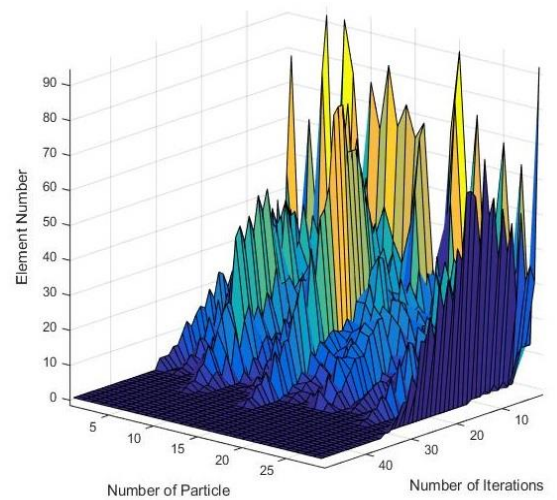
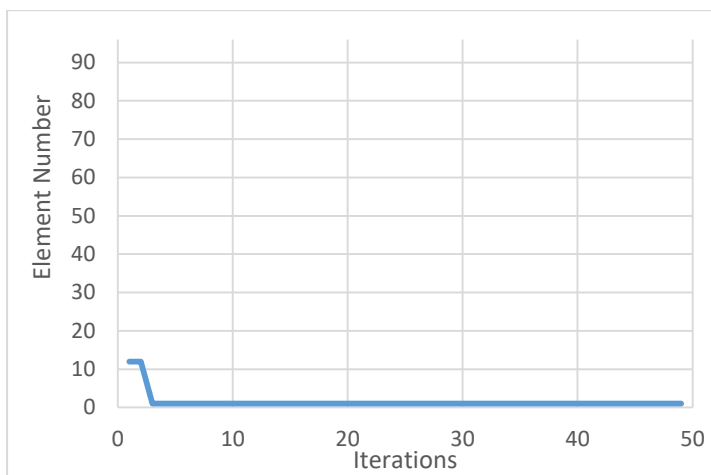


Figure (5.17) History of damaged element number and damage percentage for third crack scenario of brick masonry wall

The SHM technique was efficiency where it detected the damaged element and damage percentage in iteration number 9 and in iteration 37 all particles convergence toward the damaged element and damage percentage. The SHM technique used about 7.802083% from search space 9600 to convergence all particles.

#### **5.5.2.4. Fourth crack scenario of brick masonry wall**

In this scenario the crack was in element 50 with the damage percentage decreasing to the half modulus of elasticity. The objective function as shown in figure (5.18), while figure (5.19) shows the discovery of the damage location and its percentage.

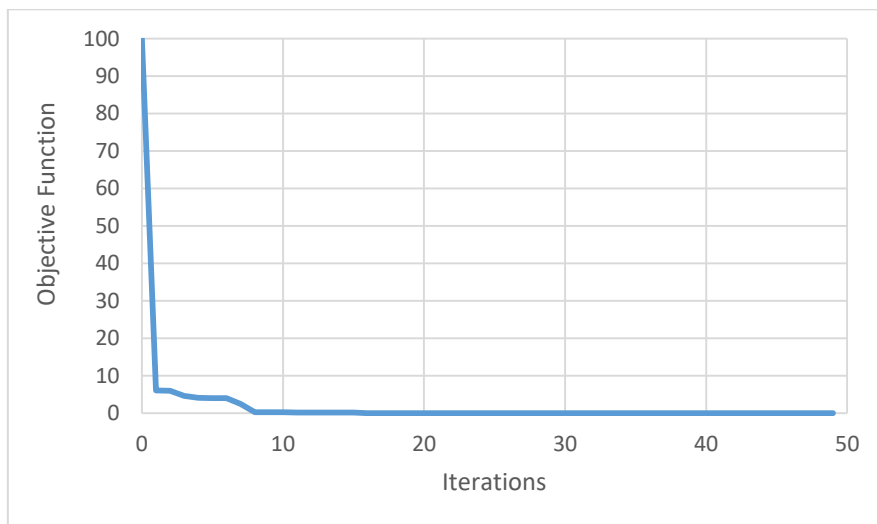


Figure (5.18) Convergence of objective function for fourth crack scenario of brick masonry wall

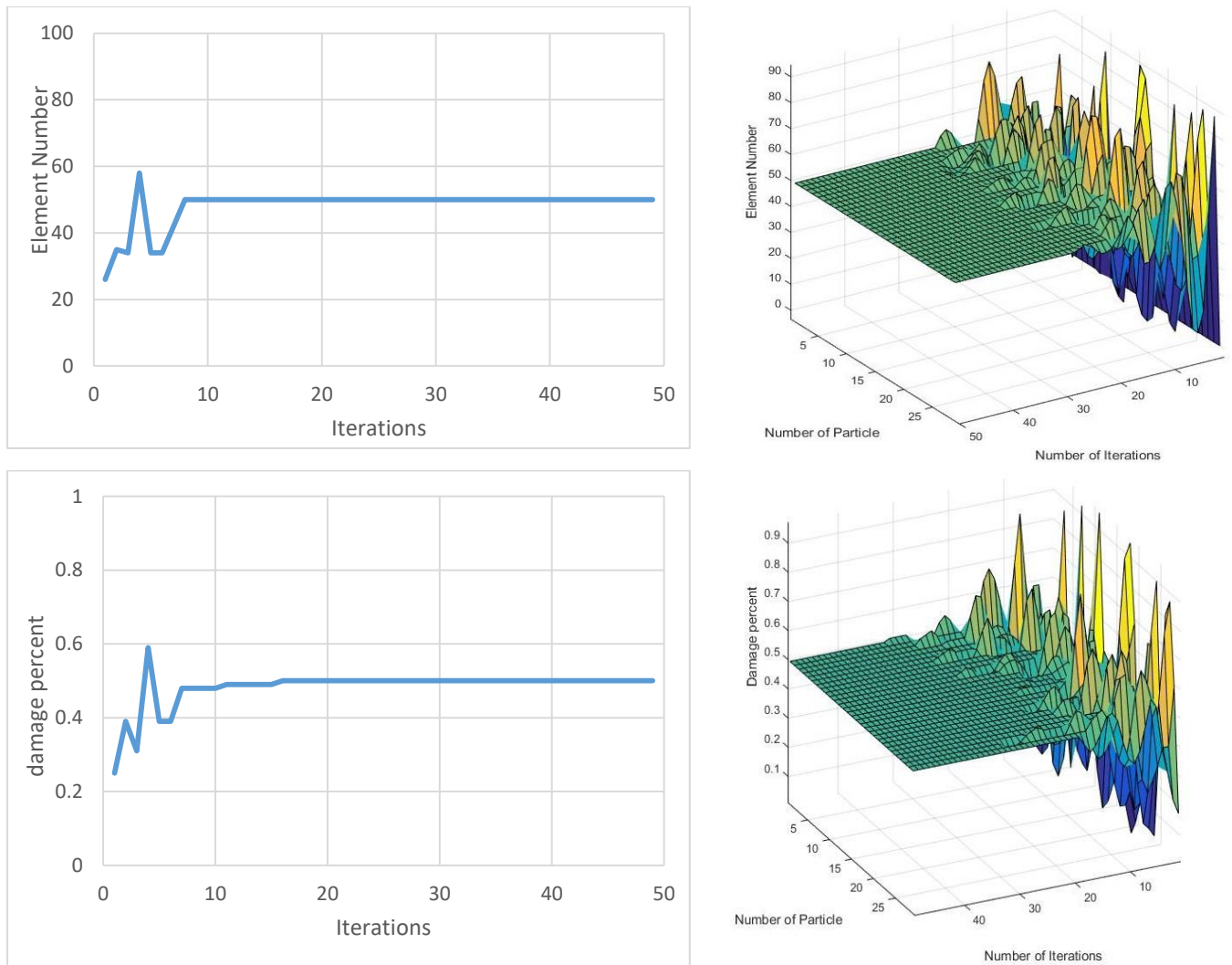


Figure (5.19) History of damaged element number and damage percentage for fourth crack scenario of brick masonry wall

The SHM technique was efficiency where it detected the damaged element and damage percentage in iteration number 16 and in iteration 32 all particles convergence toward the damaged element and damage percentage. The SHM technique used about 6.520833% from search space 9600 to convergence all particles.

## 5.6. Parametric Study to select Iteration and Particle Number in Adopted SHM Technique of Minaret

### 5.6.1. Estimation iteration number

Three different numbers of iteration were used in the PSO method these are 75, 100 and 125 iteration with keeping the same number of particles, damage element, damage percentage and other parameters of this technique. Table (5.7) shows three cases with difference in number of iterations.

Table (5.7) Parameter Description of PSO method for three cases with change in iterations

Parameter Description	case 1	case 2	case 3
Iteration	75	100	125
particle	130	130	130
Damaged element and location	366 balcony	366 balcony	366 balcony
Damage percentage	0.9	0.9	0.9
Wd , Wf	$10^4$ , $10^{11}$	$10^4$ , $10^{11}$	$10^4$ , $10^{11}$
C1,C2 of element	0.5	0.5	0.5
C1,C2 of damage	Eq.(5.5) and (5.6)	Eq.(5.5) and (5.6)	Eq.(5.5) and (5.6)
W (weighting function)	Eq .(5.4)	Eq .(5.4)	Eq .(5.4)

#### 5.6.1.1 First case

In this case 75 iterations were used for PSO technique for damage detection in the adopted model, in this case the number of iteration is low so the PSO technique did not detect the damage and found a local position and local damage

percentage (local element number (12091), local damage percentage (0.16) as shown in Figure (5.21) and local objective function (14.3377)). Figure (5.20) shows the objective values of each iteration.

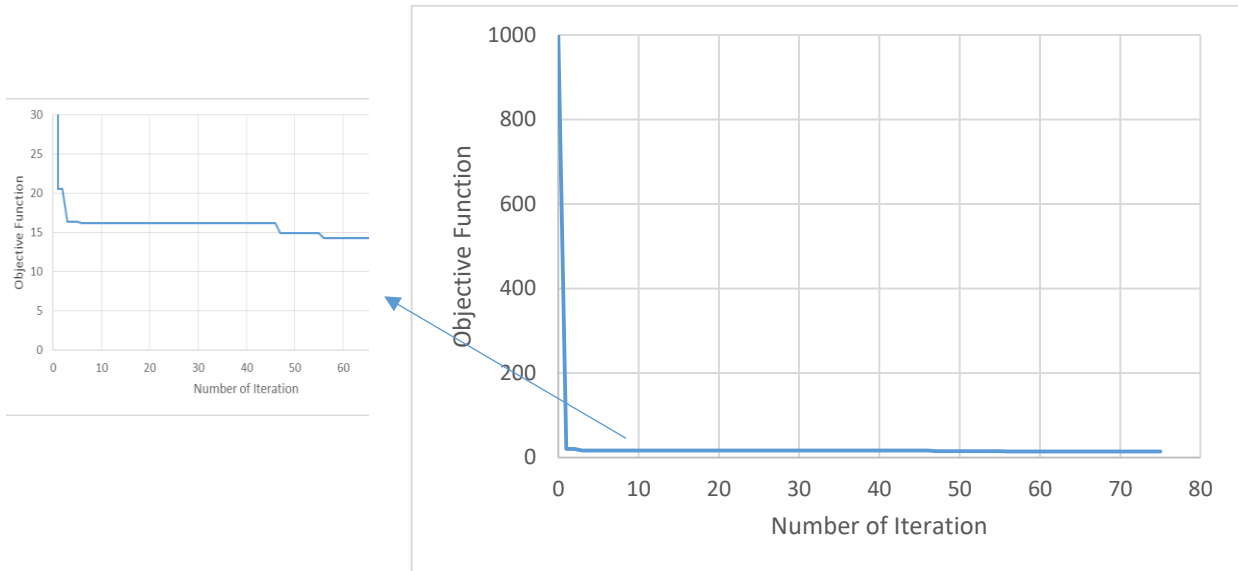


Figure (5.20) Convergence of objective function for first case

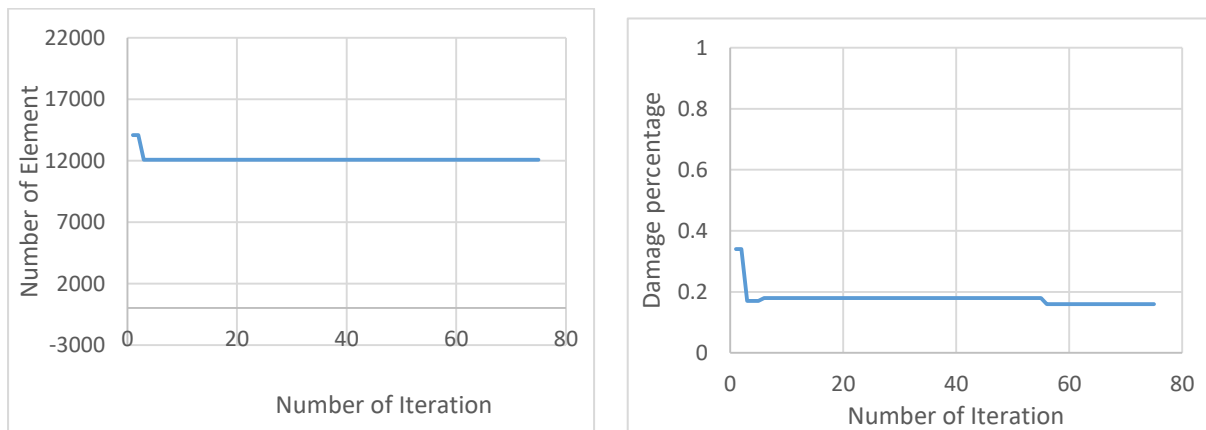


Figure (5.21) History of damaged element number and damage percentage for first case

### 5.6.1.2 Second case

In this case, the number of iterations has been increased to 100, while the number of particles remains constant, which is 130, and the parameters of the PSO technique remains constant, and for the same damaged element 366, with a

damage percentage of 0.9. The technique gave the results (the location and percentage of damage) accurately, where the damage was discovered at the 61st iteration, and then the technique began to direct all the particles on this damage. Figure (5.22) shows the objective function with each iteration for the optimum value, as it shows a match between the damaged element that was discovered with the element in which the damage was assumed, as the target function became zero at the 61st iteration.

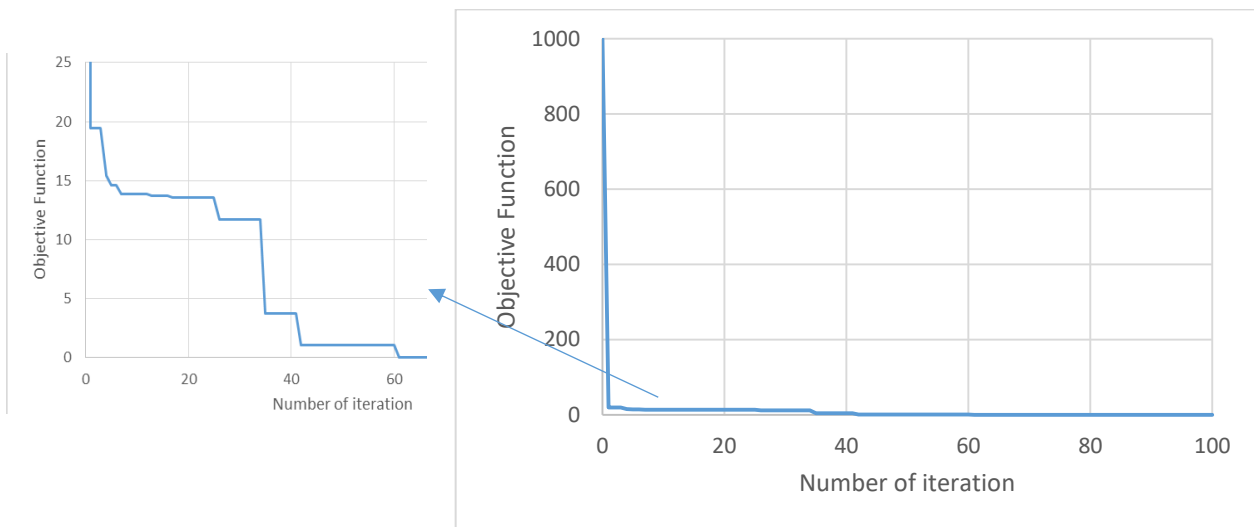


Figure (5.22) Convergence of objective function for second case

After detecting the damage, the technology approximated the particles towards the damaged element, which is 366, and the damage percentage was around to 0.9, as shown in Figure (5.23).

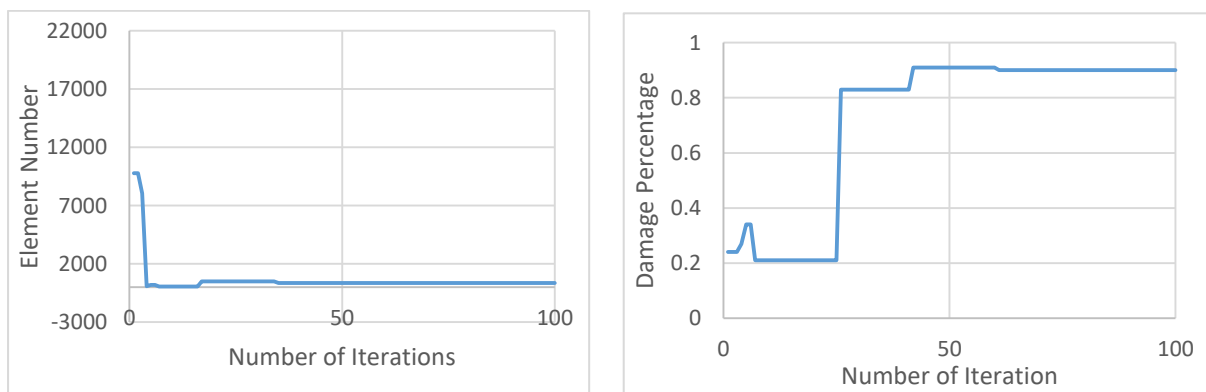


Figure (5.23) History of damaged element number and damage percentage for second case

Figure (5.24) shows the ability of the technique to approximate the particles to the damaged element and percentage, as it was noted in iteration 75 that approximately 98% of the particles approximated towards the damaged element.

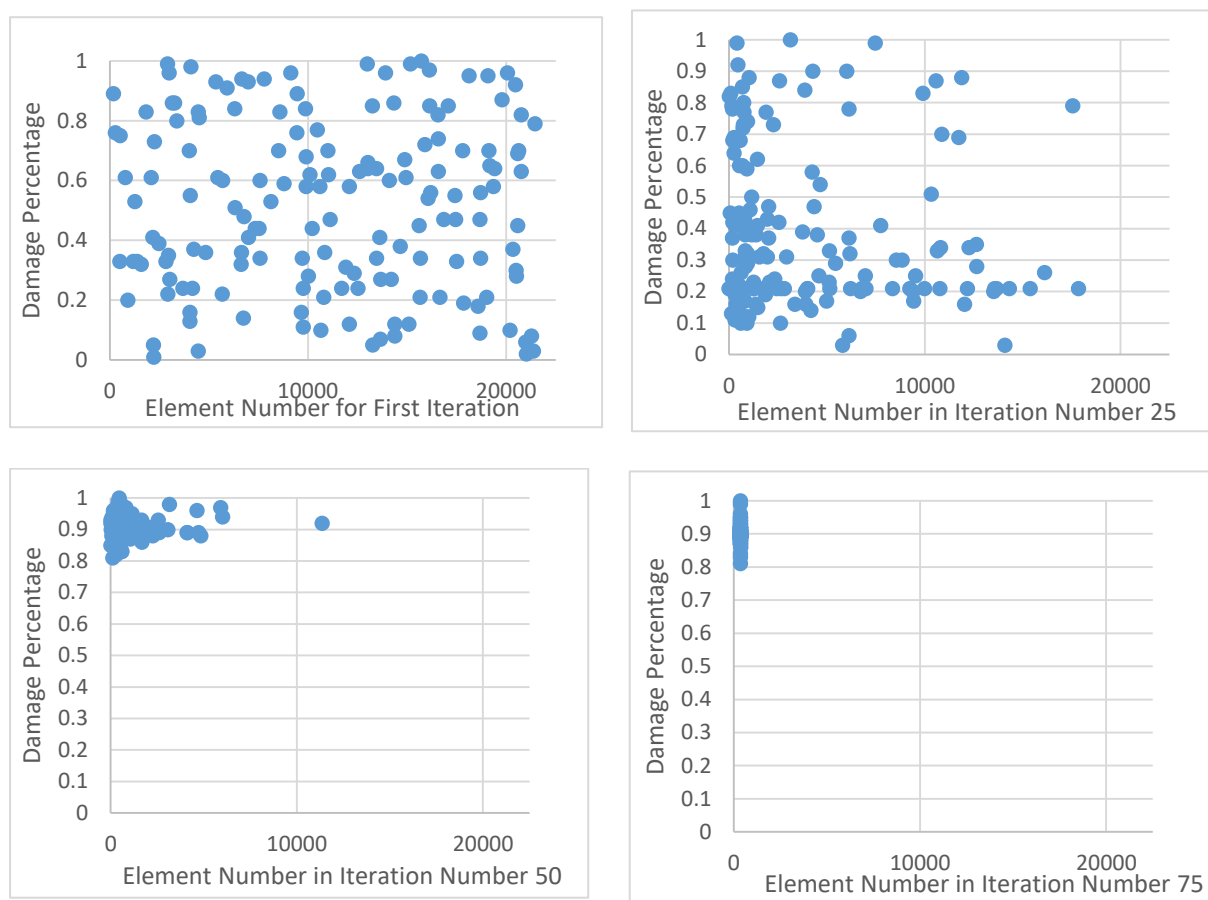


Figure (5.24) Distribution and convergence of particles towards damage in first, 25, 50 and 75 iteration

### 5.6.1.3 Third case

In this case, the number of iterations has been increased to 125. The PSO technique discovered the optimum element damage and optimum damage percentage in iteration number 71 in particle number 6. Figure (5.25) shows the

optimum objective function for each iteration. Figure (5.26) shows the ability SHM technique to approximate towards the optimum element damage and optimum damage percentage.

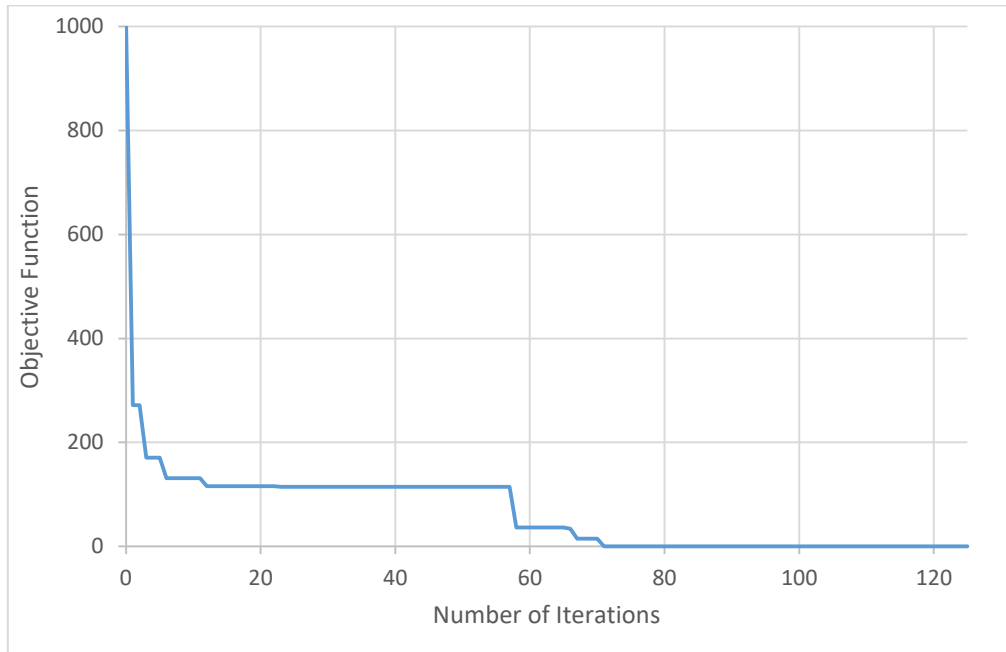


Figure (5.25) Convergence of objective function for third case

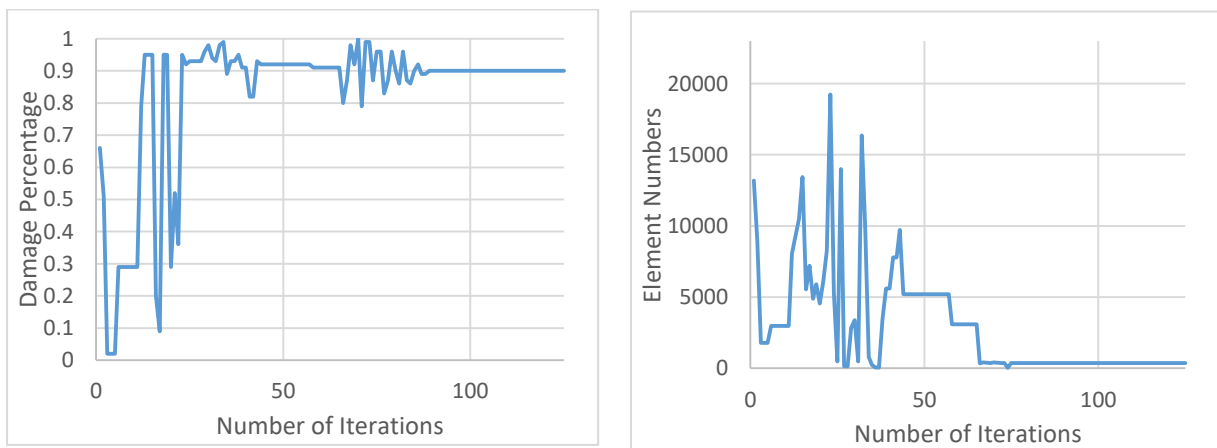


Figure (5.26) History of damaged element number and damage percentage for third case

From the results, it was noted note that in the case of 75 iterations, the damage was not detected, while the number of iterations counted 100 and 125, the damage was discovered, so the number of 100 iterations was adopted because it requires time for execution less than the number of iterations 125.

### 5.6.2. Estimation number of particles

Three different cases were used to estimate the best optimum number of particles (100, 130 and 160) for 100 iteration. Table (5.8) shows three cases with different number of particles.

Table (5.8) Parameters Description of PSO method for three cases with change in number of particles

<b>Parameter Description</b>	<b>Case 1</b>	<b>Case 2</b>	<b>Case 3</b>
Iteration	100	100	100
No. of particles	100	130	160
Damage element	366	366	366
Damage percentage	0.9	0.9	0.9
Wd , Wf	$10^4$ , $10^{11}$	$10^4$ , $10^{11}$	$10^4$ , $10^{11}$
C1,C2 of element	0.5	0.5	0.5
C1,C2 of damage	Eq .(5.5) and (5.6)	Eq .(5.5) and (5.6)	Eq .(5.5) and (5.6)
W (weighting function)	Eq .(5.4)	Eq .(5.4)	Eq .(5.4)

#### 5.6.2.1 First Case

In the first case the number of particles was 100, the PSO technique can detect the damage but the Particles are very few compared to the search space with only

82 % from particle discover the damage element and damage percentage. Figure (5.27) shows the objective function of each iteration and Figure (5.28) shows the approximation to on damage elements and damage percentage.

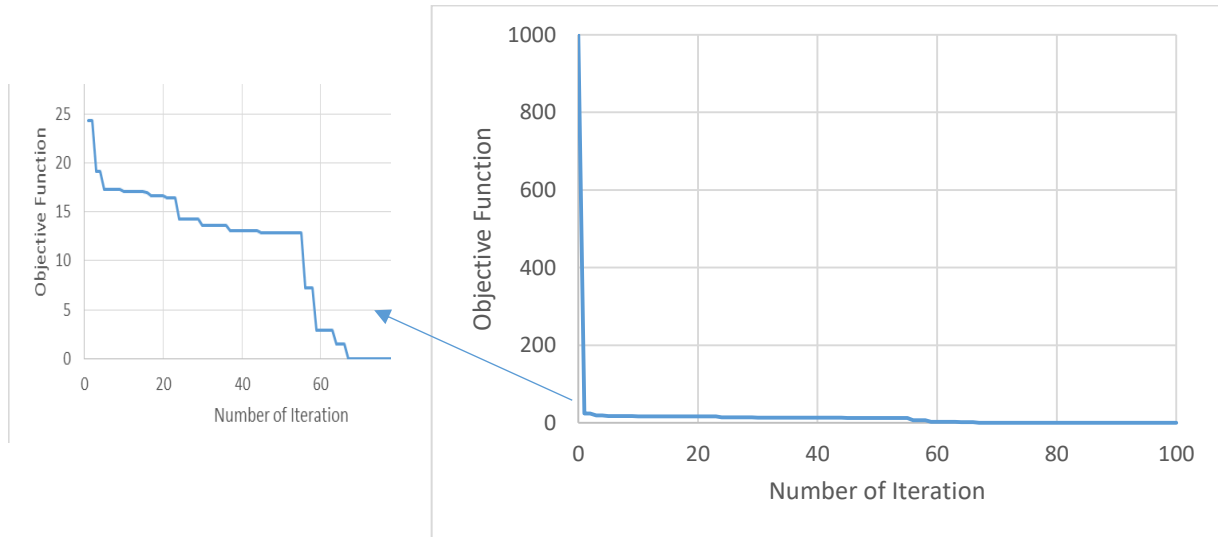


Figure (5.27) Convergence of objective function for first case

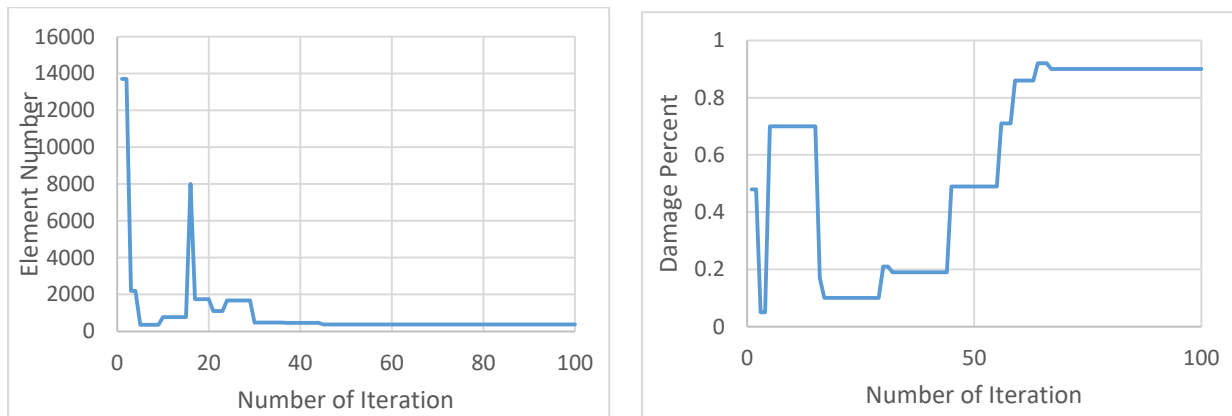


Figure (5.28) History of damaged element number and damage percentage for first case

### 5.6.2.2 Second Case

In the second case the number of particles was 130, from the results, the PSO technique detected the damage very rapidly in iteration no.24, and about 87.7%

of particles discovered the damaged element and damage percentage. Figure (5.29) shows the objective function for each iteration.

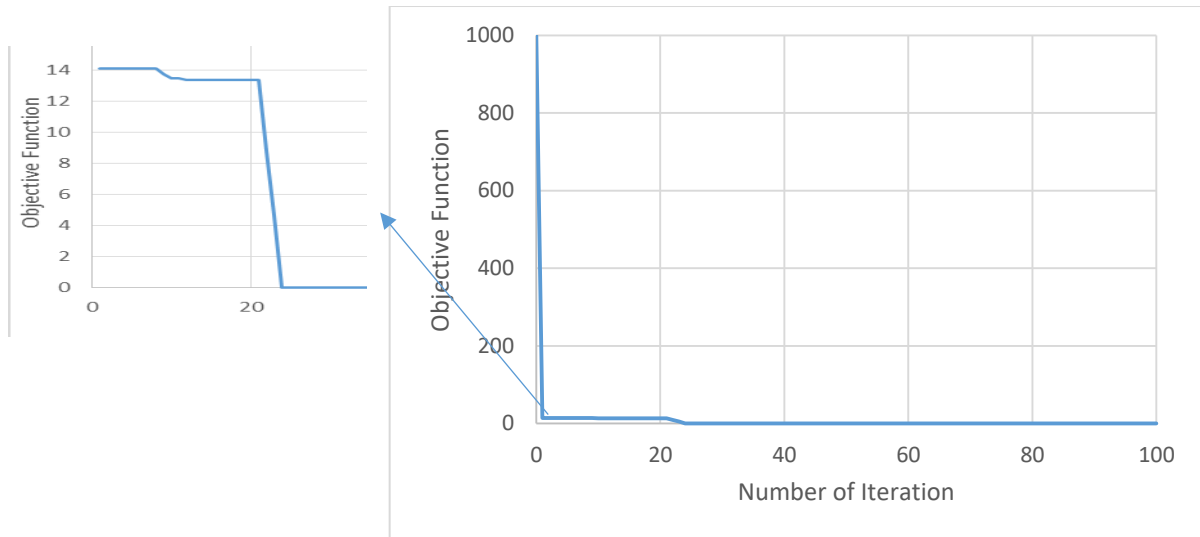


Figure (5.29) Convergence of objective function for second case

The Figure (5.30) shows the ability of the PSO technique to bring the particles closer to the damaged element 366 and also to the damage percentage 0.9.

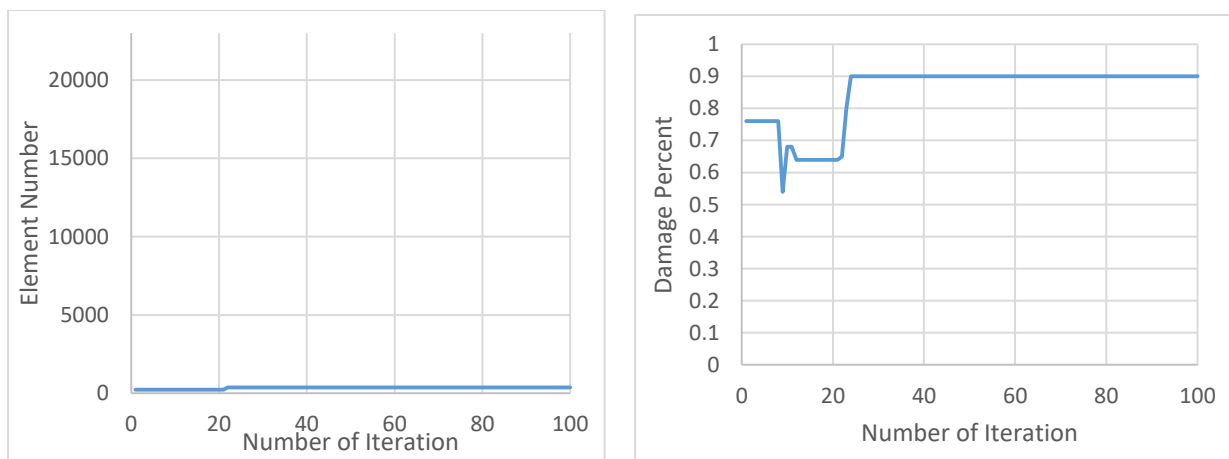


Figure (5.30) History of damaged element number and damage percentage for second case

Figure (5.31) shows the ability of the technique to approximate the particles to the damaged element and percentage, it was noted in iteration 75 that

approximately 97.7% of the particles was approximated towards the damaged element

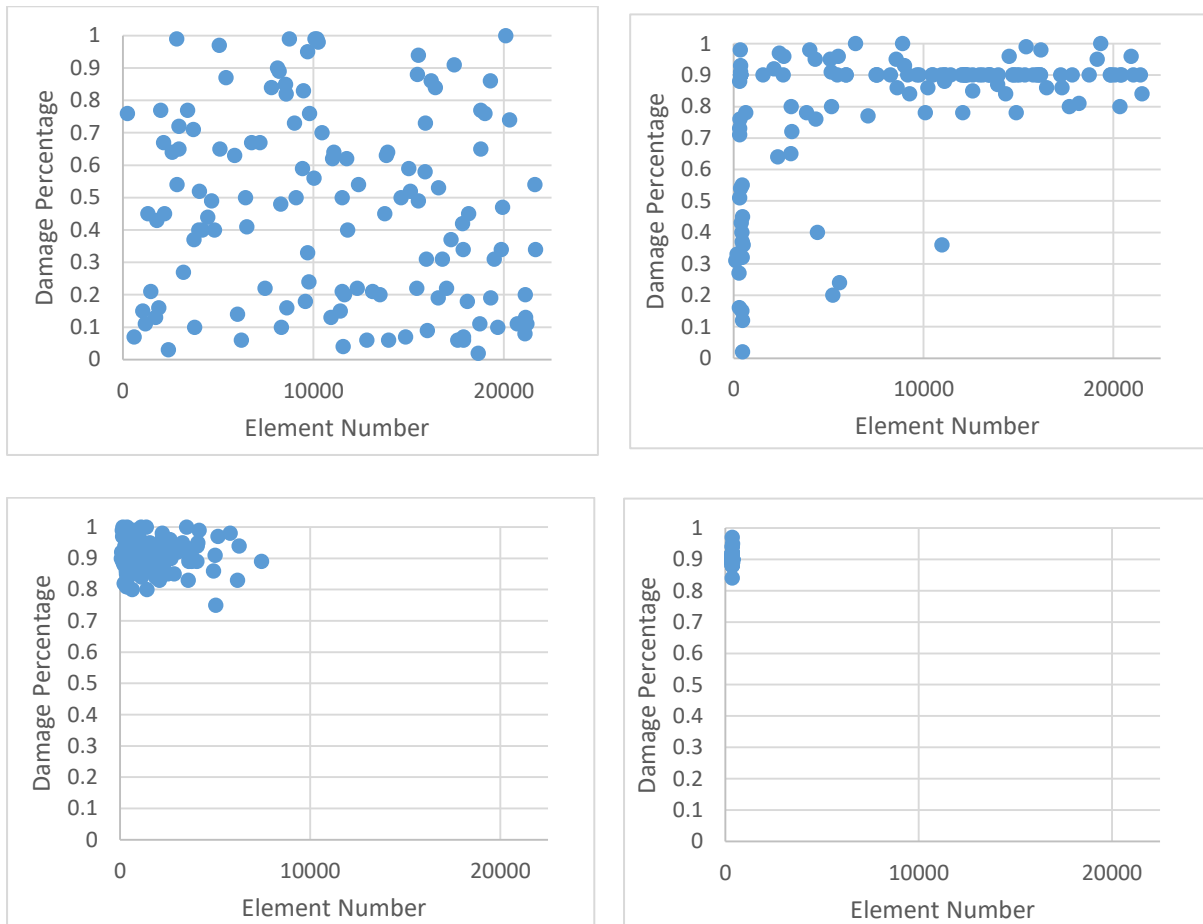


Figure (5.31) Distribution and convergence of particles towards target (damaged element and severity) in first, 25, 50 and 75 iteration for second case

### 5.6.2.3 Third Case

In the third scenario, there were 160 particles. Based on the data, the PSO technique identified the damage in iteration number 61, and approximately 86.25% of the particles revealed the damage element and damage percentage. For each iteration, objective function is shown in Figure (5.32).

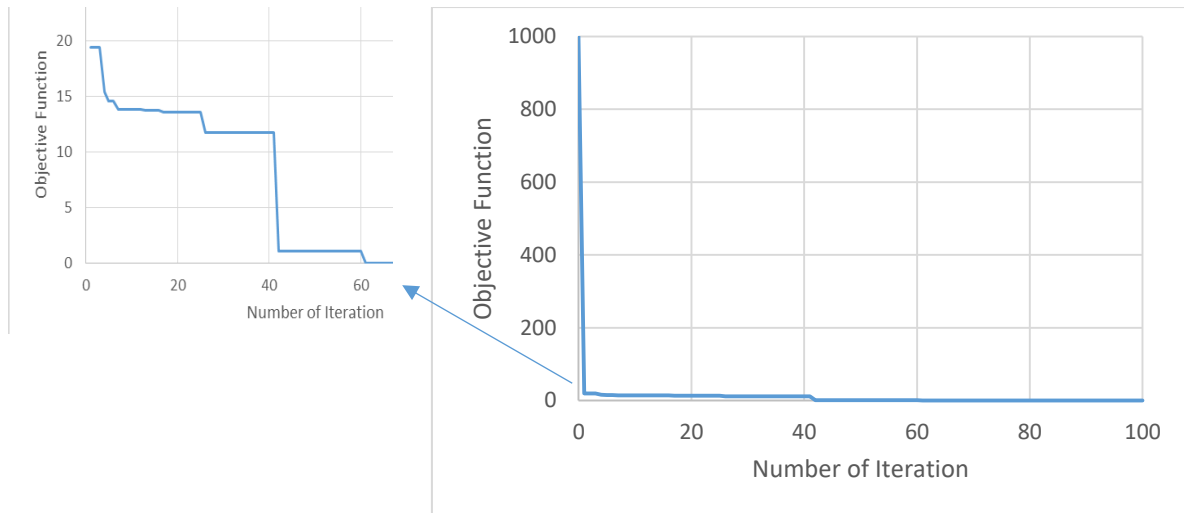


Figure (5.32) Convergence of objective function for third case

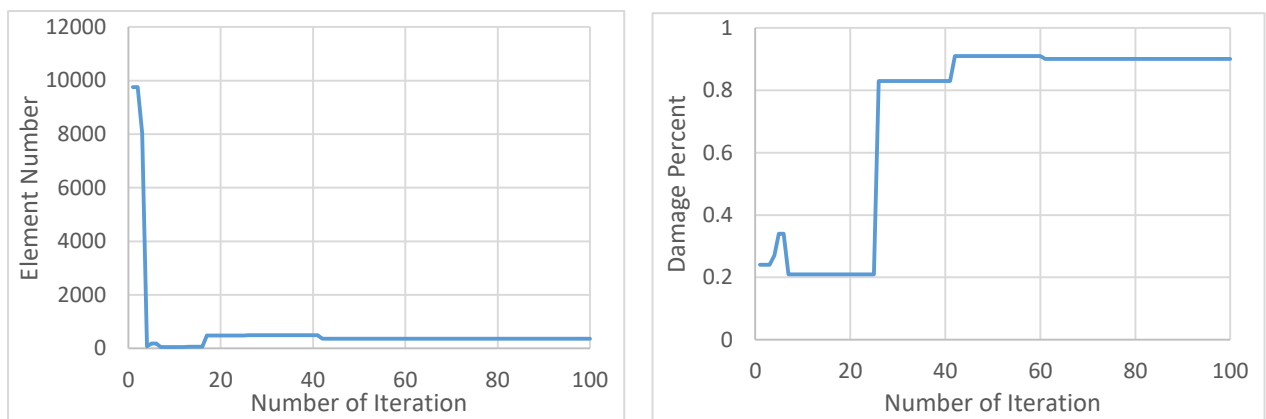


Figure (5.33) History of damaged element number and damage percentage for third case

from this three cases with different in number of particles ,when number of particles equal to 100 about only 82 % from particles discovered the damage element and damage percentage, but for 130 and 160 the particles discovered the damage about (98 %- 97.7%), respectively. So in this study the 130 particles was adopted.

# CHAPTER SIX

## CHAPTER SIX

### Damage Detection Results of Using SHM Technique for Adopted Structural Model

#### 6.1. General

In this chapter, the proposed SHM technique using PSO method was applied for the structural minaret model to detect damage and its characteristics, damage location and percentage. Four different locations of damage in FE minaret model were used. The results of adopted SHM technique were extracted and discussed. Also, three different damage percentages, (high, medium and low) were taken and the results were extracted and discussed.

#### 6.2. Selecting Weighting Factors in the Adopted SHM Technique

There are significant effect of weighting factors for the parameters included in the objective functions adopted for PSO method used in the proposed SHM technique. To select the two weighting factors ( $Wf$  and  $Wd$ ) in the chosen target function, three different damage scenarios were used as listed in Table (6.1) as a sensitivity analysis. Those two factors,  $Wf$  and  $Wd$ , are multiply by the parameters  $Freq$  and  $Disp$ , respectively as mention in Eq. (5.1), as listed in Table (6.2).

Table (6.1) Three different scenarios of damage selecting in sensitivity analysis

	Scenario 1	Scenario 2	Scenario 3
Element damaged	14697	1000	1000
Damage percentage	0.9	0.9	0.5

Table (6.2) Result of *Freq* and *Disp* values for three different scenarios

Scenario number	<i>Freq</i>	<i>Disp</i>
Scenario 1	2.12E-07	3.30E-03
Scenario 2	2.59E-08	3.74E-03
Scenario 3	1.18E-08	3.30E-03
average	1.18E-08	0.344E-04

from results, the final adopted values of weighting factors,  $Wf$  and  $Wd$ , in the proposed SHM technique are  $10^8$  and  $10^4$ , respectively.

### 6.3. Damage Detection for Different Scenario Cases (Damage Location and Percentage) for the Minaret Structural Model

In this study, six damage scenarios were adopted, in the first scenario the damaged element is near the base with damage percentage of 0.9, the second scenario the damaged element is in the middle of the minaret body with damage percentage of 0.9, in the third scenario the damaged element is on balcony with damage percentage of 0.9 and in the fourth, fifth and sixth scenarios the same damaged element is in the dome with different damage percentages 0.9, 0.5 and 0.1), respectively, as shown in Table (6.3).

Table (6.3) Damaged element and percentage and location for damage scenarios

No. of scenarios	Sc.1	Sc. 2	Sc. 4	Sc. 3	Sc. 5	Sc. 6
Damage element	3055	14697	445	1000	1000	1000
Damage percentage	0.9	0.9	0.9	0.9	0.5	0.1
Damage location	base	body	balcony	dome	dome	dome

The results of modal analysis, natural frequencies and mode shapes, for six damage scenarios model were display to compare with the result of intact model as listed in Table (6.4).

Table (6.4) Natural frequencies of intact, 1<sup>st</sup>, 2<sup>nd</sup>, 3<sup>rd</sup>, 4<sup>th</sup>, 5<sup>th</sup>, 6<sup>th</sup> and 7<sup>th</sup> modes

mode	intact	first scenario	second scenario	third scenario
1	3.393412268913	3.393412046166	3.393355187526	3.393370575629
2	3.479856104073	3.479856098387	3.479833668905	3.479703969119
3	11.91664111322	11.91664057788	11.91651012791	11.91593646978
4	12.16794926303	12.16794926100	12.16787759511	12.16627318591
5	21.34992632022	21.34992629970	21.34946637354	21.34823164126
6	27.17613329718	27.17613033376	27.17488015028	27.17540848702
7	29.13207558373	29.13207557116	29.13190267611	29.13153108964

fourth scenario	fifth scenario	sixth scenario
3.393394896588	3.393403176969	3.393410549632
3.479841530921	3.479848556528	3.479854689847
11.91594406646	11.91627584037	11.91657196519
12.16744041902	12.16768613246	12.16790001703
21.34982495374	21.34987380453	21.34991647450
27.17567351100	27.17589299807	27.17608790364
29.13037817111	29.13119851301	29.13191146589

As listed in the Table (6.4), the differences of natural frequency values among damage scenarios and intact model are very small. Even with very small differences, the proposed SHM technique is able to detect damage due to the significant sensitivity for objective function used in PSO method.

For SHM technique the number of the included elements is 21685, Range of Damage Reduction Factor (0.01 - 1) and the Size of Searching Space is (2168500) the number of iterations and number of particles were (100 - 130) respectively. The weighting factors  $W_f$  and  $W_d$  are shown in **section (6.2)** is ( $10^8$  and  $10^4$ ) respectively, as listed in Table (6.5) .

Table (6.5) Input Parameters in SHM technique for damage detection

Parameter Description	Parameter Value
Number of Included Elements	21685
Range of Damage Reduction	0.01 - 1
Size of Searching Space	2168500
Number of particle	130
Number of Iterations	100
Weighting Factors ( $W_f$ , $W_d$ )of obj- fun	( $10^8$ and $10^4$ )

The coefficients for PSO method ( $W$  ,  $C_1$  ,  $C_2$ ) was adopted the Eq. (5.4) (5.5) (5.6) respectively.

### 6.3.1. First scenario

In the first scenario, the crack occurred in the base of the minaret, which is 0.25 m away from the fixed support. The damage was represented by decreasing the modulus of elasticity 90% that means the residual value is 10%. The material properties of the intact and damaged element are listed in Table (6.6).

Table (6.6) Material properties of intact and damaged element for first scenario

Material properties	Intact elements	Damage element
Modulus of Elasticity (MPa)	3400	340

Mass Density (kg/m <sup>3</sup> )	1200	1200
Poisson's Ratio	0.2	0.2

The Figure (6.1) shows the damaged element number of 3055 and damage percentage of 0.9 with its position in the FE minaret model for the first damage scenario case.

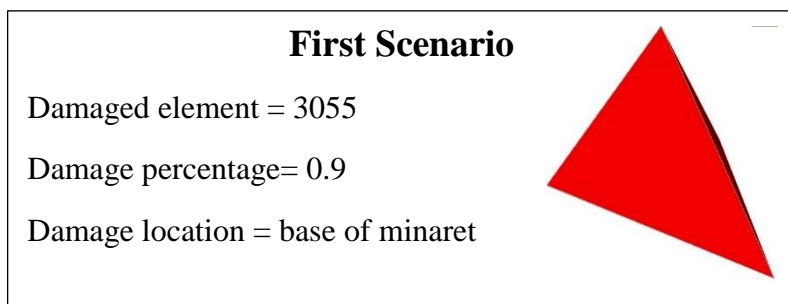


Figure (6.1) The damaged element, damage percentage and damage location of first scenario

After performing the proposed SHM technique to detect the damage using particle swarm optimization (PSO) method by MATLAB software, the first scenario showed very efficient of the convergence of objective function in the SHM technique. Where the SHM technique detected the damage in iteration number 42 by particle number 33. After that, in iteration number 50 about 12.3% of particles detected the damage. In the iteration number 74, all particles (130)

have detected the exact target solution, damaged element and percentage. While, the SHM technique used only 0.44% to detect the optimum solution from the searching space size of 2168500 solutions. Figure (6.2) shows convergence of objective function with optimum iterations during the SHM technique procedures.

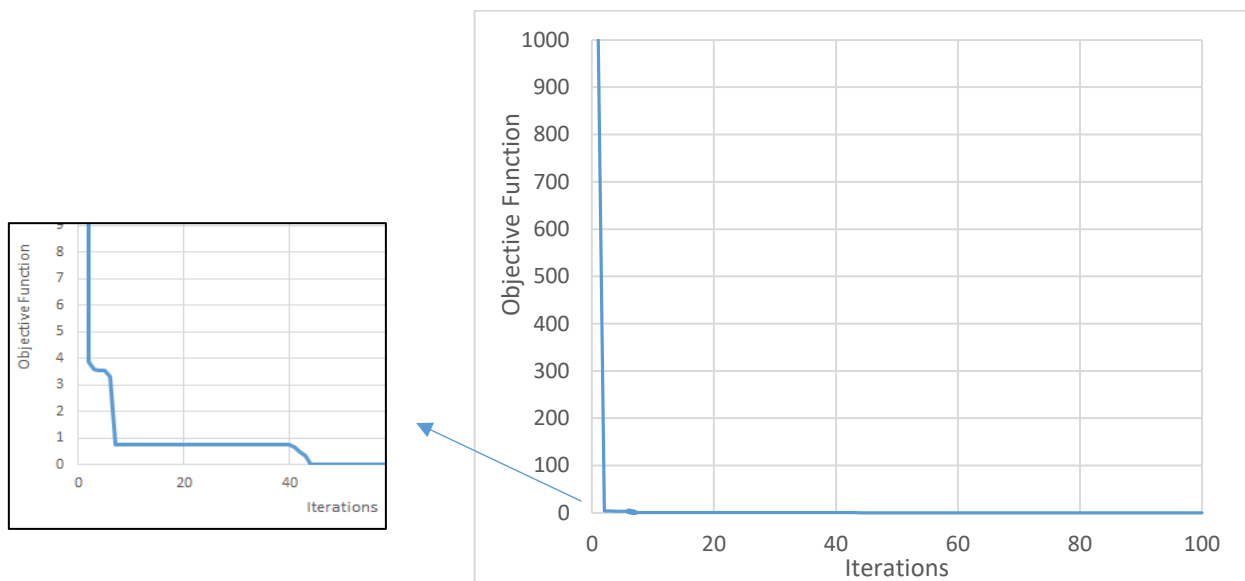
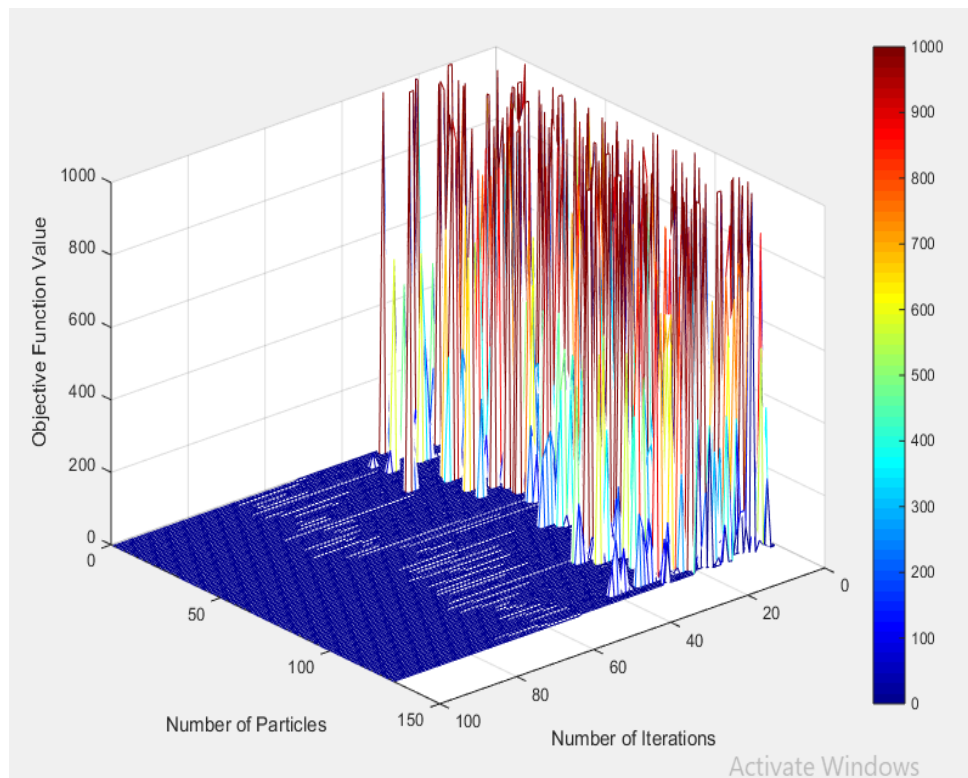


Figure (6.2) Convergence of objective function for first scenario

From Figure (6.2), it is noticed the line of objective function goes down directly from the assumed initial value of 1000 to almost down because the optimum objective function in the first iteration was at lower value of 3.86 in element 3001 and damage percentage of 0.7. The damaged element was detected in iteration number 6, as shown in Figure (6.3) with a high convergence of optimum element number, but the damage percentage was detected in iteration number 42 as shown in figure (6.4).

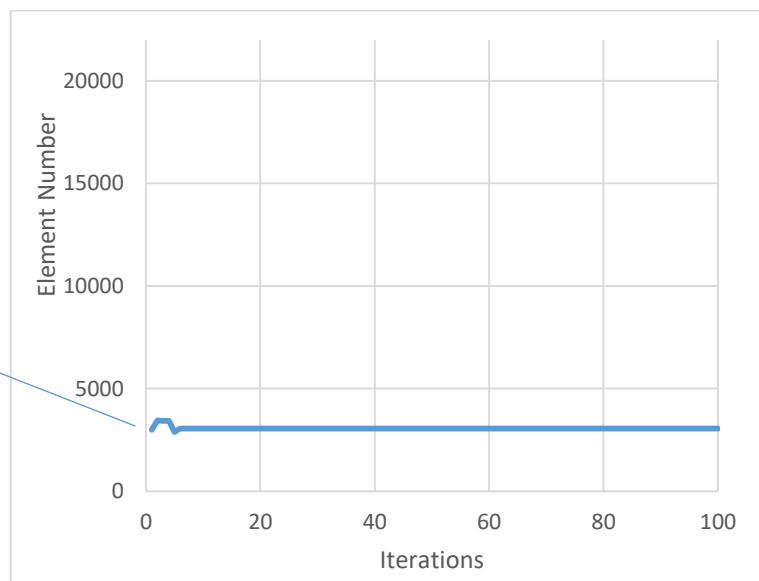
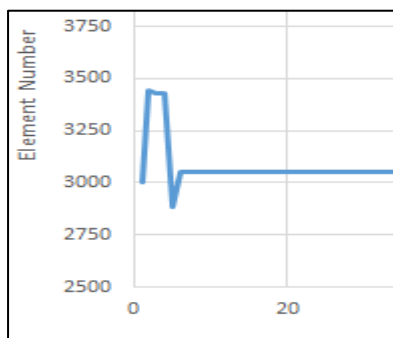
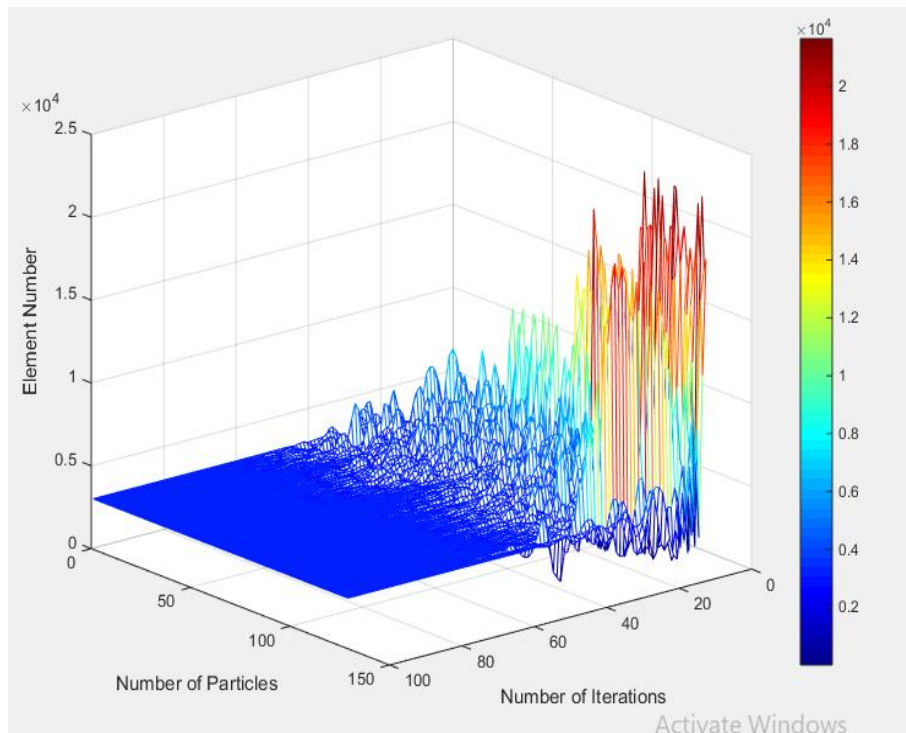


Figure (6.3) History of damaged element number for first scenario

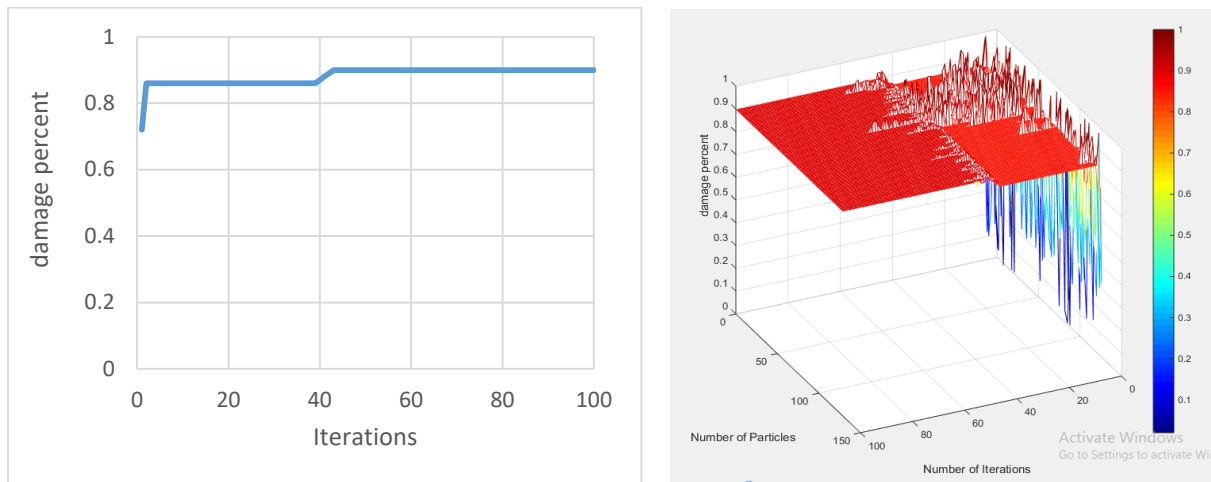


Figure (6.4) History of damage percentage for first scenario

From Figure (6.3), it is obvious that the first optimum element is 3001 which is very close to damaged element 3055 compared with the total number of elements. Therefore, the adopted technique needed just 6 iterations to detect the damaged element, but Figure (6.4) shows the first optimum damage percentage of 72%, while, the technique needed to 42 iterations to reach damage percentage of 90%.

The convergence of the particles towards the damage value within the searching space can be illustrated in Figure (6.5), where it shows the distribution of particles in the searching space for the first iteration and iteration number of 25, 50, 75 and 100. It is noted that in iteration number 75 all particles of 130 discovered the exact target (solution), damaged element and the percentage of damage.

## Model

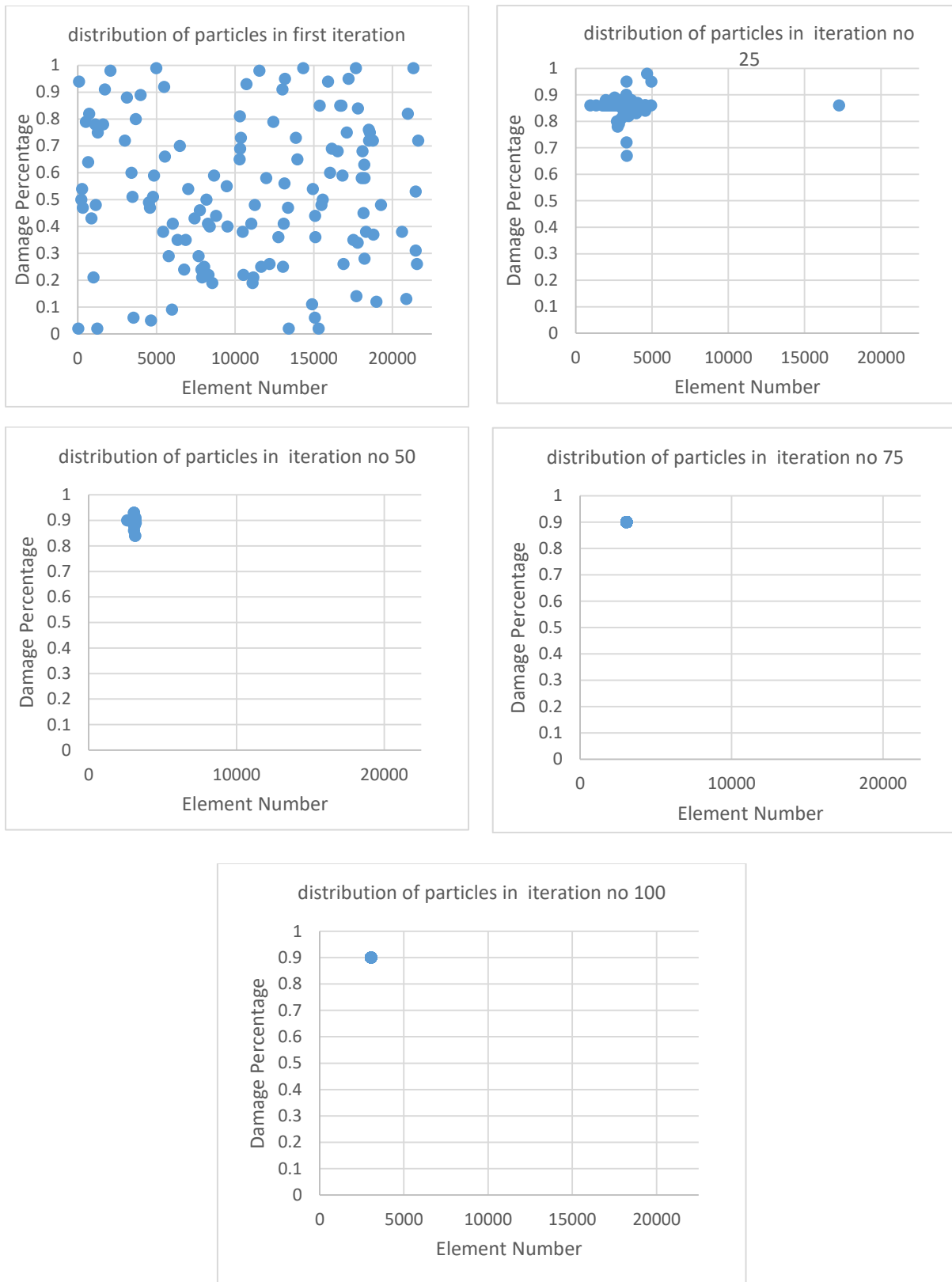


Figure (6.5) Distribution and convergence of particles towards damage in first, 25, 50, 75 and 100 iteration

Also from Figure (6.5), it can be seen how powerful a single particle is in detecting damage. Therefore, the ability of a single particle to move towards the detected damaged element and its percentage can be illustrated as in Figure (6.6) which shows the ability of the first particle to move towards the detected damage element and damage percentage.

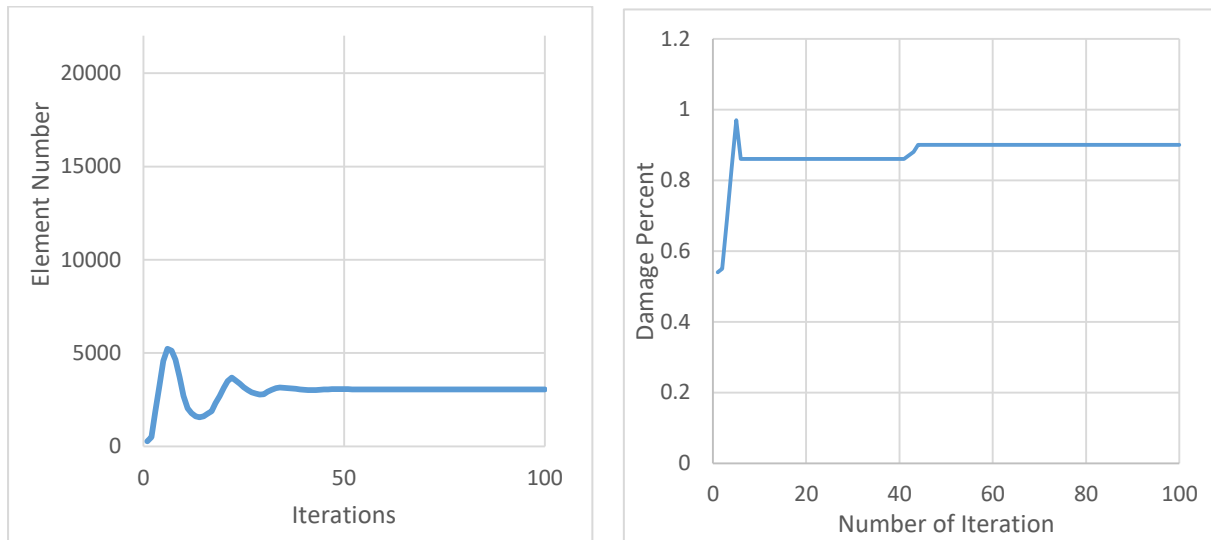


Figure (6.6) Ability the first particle to move towards the detected damaged element

As a result, the SHM technique detected the exact damaged element and percentage with only 74 iterations, this proved the efficiency of the adopted technique.

### 6.3.2. Second scenario

In the second scenario, the crack occurred in the middle of the minaret body, near the end area fixed with the shrine. The damage was represented by decreasing the modulus of elasticity 90% that means the residual value is 10%. The material properties of the intact and damaged element are listed in Table (6.7).

Table (6.7) Material properties of intact and damaged element for second scenario

material properties	Intact elements	Damage element
Modulus of Elasticity (MPa)	3400	340
Mass Density (kg/m <sup>3</sup> )	1200	1200
Poisson's Ratio	0.2	0.2

The Figure (6.7) shows the damaged element number of 14697 and damage percentage of 0.9 with its position in the FE minaret model for the second damage case.

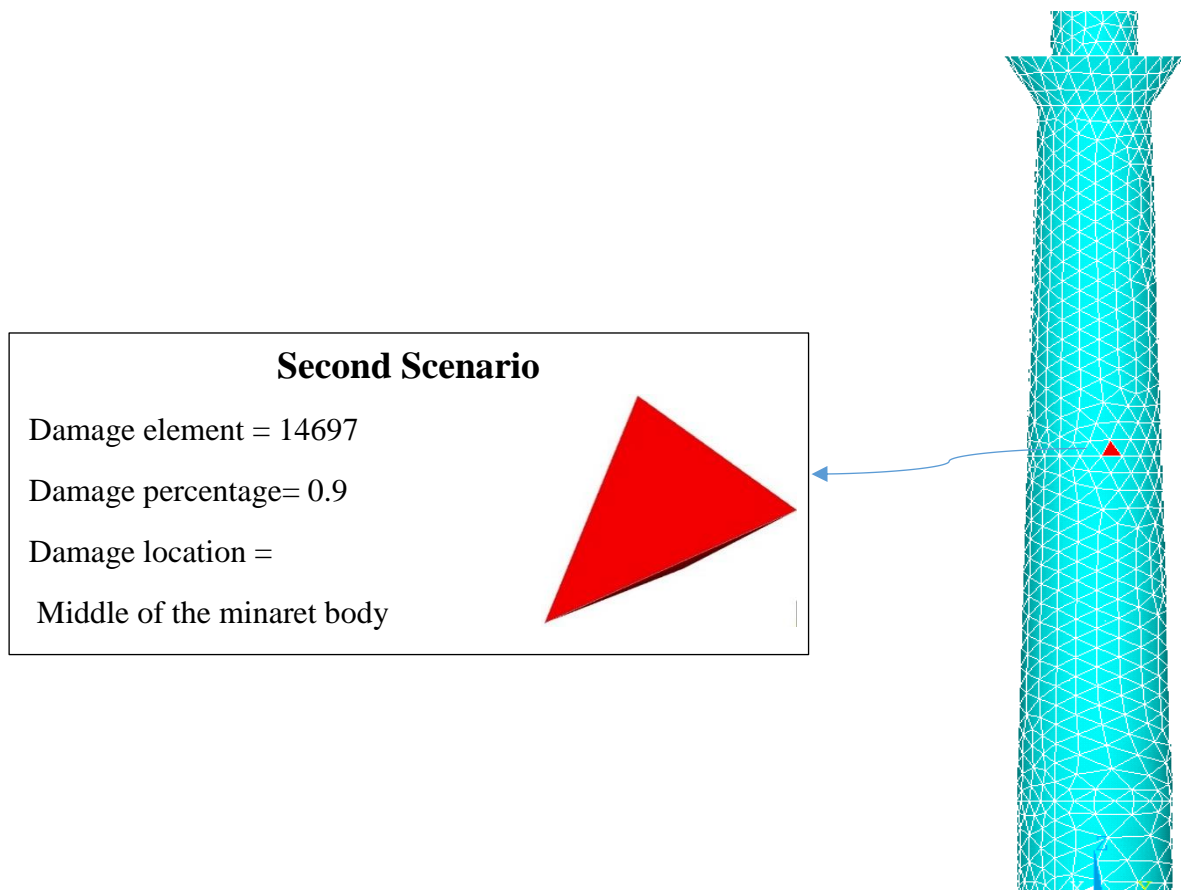


Figure (6.7) The damaged element, damage percentage and damage location of second scenario

The second scenario showed a good convergence of objective function in the SHM technique. Where the SHM technique detected the damage in iteration number 70 by particle number 19. After that, in the iteration number 95, all particles (130) have detected the exact target solution, damaged element and percentage. While, the SHM technique used only 0.57% to detect the optimum solution from the searching space size of 2168500 solutions. Figure (6.8) shows convergence of objective function with optimum iterations during the SHM technique procedures.

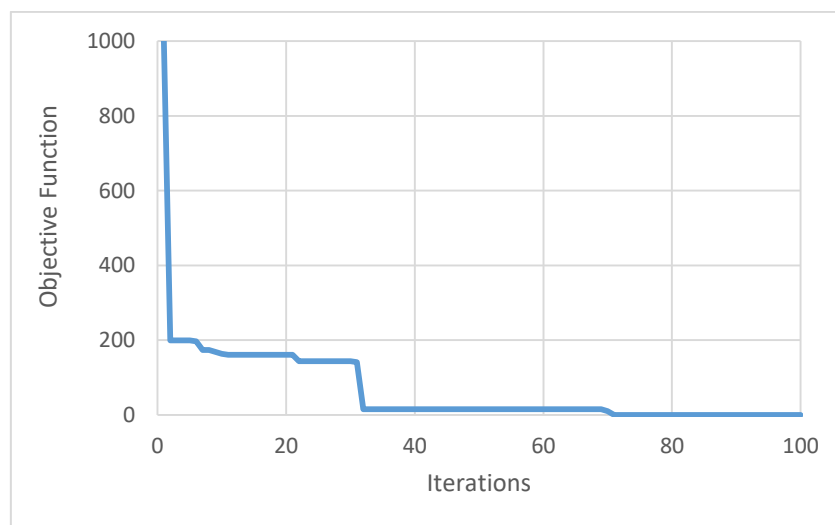
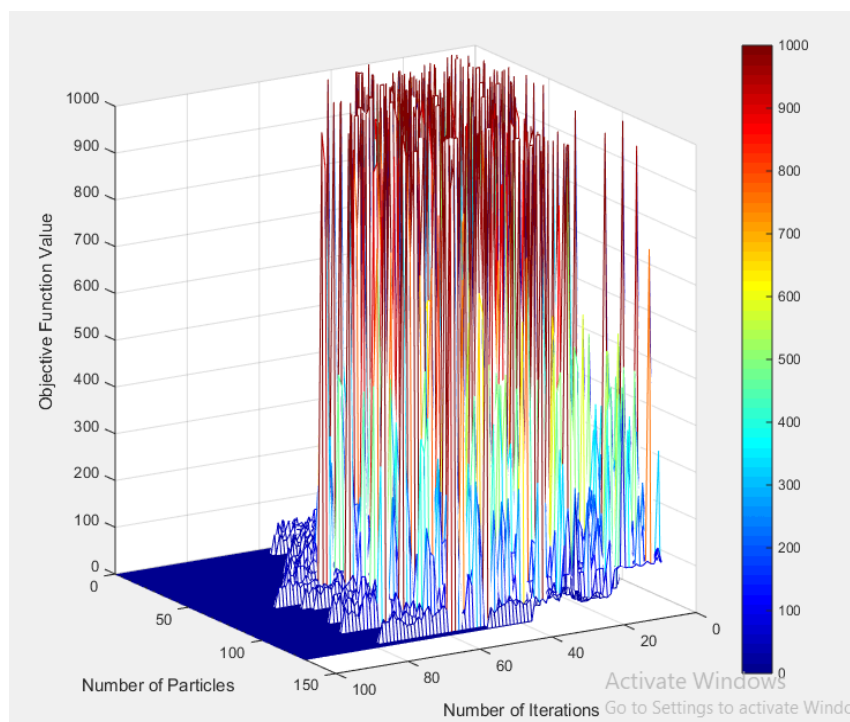


Figure (6.8) Convergence of objective function for second scenario

From Figure (6.8), it is noticed the line of objective function goes down directly from the assumed initial value of 1000 to about 200 because the optimum objective function in the first iteration was 199.0461 in element 12728 and the damage percentage of 0.45. The damaged element was detected in iteration number 31, as shown in Figure (6.9) with a high convergence of optimum element number, but the damage percentage was detected in iteration number 70 as shown in Figure (6.10).

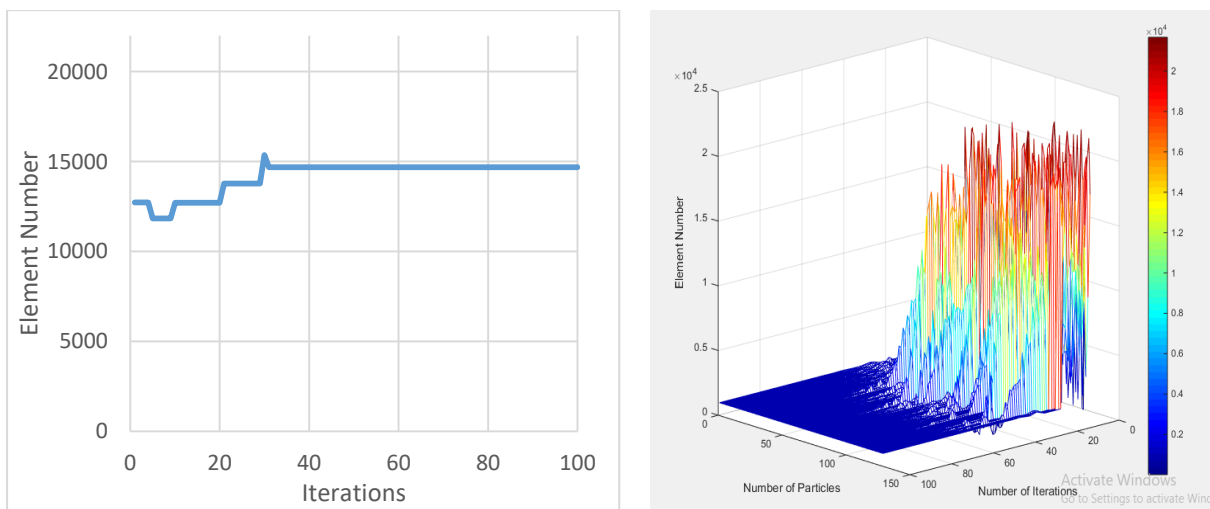


Figure (6.9) History of damaged element number for second scenario

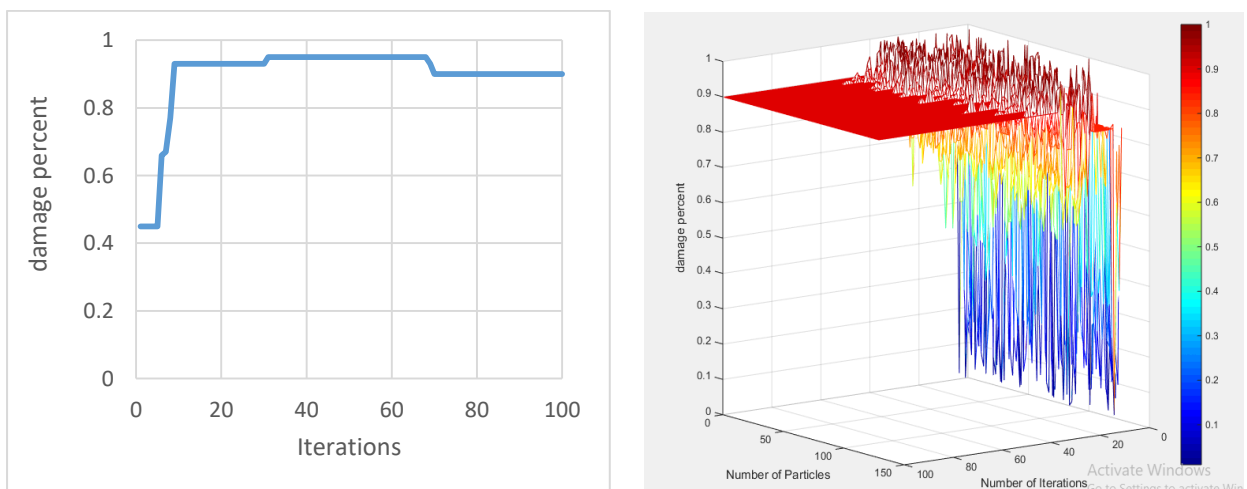


Figure (6.10) History of damage percentage for second scenario

From Figure (6.9), it is obvious that the first optimum element is 12728 which is far from damaged element 14697 compared with the first scenario. Therefore, the adopted technique needed just 31 iterations to detect the damaged element, but Figure (6.10) shows the first optimum damage percentage of 45% is far from damage percentage 90% compared with the first scenario, so the technique needed to 70 iterations to reach damage percentage of 90%.

The convergence of the particles towards the damage value within the searching space can be illustrated in Figure (6.11), where it shows the distribution of particles in the searching space for the first iteration and iteration number of 25, 50, 75 and 100. It is noted that in iteration number 100 all particles of 130 discovered the exact target (solution), damaged element and the percentage of damage.

## Model

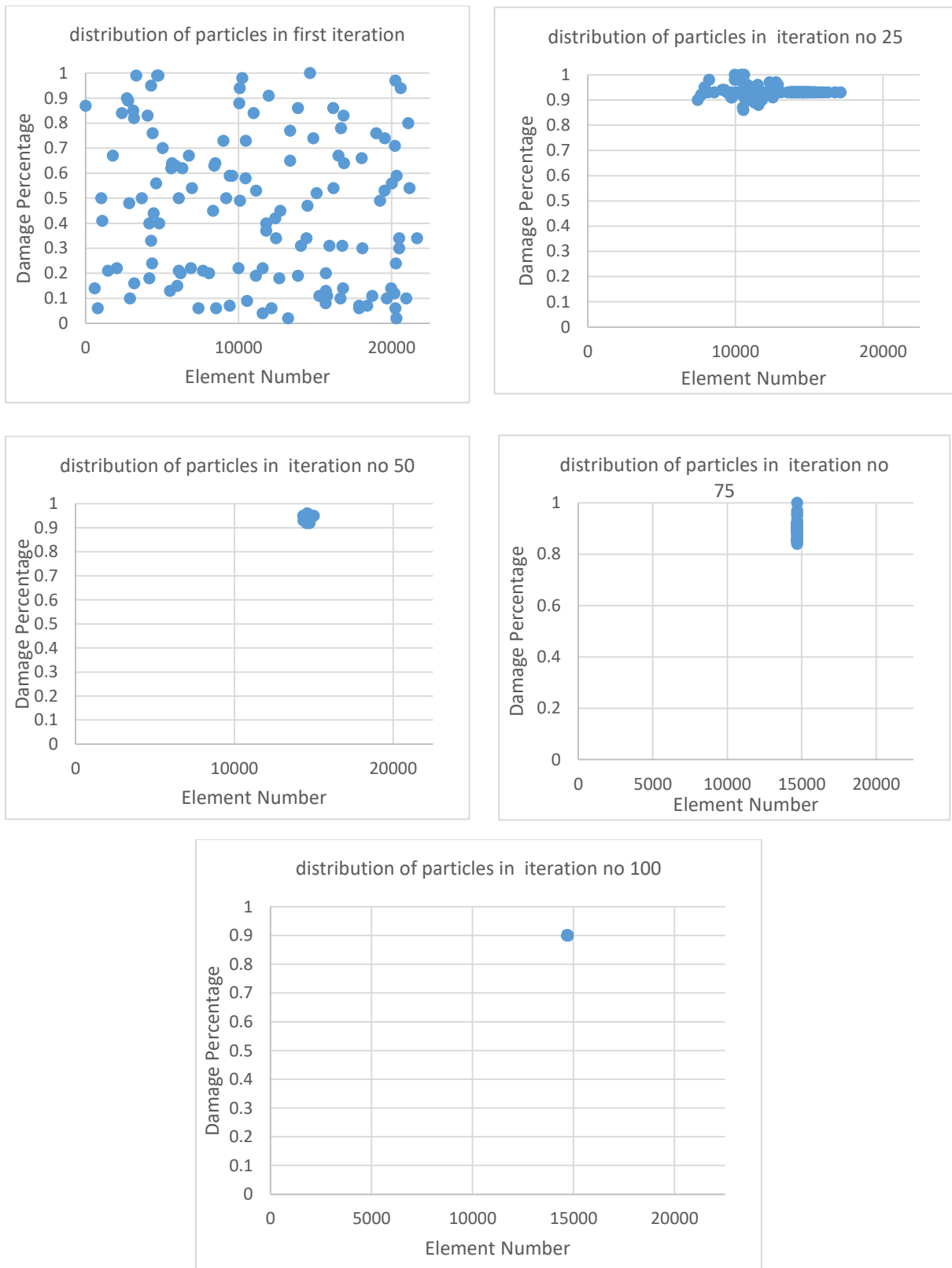


Figure (6.11) Distribution and convergence of particles towards damage in first, 25, 50, 75 and 100 iteration

The ability of a single particle to move towards the detected damaged element and damage percentage can be illustrated as in Figure (6.12) which shows the ability of the first particle to move towards the detected damaged element and damage percentage.

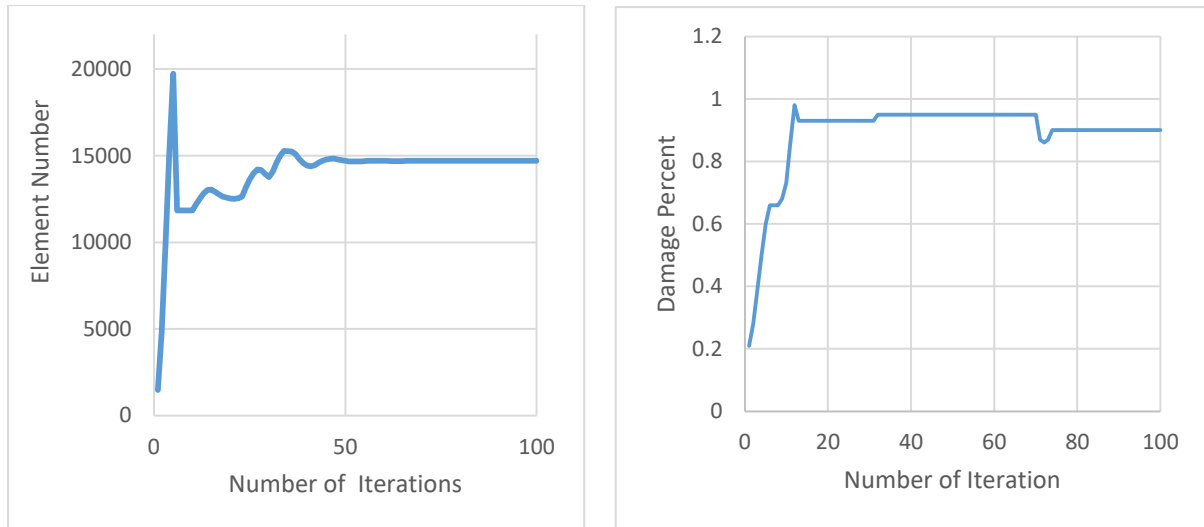


Figure (6.12) Ability the first particle to move towards the detected damaged element

As a result, the SHM technique detected the exact damaged element and percentage with only 90 iterations, this proved the efficiency of the adopted technique.

### 6.3.3. Third scenario

In the third scenario, the crack occurred in balcony. The damage was represented by decreasing the modulus of elasticity 90% that means the residual value is 10%. The material properties of the intact and damaged element are listed in Table (6.8).

Table (6.8) Material properties of intact and damaged element for third scenario

Material properties	Intact elements	Damage element
Modulus of Elasticity (MPa)	3400	340
Mass Density (kg/m <sup>3</sup> )	1200	1200
Poisson's Ratio	0.2	0.2

The Figure (6.13) shows the damaged element number of 445 and damage percentage of 0.9 with its position in the FE minaret model for the third damage scenario case.

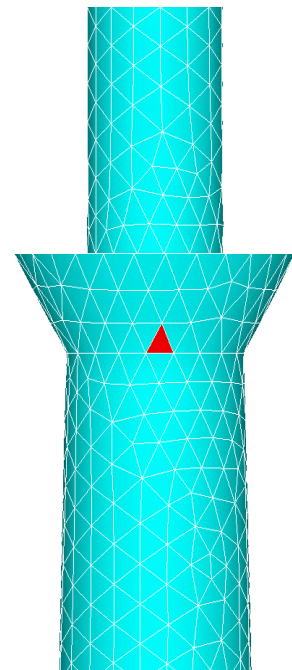
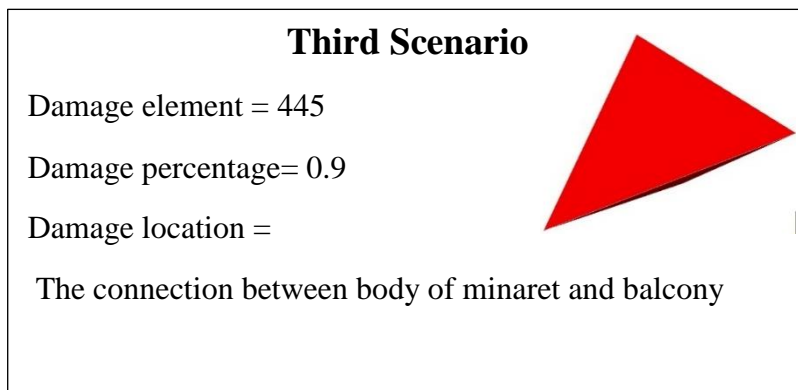


Figure (6.13) The damaged element, damage percentage and damage location of third scenario

After performing the proposed SHM technique to detect the damage using particle swarm optimization (PSO) method by MATLAB software, the first scenario showed very efficient of the convergence of objective function in the

SHM technique. Where the SHM technique detected the damage in iteration number 27 by particle number 71. After that, in the iteration number 84, all particles (130) have detected the exact target solution, damaged element and percentage. While, the SHM technique used only 0.50% to detect the optimum solution from the searching space size of 2168500 solutions. Figure (6.14) shows convergence of objective function with optimum iterations during the SHM technique procedures.

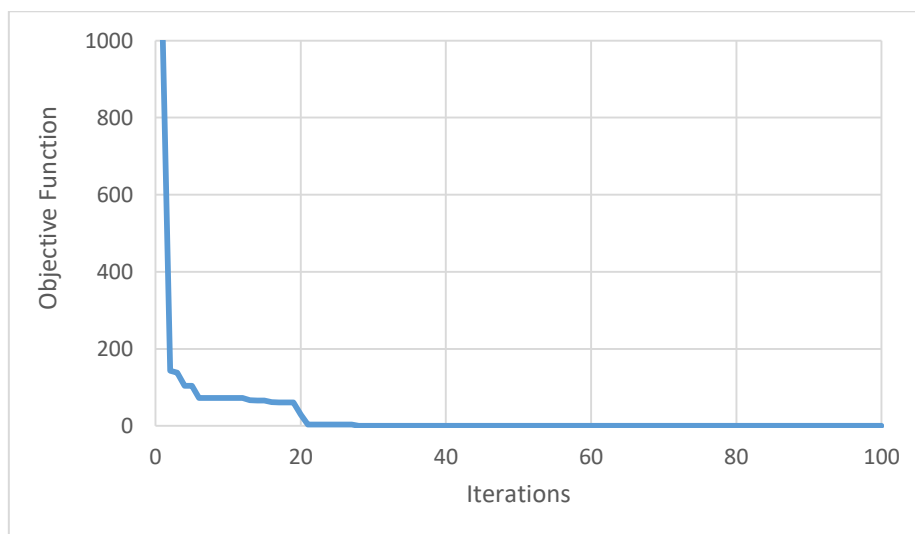
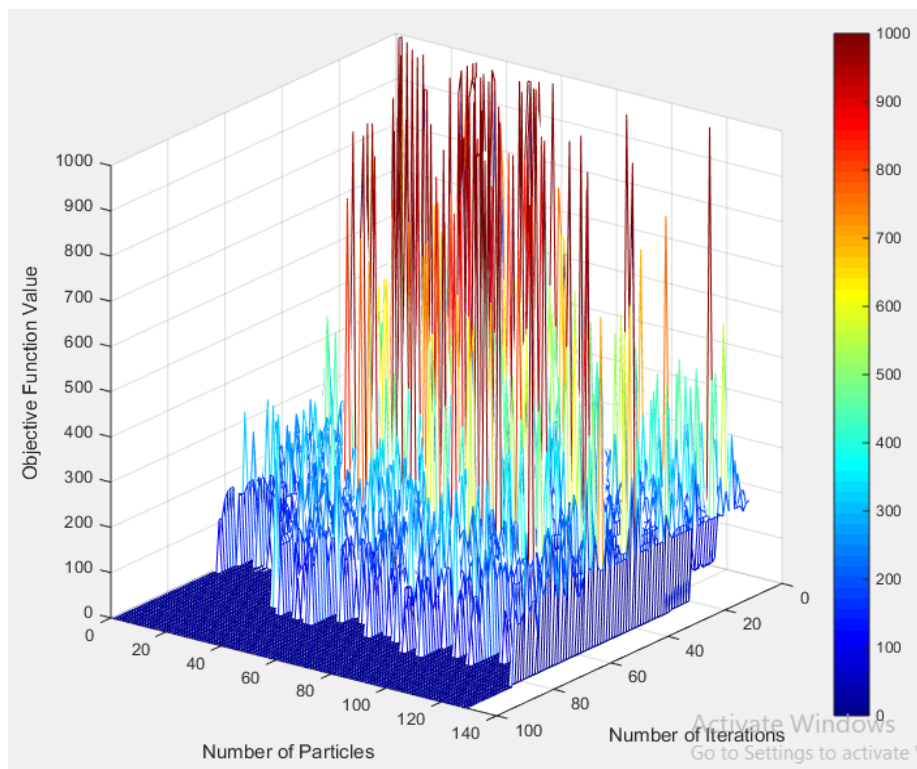


Figure (6.14) Convergence of objective function for third scenario

From Figure (6.14), it is noticed the line of objective function goes down directly from the assumed initial value of 1000 to the optimum objective function in the first iteration was 142.8465 in element 573 and damage percentage of 0.61. The damaged element was detected in iteration number 19, as shown in Figure (6.15) with a high convergence of optimum element number, but the damage percentage was detected in iteration number 27 as shown in Figure (6.16).

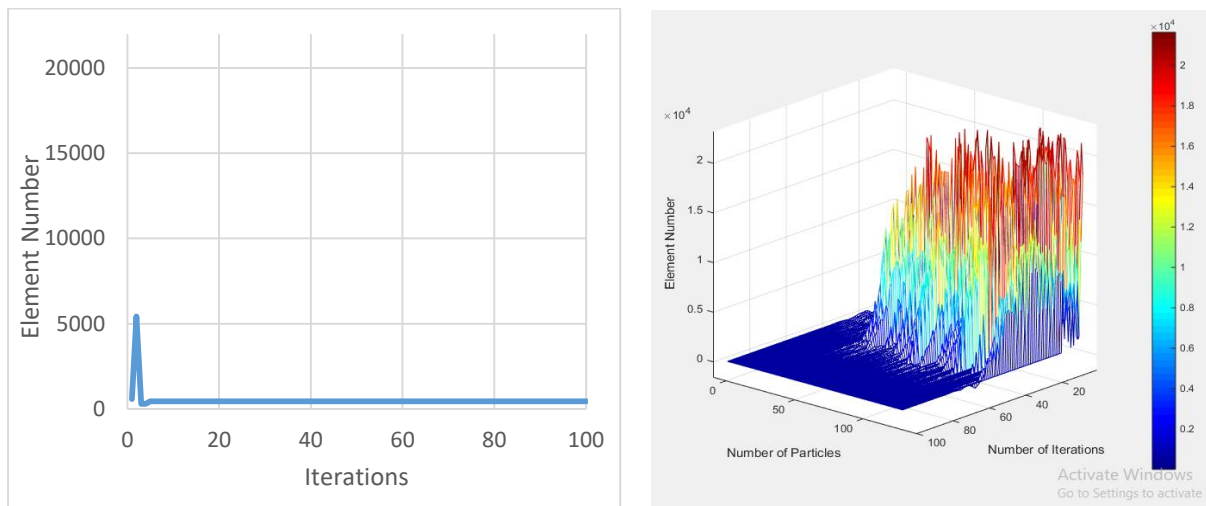


Figure (6.15) History of damaged element number for third scenario

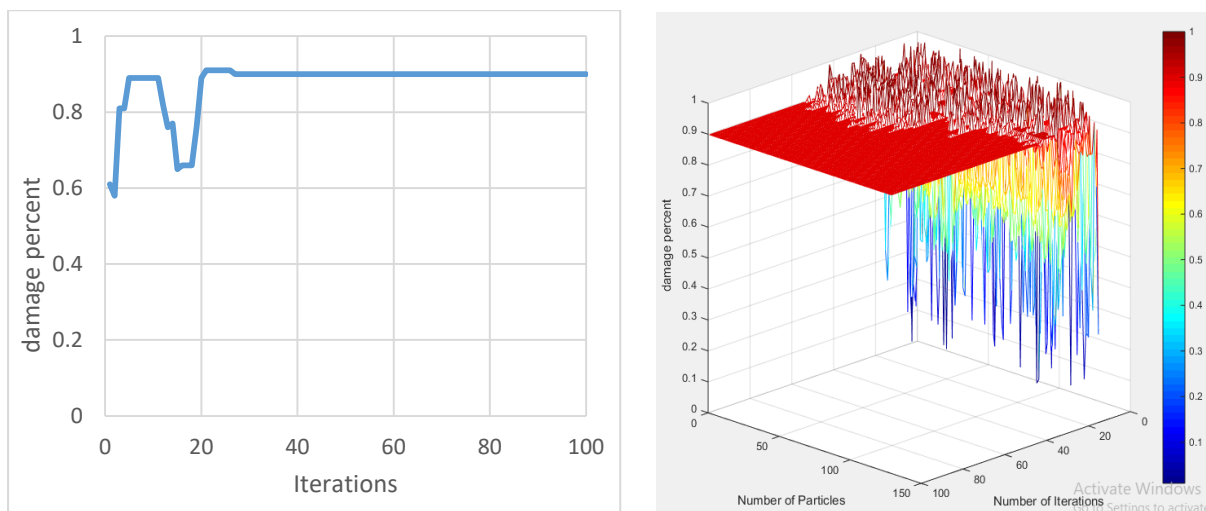


Figure (6.16) History of damage percentage for third scenario

From Figure (6.15), it is obvious that the first optimum element is 573 which is close to damaged element 1000 compared with the total number of elements. Therefore, the adopted technique needed just 19 iterations to detect the damaged element, but Figure (6.16) shows the first optimum damage percentage of 61%, while, the technique needed to 27 iterations to reach damage percentage of 90%.

The convergence of the particles towards the damage value within the searching space can be illustrated in Figure (6.17), where it shows the distribution of particles in the searching space for the first iteration and iteration number of 25, 50, 75 and 100. It is noted that in iteration number 75 that 90% of particles 130 discovered the exact target (solution), damaged element and the percentage of damage.

## Model

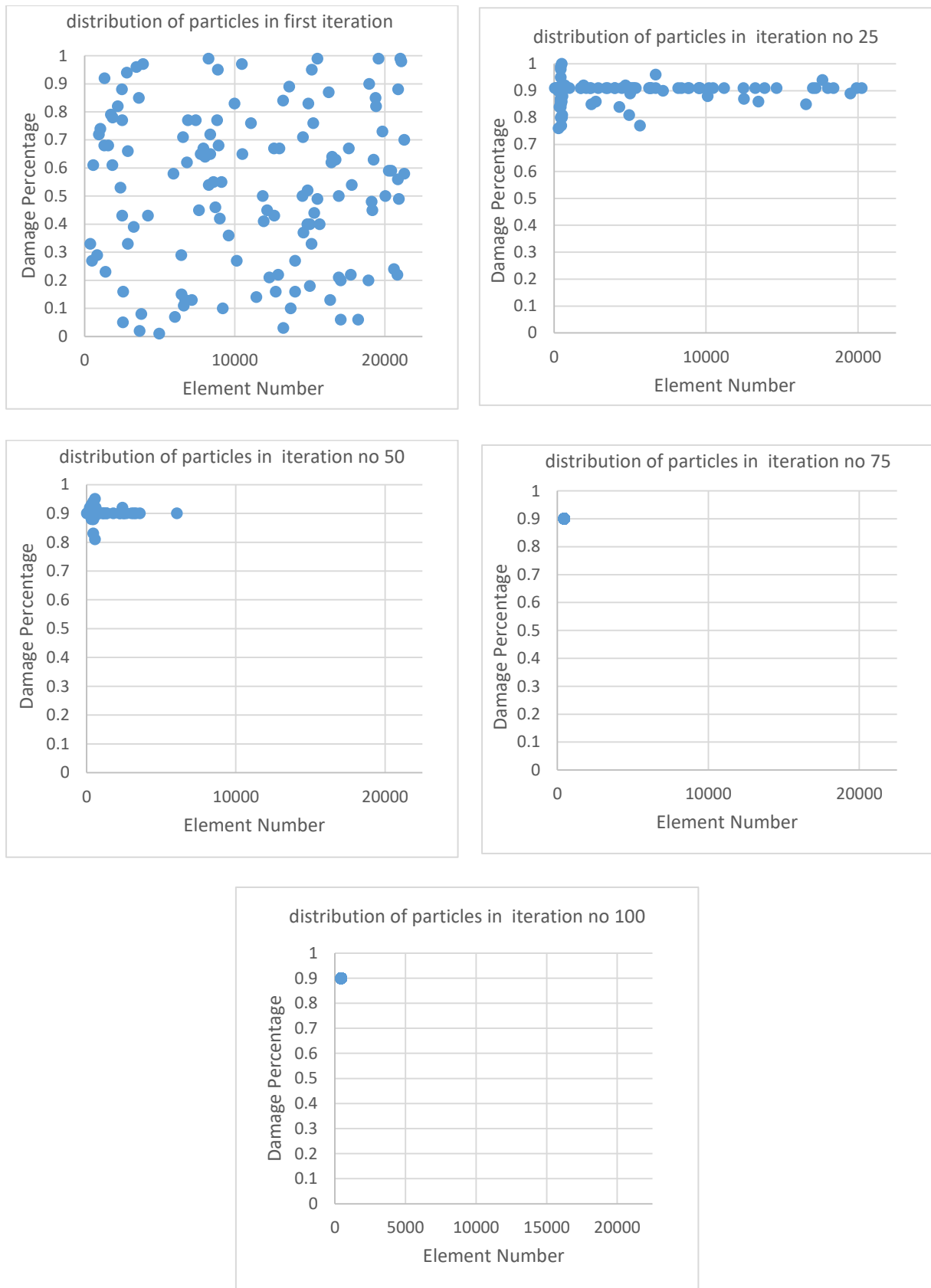


Figure (6.17) Distribution and convergence of particles towards damage in first, 25, 50 and 75 iteration

As a result, the SHM technique detected the exact damaged element and percentage with only 84 iterations, this proved the efficiency of the adopted technique.

#### 6.3.4. Fourth scenario

In the fourth scenario, the crack occurred in the dome of the minaret, which is very far from the fixed support. The damage was represented by decreasing the modulus of elasticity 90% that means the residual value is 10%. The material properties of the intact and damaged element are listed in Table (6.9).

Table (6.9) Material properties of intact and damaged element for fourth scenario

material properties	Intact elements	Damage element
Modulus of Elasticity (MPa)	3400	340
Mass Density (kg/m <sup>3</sup> )	1200	1200
Poisson's Ratio	0.2	0.2

The Figure (6.18) shows the damaged element number of 1000 and damage percentage of 0.9 with its position in the FE minaret model for the fourth damage scenario case.

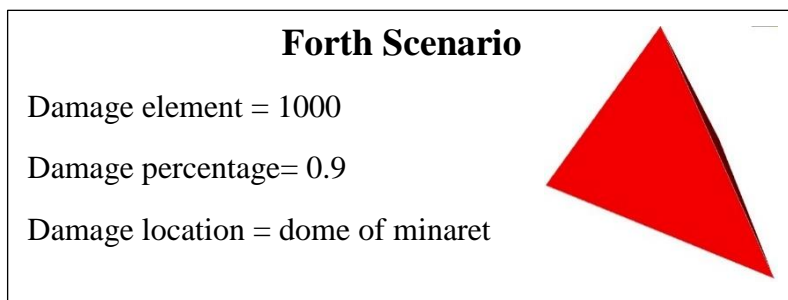


Figure (6.18) the damaged element, damage percentage and damage location of fourth scenario

The fourth scenario showed very efficient of the convergence of objective function in the SHM technique. Where the SHM technique detected the damage in iteration number 26 by particle number 74. After that, in the iteration number 83, all particles (130) have detected the exact target solution, damaged element and percentage. While, the SHM technique used only 0.50% to detect the optimum solution from the searching space size of 2168500 solutions. Figure (6.19) shows convergence of objective function with optimum iterations during the SHM technique procedures.

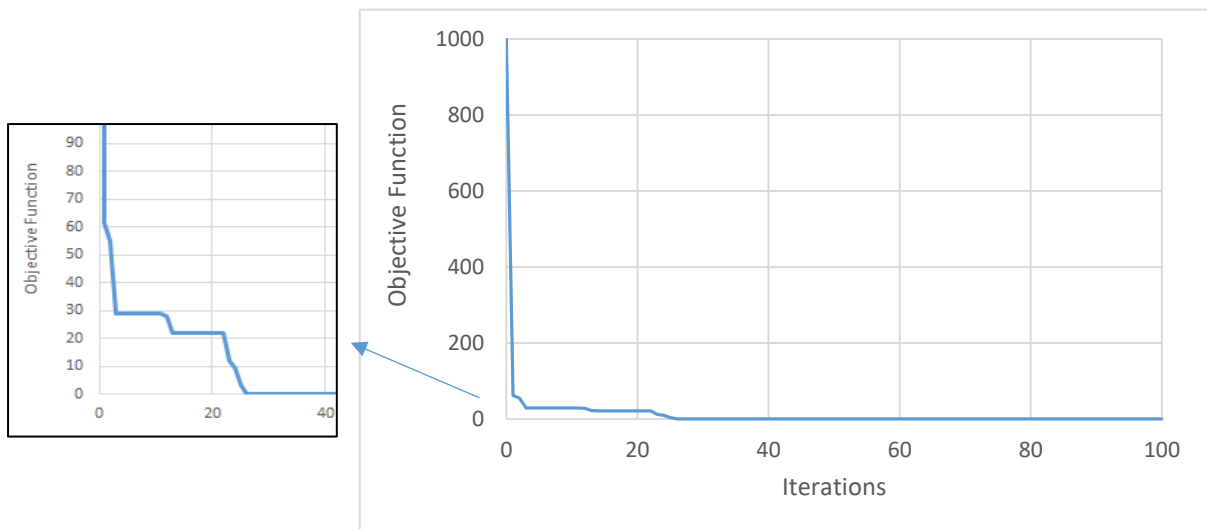
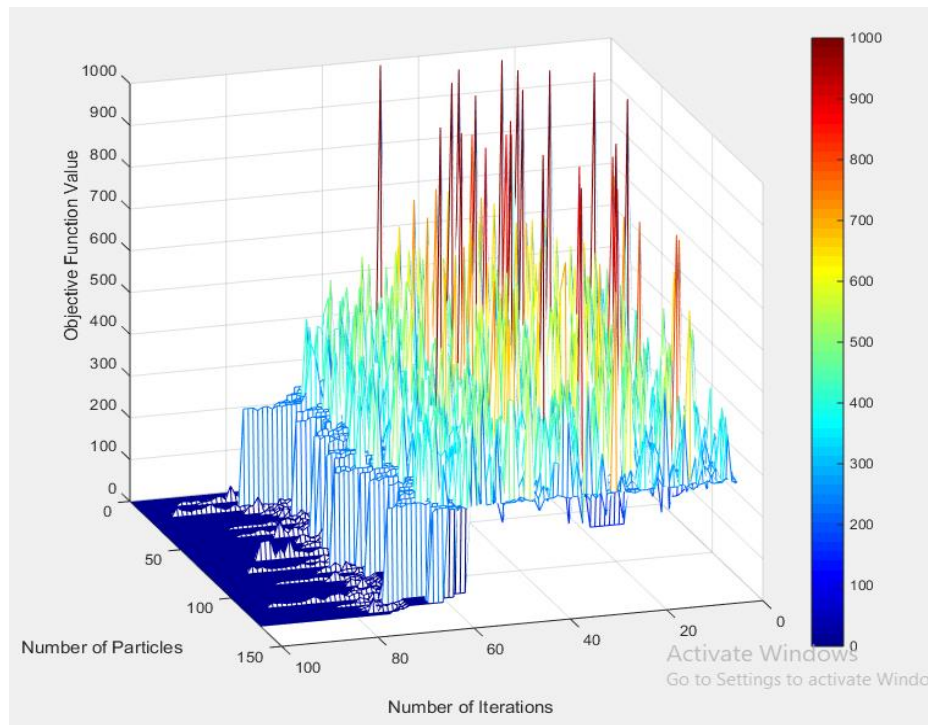


Figure (6.19) Convergence of objective function for fourth scenario

From Figure (6.19), it is noticed the line of objective function goes down directly from the assumed initial value of 1000 to the optimum objective function in the first iteration was 61.56 in element 2046 and damage percentage of 0.22. The damaged element was detected in iteration number 23, as shown in Figure (6.20)

with a high convergence of optimum element number, but the damage percentage was detected in iteration number 26 as shown in Figure (6.21).

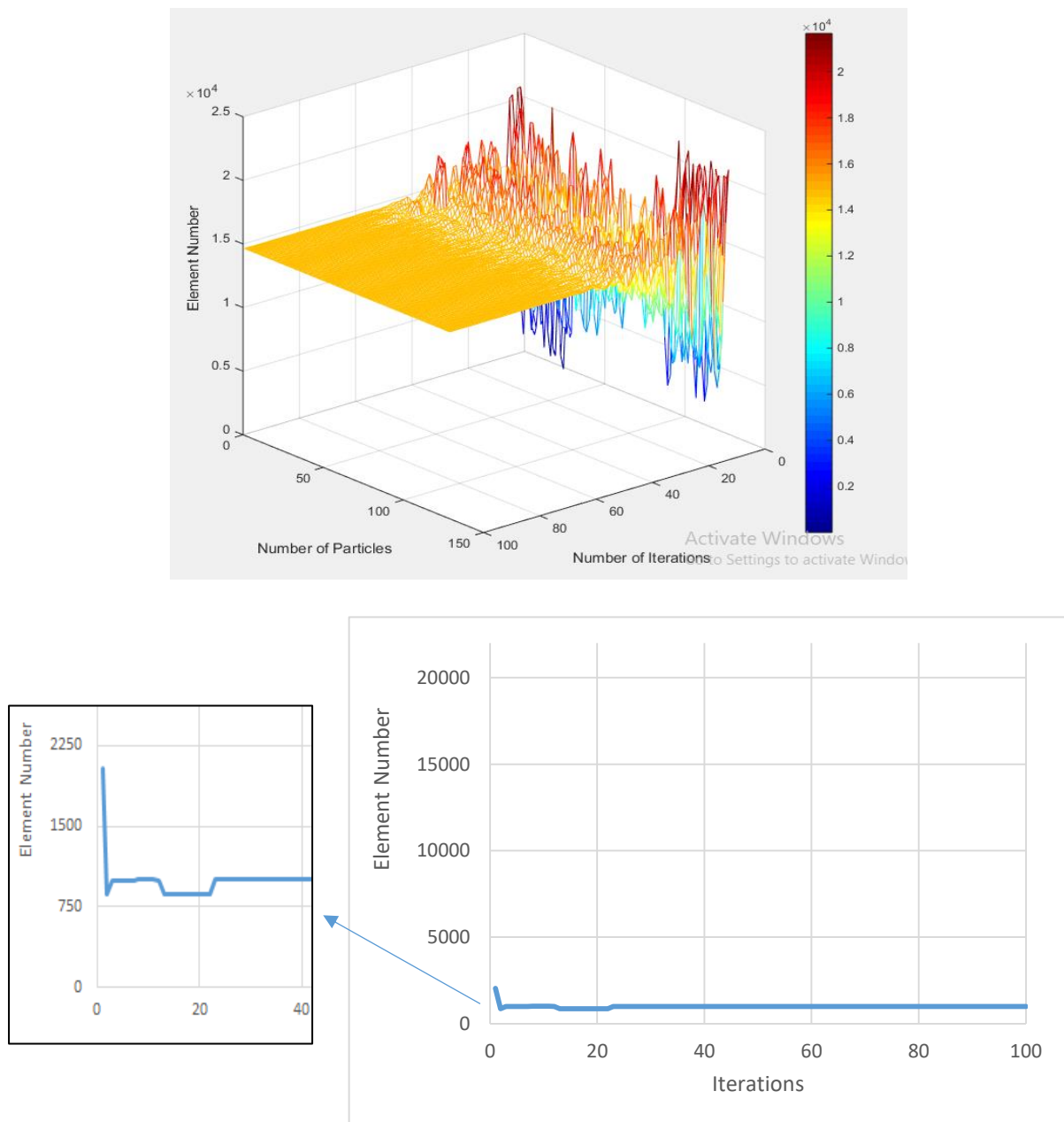


Figure (6.20) History of damaged element number for fourth scenario

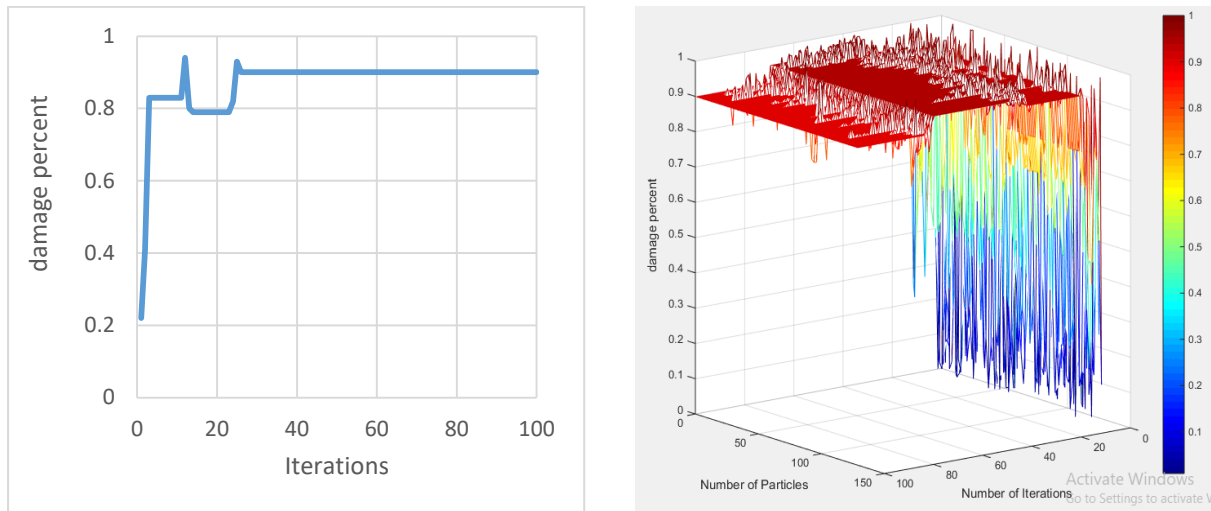


Figure (6.21) History of damage percentage for fourth scenario

From Figure (6.20), it is obvious that the first optimum element is 2064 which is close to damaged element 1000 compared with the total number of elements. Therefore, the adopted technique needed just 23 iterations to detect the damaged element, but Figure (6.21) shows the first optimum damage percentage of 22%, while, the technique needed to 26 iterations to reach damage percentage of 90%.

The convergence of the particles towards the damage value within the searching space can be illustrated in Figure (6.22), where it shows the distribution of particles in the searching space for the first iteration and iteration number of 25, 50, 75 and 100. It is noted that in iteration number 75 that 93% of particles 130 discovered the exact target (solution), damaged element and the percentage of damage.

## Model

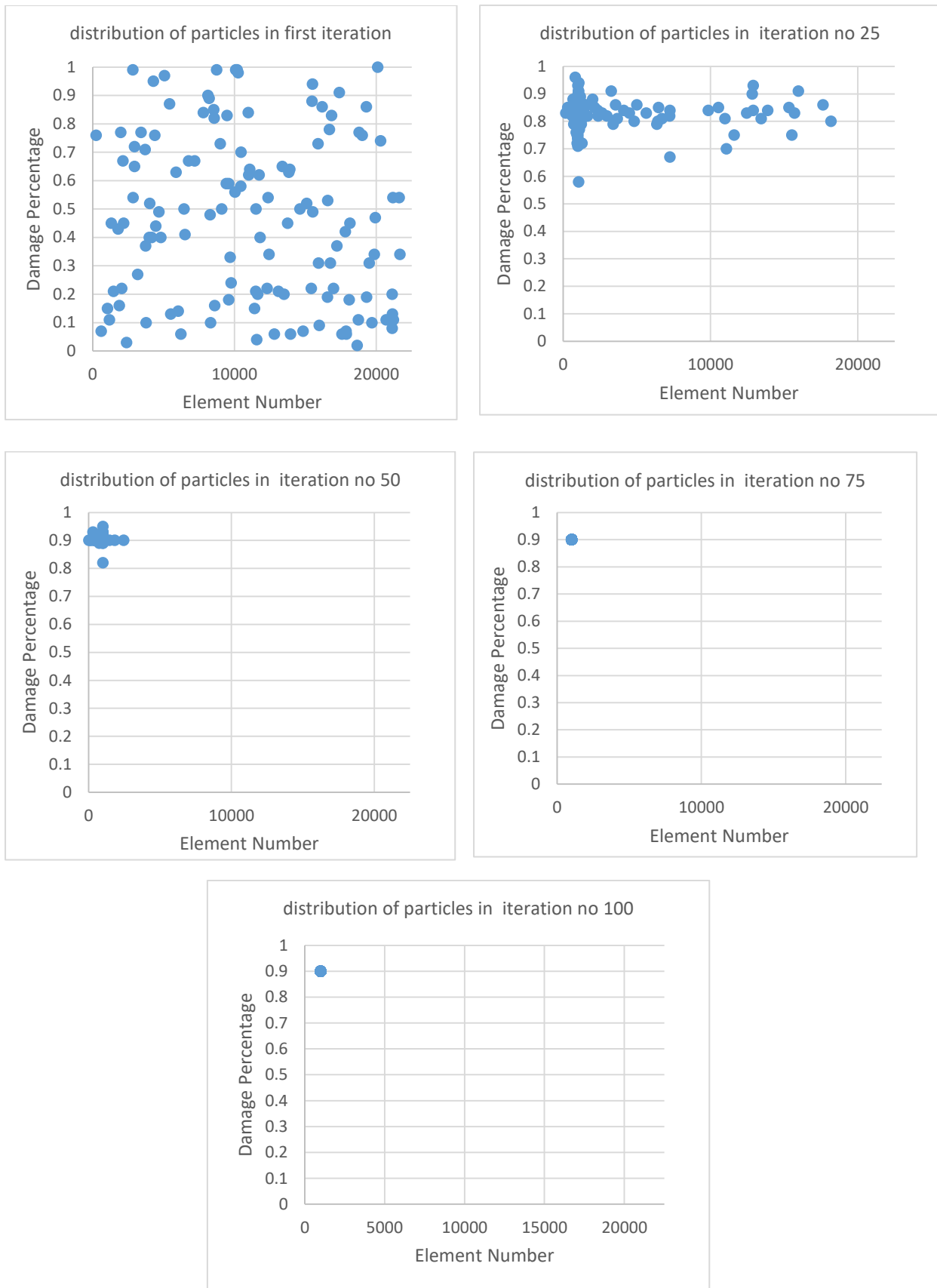


Figure (6.22) Distribution and affinity of particles towards damage in first, 25, 50, 75 and 100 iteration

Also from Figure (6.22) it can be seen how powerful a single particle is in detecting damage. Therefore, the ability of a single particle to move towards the detected damage element can be illustrated in the Figure (6.23) which shows the ability of the first particle to move towards the detected damage.

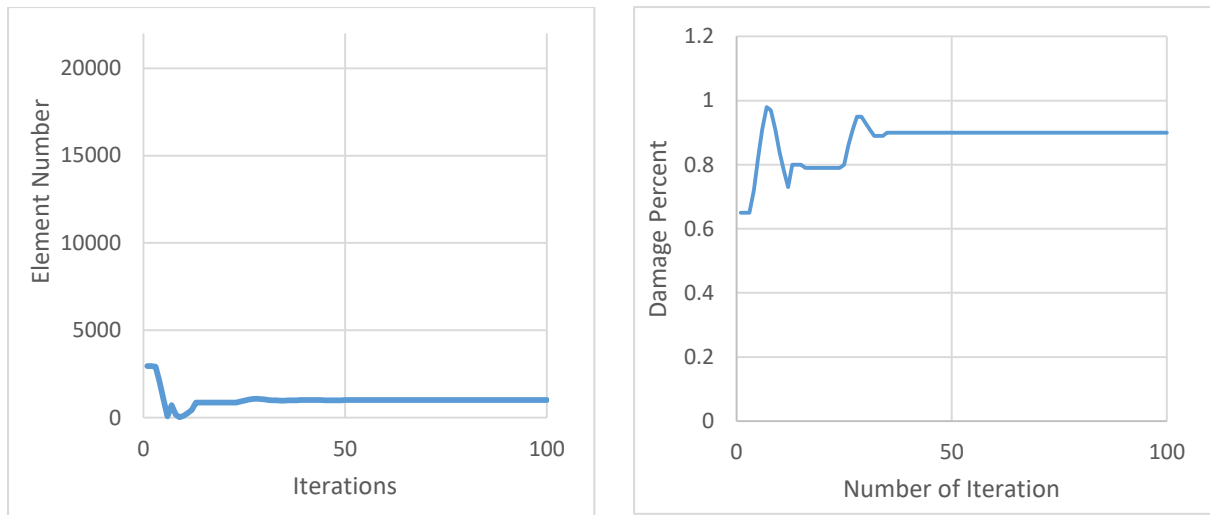


Figure (6.23) Ability the first particle to move towards the detected damaged element

As a result, the SHM technique detected the exact damaged element and percentage with only 83 iterations, this proved the efficiency of the adopted technique.

### 6.3.5. Fifth scenario

In the fifth scenario, the crack occurred in the dome of the minaret. The damage was represented by decreasing the modulus of elasticity 50% that means the residual value is 50%. The material properties of the intact and damaged element are listed in Table (6.10).

Table (6.10) Material properties of intact and damaged element for fifth scenario

Material properties	Intact elements	Damage element
Modulus of Elasticity (MPa)	3400	1700
Mass Density (kg/m <sup>3</sup> )	1200	1200
Poisson's Ratio	0.2	0.2

The Figure (6.24) shows the damaged element number of 1000 and damage percentage of 0.5 with its position in the FE minaret model for the fifth damage scenario case.

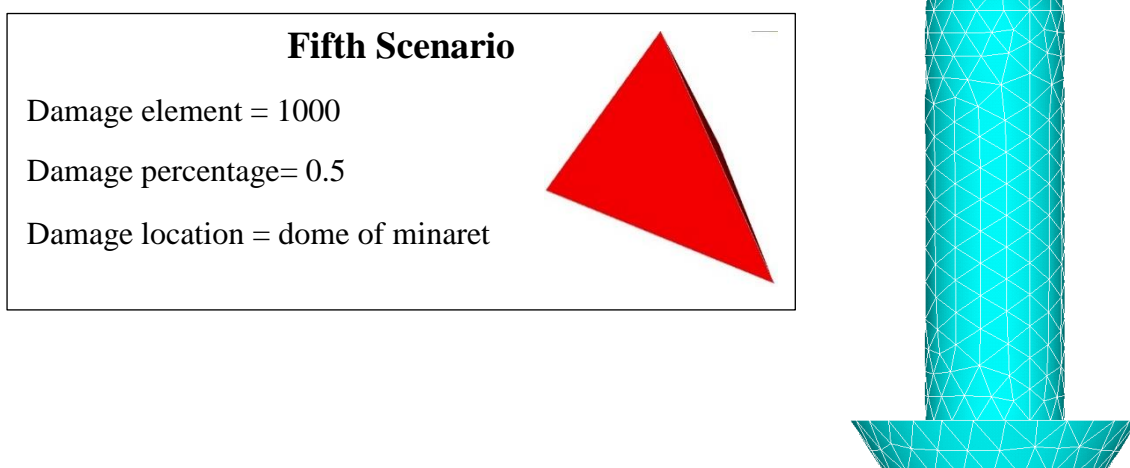


Figure (6.24) The damaged element, damage percentage and damage location of fifth scenario

The fifth scenario showed very efficient of the convergence of objective function in the SHM technique although the damage percentage was reduced by half compared with the first four scenarios. Where the SHM technique detected the damage in iteration number 36 by particle number 103. After that, in the iteration number 80, all particles (130) have detected the exact target solution, damaged

element and percentage. While, the SHM technique used only 0.48% to detect the optimum solution from the searching space size of 2168500 solutions. Figure (6.25) shows convergence of objective function with optimum iterations during the SHM technique procedures.

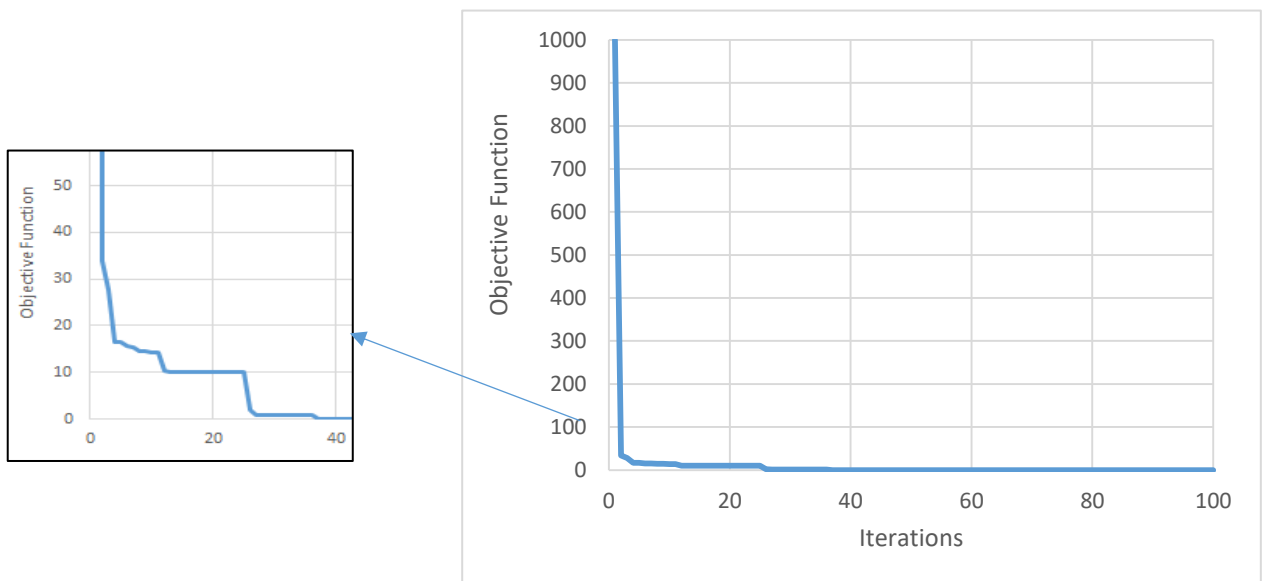
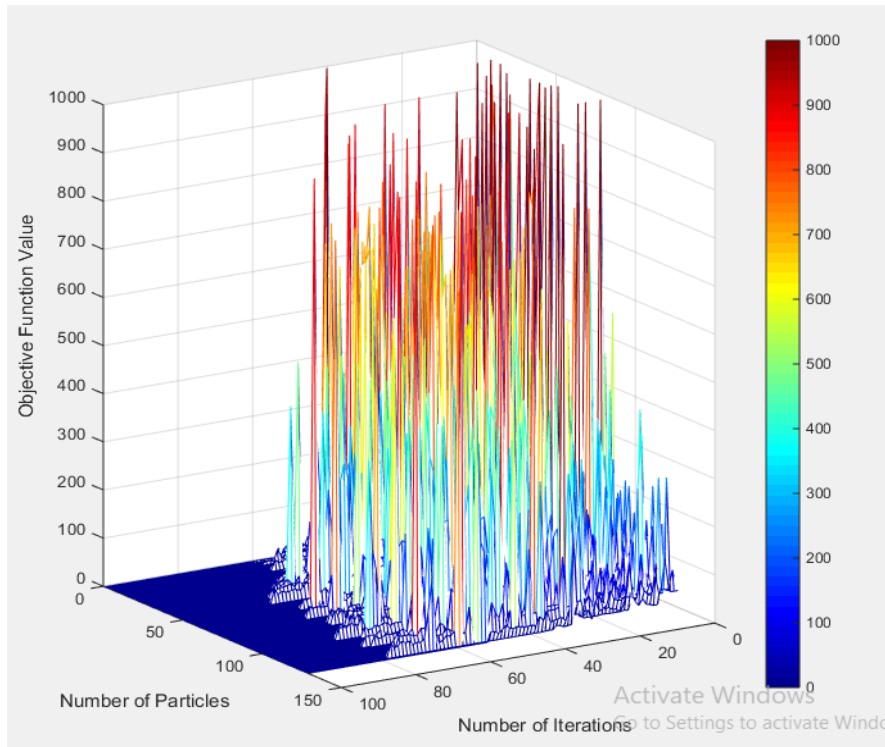


Figure (6.25) Convergence of objective function for fifth scenario

From Figure (6.25), it is noticed the line of objective function goes down directly from the assumed initial value of 1000 to the optimum objective function in the first iteration was 33.78 in element 1889 and damage percentage of 0.05. The damaged element was detected in iteration number 25, as shown in Figure (6.26) with a high convergence of optimum element number, but the damage percentage was detected in iteration number 36 as shown in Figure (6.27).

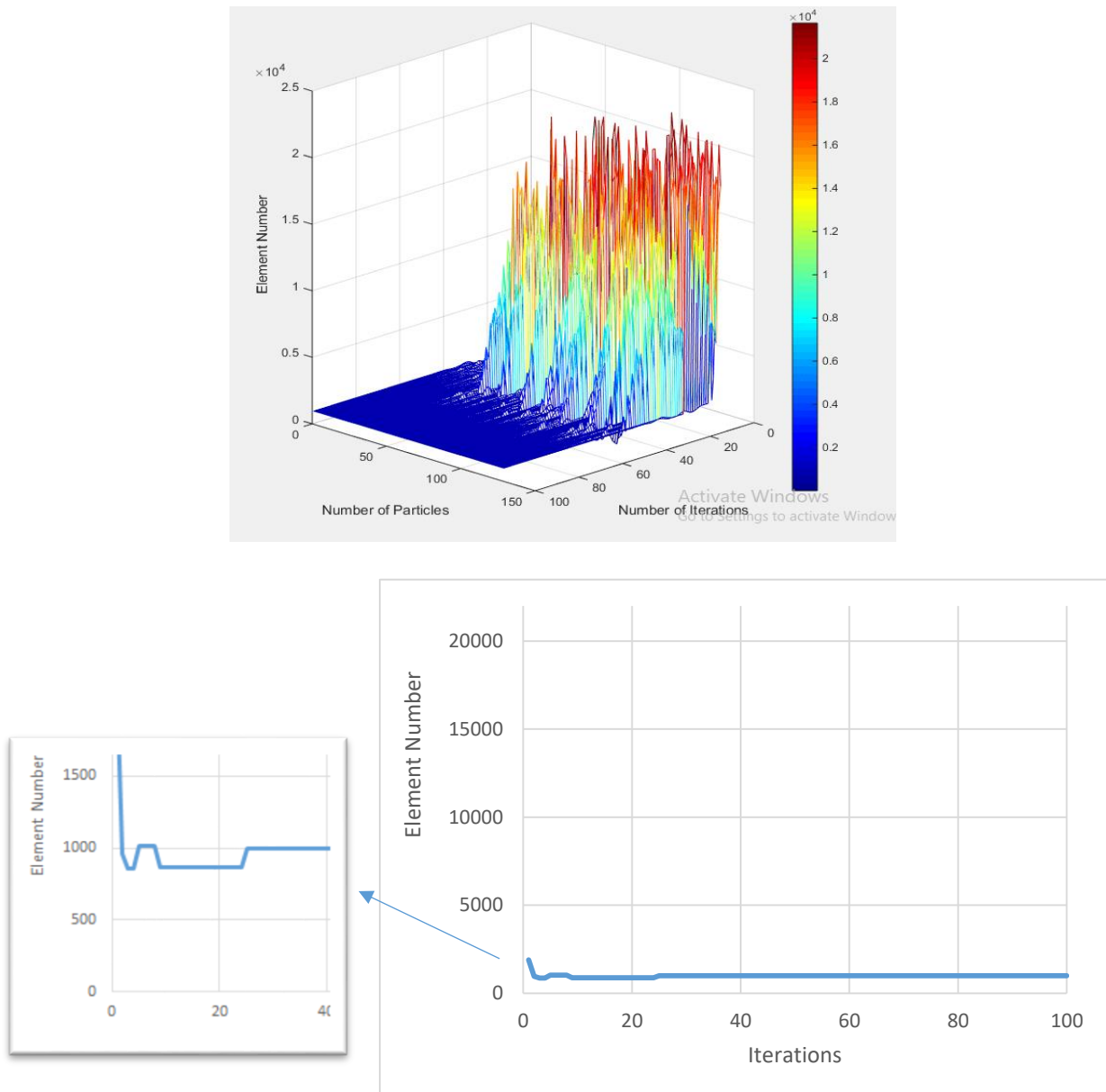


Figure (6.26) History of damaged element number for fifth scenario

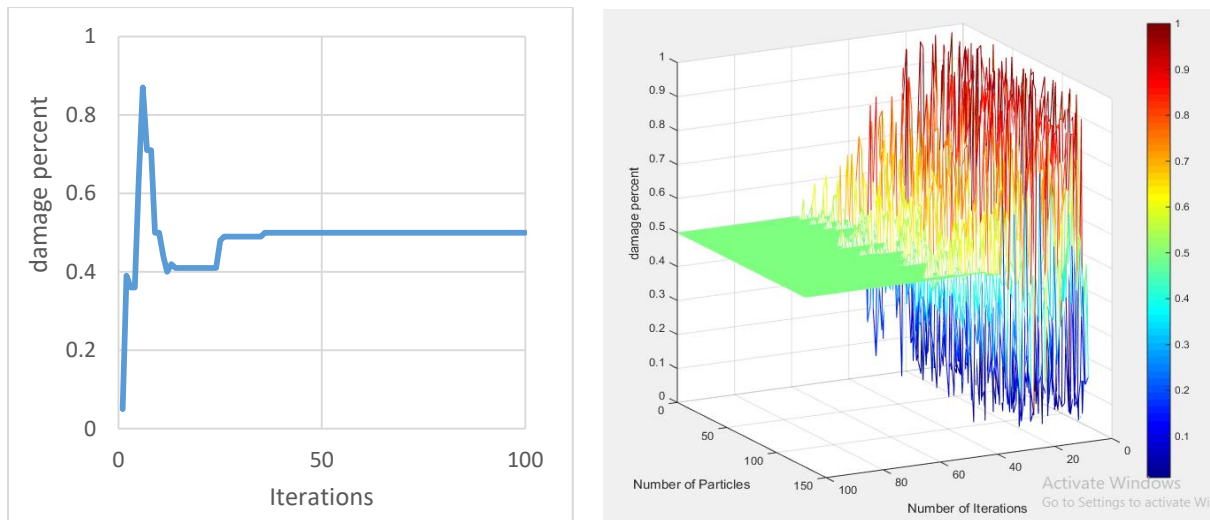


Figure (6.27) History of damage percentage for fifth scenario

From Figure (6.26), it is obvious that the first optimum element is 1889 which is close to damaged element 1000 compared with the total number of elements. Therefore, the adopted technique needed just 25 iterations to detect the damaged element, but Figure (6.27) shows the first optimum damage percentage of 5%, while, the technique needed to 36 iterations to reach damage percentage of 50%.

The convergence of the particles towards the damage value within the searching space can be illustrated in Figure (6.28), where it shows the distribution of particles in the searching space for the first iteration and iteration number of 25, 50, 75 and 100. It is noted that in iteration number 75 that 94.6% of particles 130 discovered the exact target (solution), damaged element and the percentage of damage.

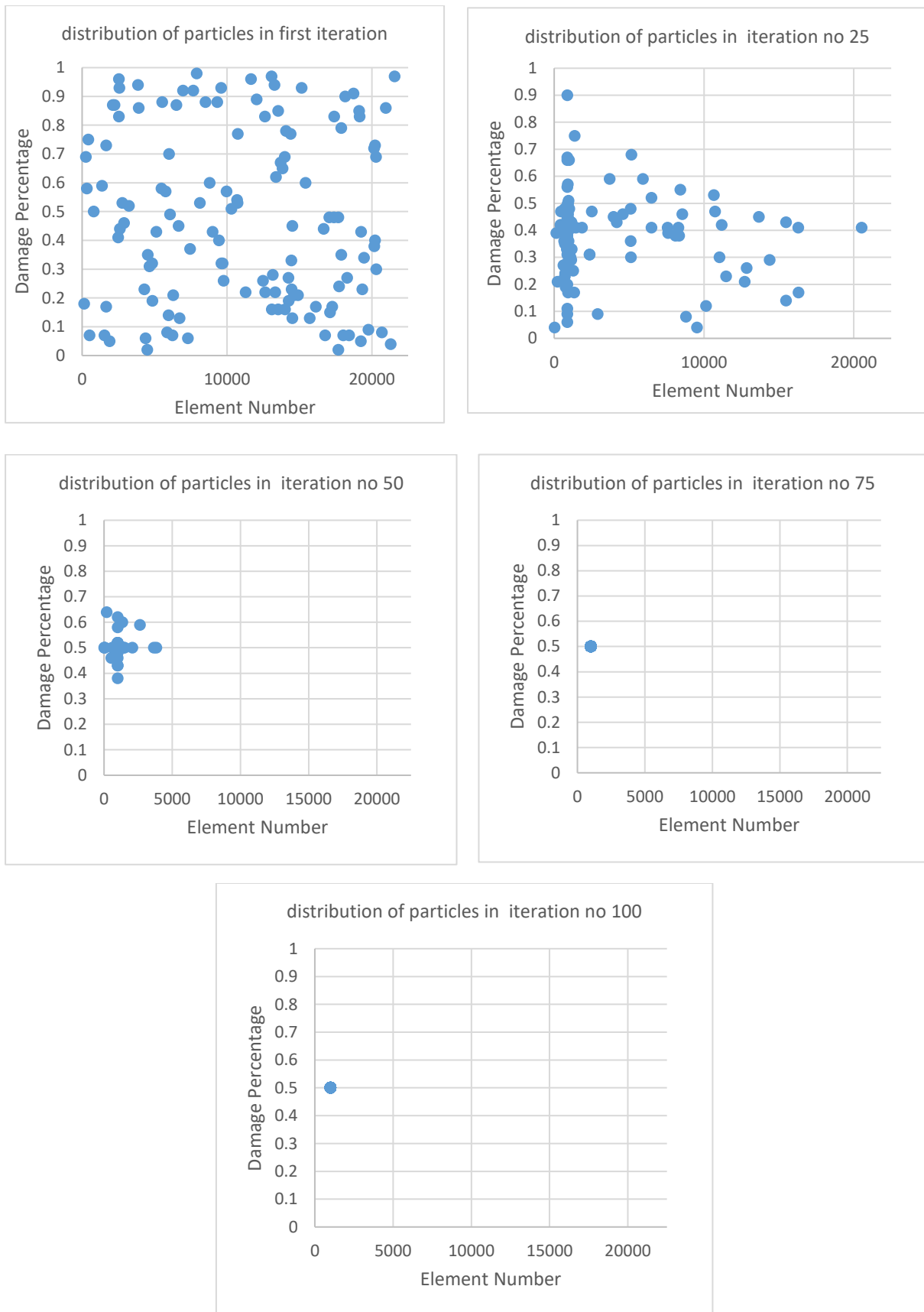


Figure (6.28) Distribution and convergence of particles towards damage in first, 25, 50, 75 and 100 iteration

Also from Figure (6.28) it can be seen how powerful a single particle is in detecting damage. Therefore, the ability of a single particle to move towards the detected damage can be illustrated as in Figure (6.29) where the ability of the first particle to move towards the detected damage is shown.

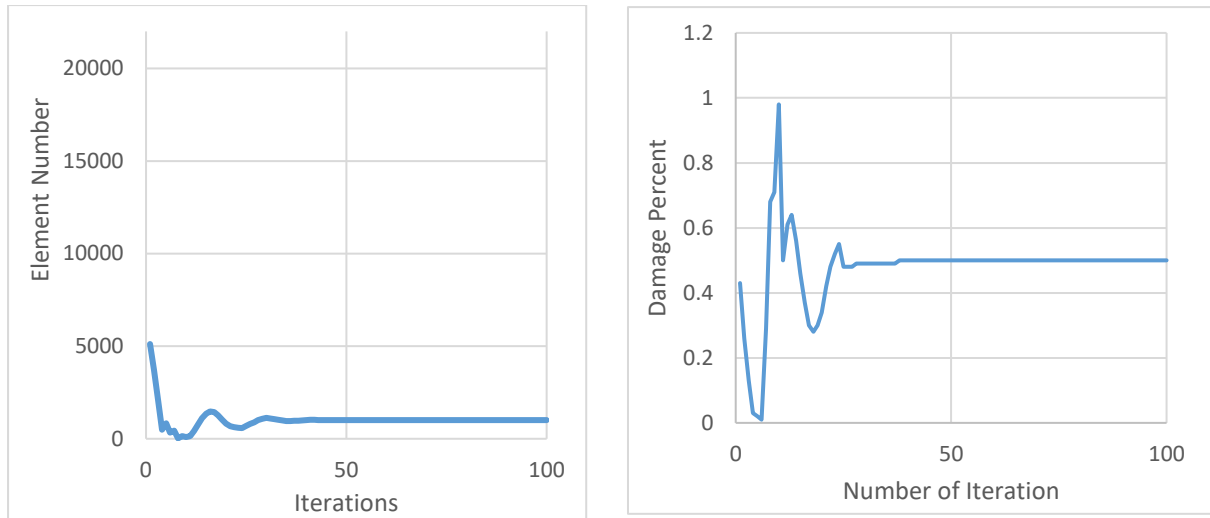


Figure (6.29) Ability the first particle to move towards the detected damage.

As a result, the SHM technique detected the exact damaged element and percentage with only 80 iterations, this proved the efficiency of the adopted technique.

### 6.3.6. Sixth scenario

In the sixth scenario, the crack occurred in the dome of the minaret. The damage was represented by decreasing the modulus of elasticity 10% that means the residual value is 90%. The material properties of the intact and damaged element are listed in Table (6.11).

Table (6.11) Material properties of intact and damaged element for sixth scenario

material properties	Intact elements	Damage element
Modulus of Elasticity (MPa)	3400	3060

Mass Density (kg/m <sup>3</sup> )	1200	1200
Poisson's Ratio	0.2	0.2

The Figure (6.30) shows the damaged element number of 1000 and damage percentage of 0.1 with its position in the FE minaret model for the sixth damage scenario case.

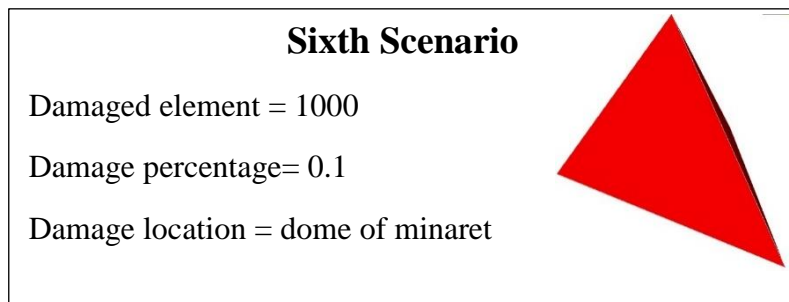


Figure (6.30) The damaged element, damage percentage and damage location of sixth scenario

The fifth scenario showed very efficient of the convergence of objective function in the SHM technique although the damage percentage is very low about just 10% from the modulus of elasticity compare with the first five scenarios. Where the SHM technique detected the damage in iteration number 27 by particle number 1. After that, in the iteration number 67, all particles (130) have detected the exact target solution, damaged element and percentage. While, the SHM technique used only 0.40% to detect the optimum solution from the searching space size of 2168500 solutions. Figure (6.31) shows convergence of objective function with optimum iterations during the SHM technique procedures.

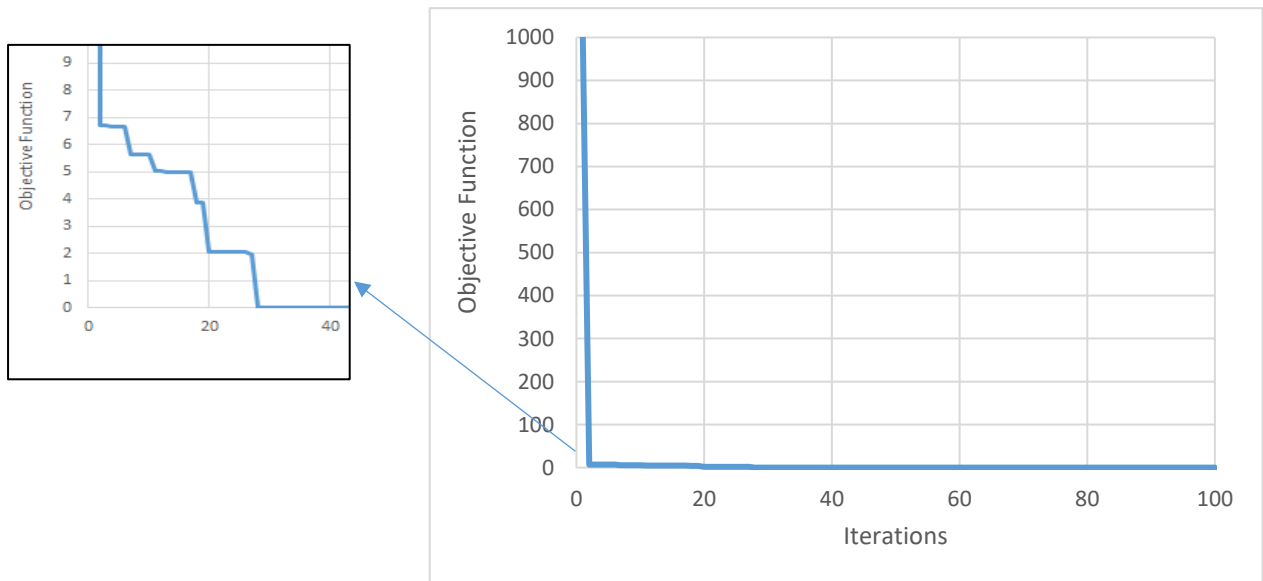
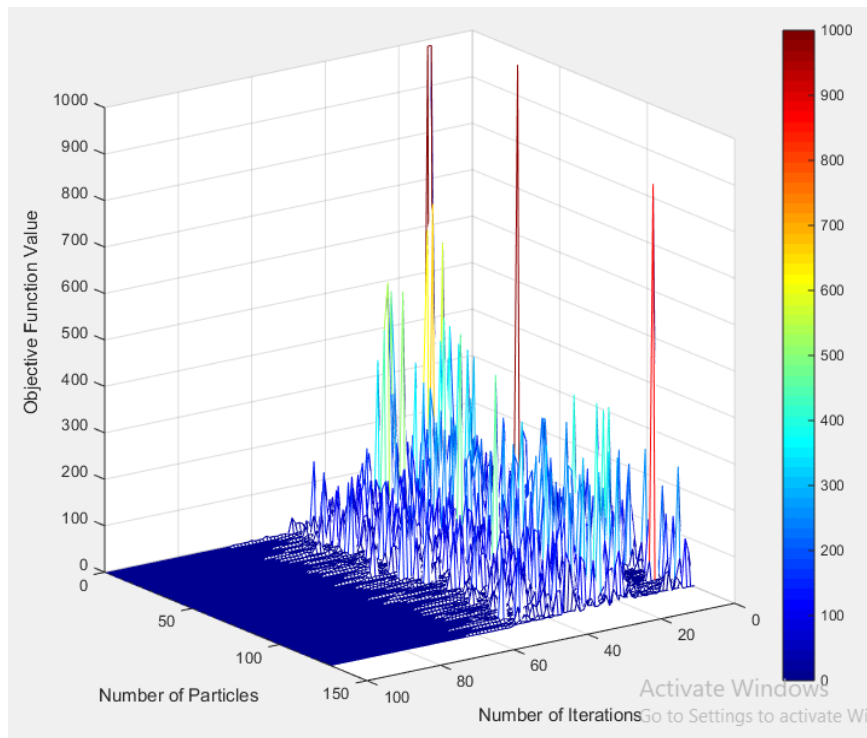


Figure (6.31) Convergence of objective function for sixth scenario

From Figure (6.31), it is noticed the line of objective function goes down directly from the assumed initial value of 1000 to the optimum objective function in the

first iteration was 6.68 in element 10764 and damage percentage of 0.02. The damaged element was detected in iteration number 27, as shown in Figure (6.32) with a high convergence of optimum element number, but the damage percentage was detected also in iteration number 27 as shown in Figure (6.33).

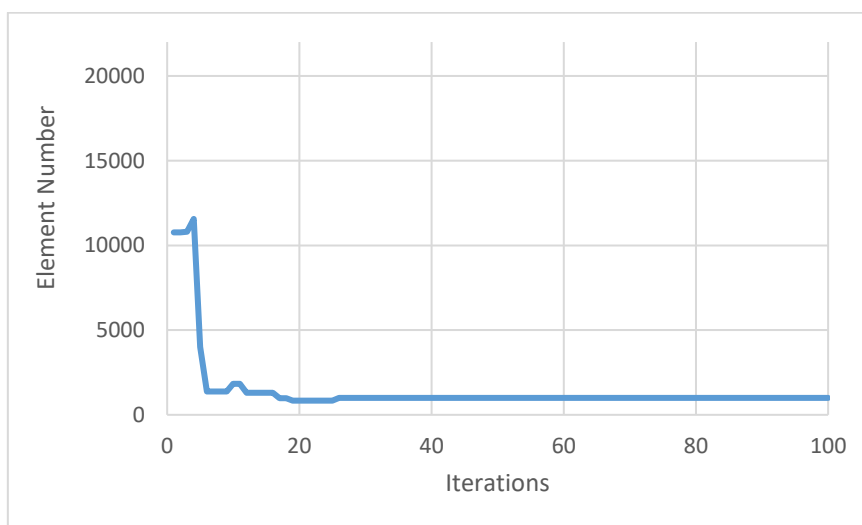
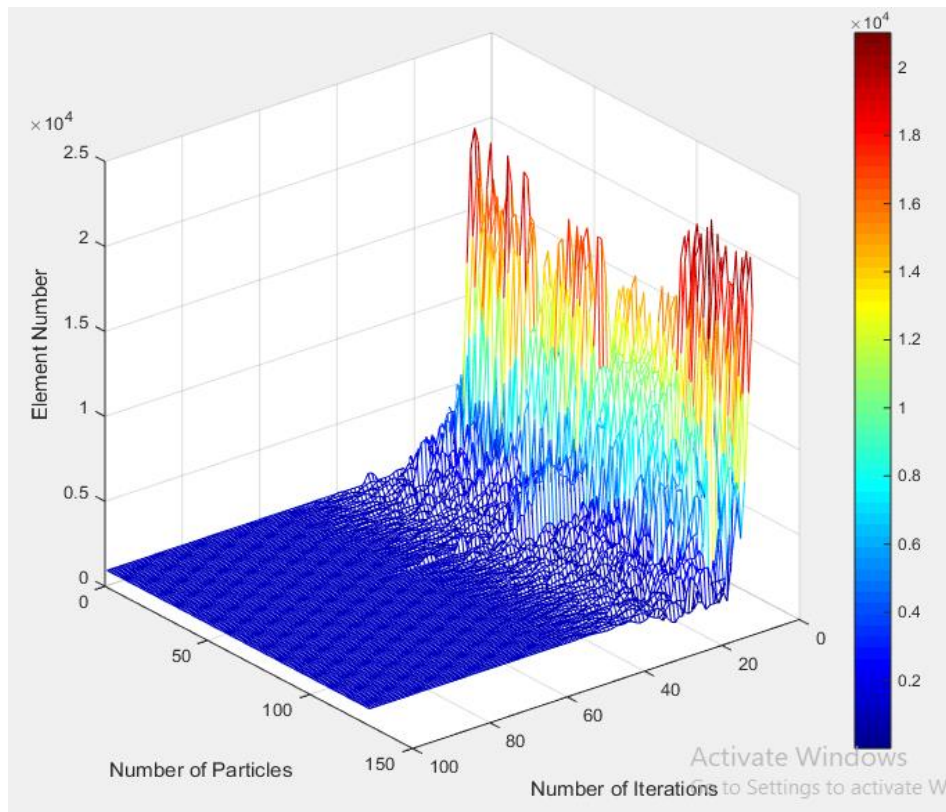


Figure (6.32) History of damaged element number for sixth scenario

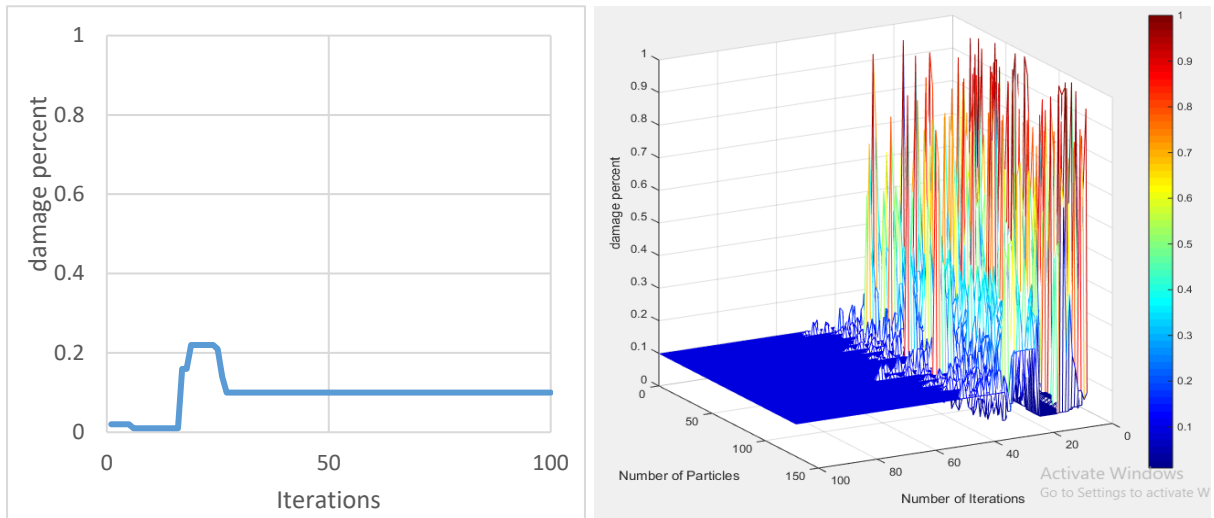


Figure (6.33) History of damage percentage for sixth scenario

The convergence of the particles towards the damage value within the searching space can be illustrated in Figure (6.34), where it shows the distribution of particles in the searching space for the first iteration and iteration number of 25, 50 and 75. It is noted that in iteration number 75 all particles 130 discovered the exact target (solution), damaged element and the percentage of damage.

## Model

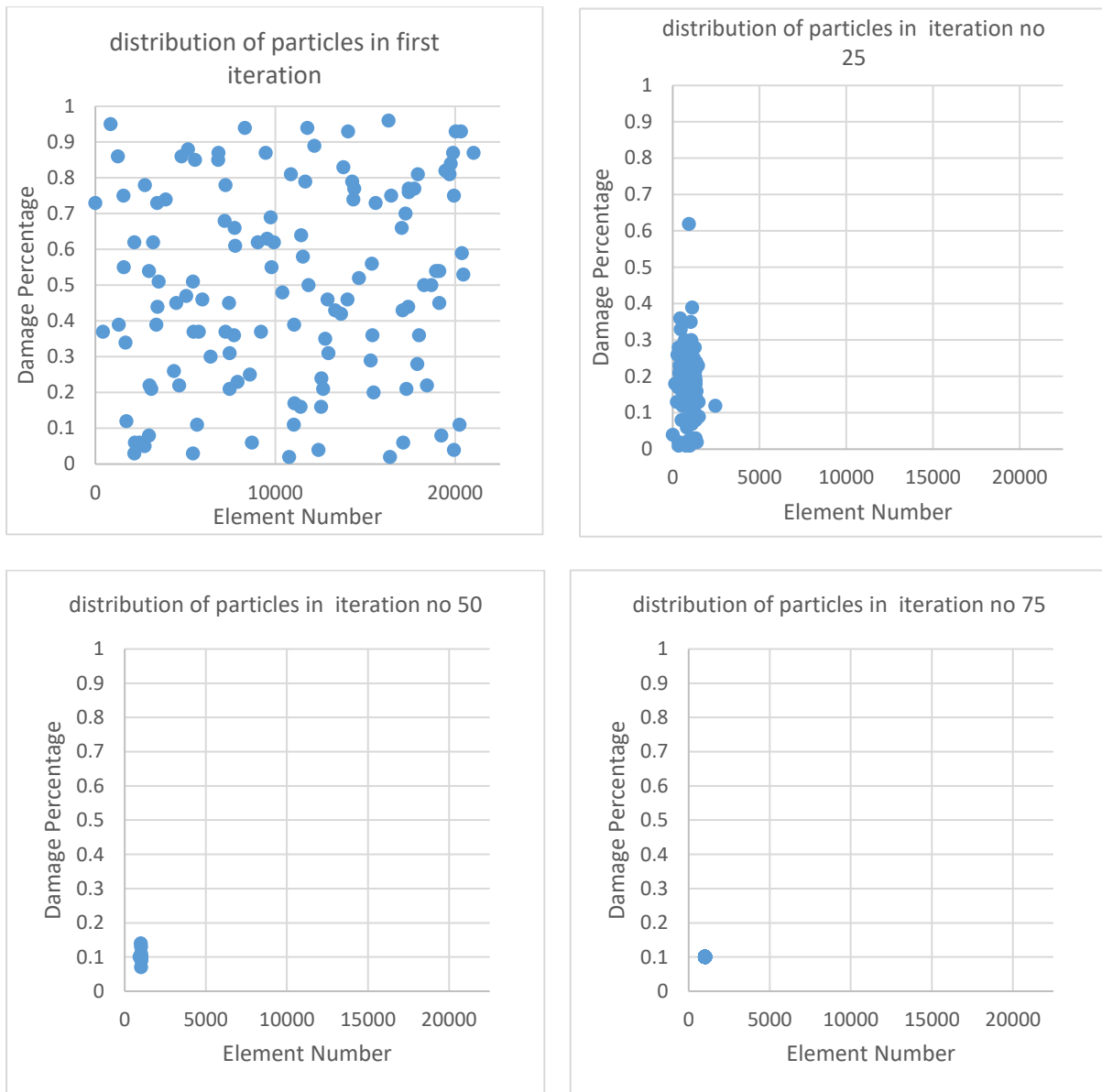


Figure (6.34) Distribution and convergence of particles towards damage in first, 25, 50 and 75 iteration

Also from the figure (6.36) it can be seen how powerful a single particle is in detecting damage. Therefore, the ability of a single particle to move towards the detected damage can be illustrated as in Figure (6.37) which shows the ability of first particle to move towards the detected damage.

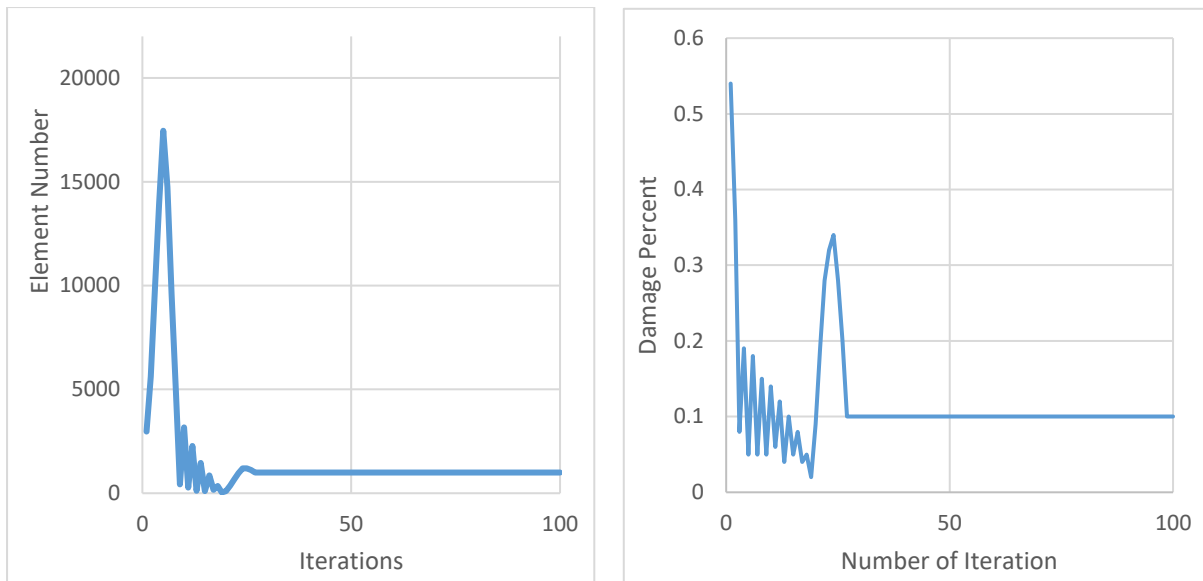


Figure (6.35) Ability the first particle to move towards the detected damage.

As a result, the SHM technique detected the exact damaged element and percentage with only 67 iterations, this proved the efficiency of the adopted technique.

# CHAPTER SEVEN

# CHAPTER SEVEN

## Conclusions and Recommendations

### 7.1. Conclusions

This study introduces the structural health monitoring technique of Imam Ali holy building and many conclusions are extracted which listed as below:

1- From the static analysis of adopted structure the maximum displacement was in the top of minaret about 1.306mm. The maximum von Mises stress is 0.336 MPa in the area middle of minaret between fixed walls of free part from minaret. The maximum tensile stress is located in the middle of minaret between fixed support walls and free part of minaret, therefore the first crack may be appeared in this regen.

2- From the modal (dynamic) analysis, the first seven natural frequencies values of brick minaret structural model was adopted in the range of (3.353-29.162) Hz with mass participation of 99.5%. The first seven mode shapes characters are 1<sup>st</sup> bending about y and x-axis, 2<sup>nd</sup> bending about y and x-axis, torsion about z-axis and 3<sup>rd</sup> bending about y and x-axis.

3- In the parametric analysis, when changing elastic modulus of the FE minaret model by percent of  $\pm 5\%$  (3060–3740) MPa, has significant effect with gradually increasing on the natural frequencies values. The first and third natural frequency values differ by 0.335 and 1.161 Hz, respectively, whereas, the fifth and sixth natural frequency values differ by 2.108 and 2.745 Hz, respectively, indicating that last modes were more responsive to the elastic modulus changing.

4- The natural frequency value has significant decreasing as the mass density increased, with changing percent of  $\pm 5\%$  in mass density of 1080-1320 kg/m<sup>3</sup>. Additionally, the four modes have a same decreasing ratio of 9.5% percent.

5- From the modal analysis between the intact and damaged minaret model for the six damage scenarios cases, the differences of extracted first seven natural frequencies values were very small as in the fourth digit.

6- In first scenario which was near the base with 90% damage percentage, the SHM technique detected the target (optimum) solution (damage) in iteration number 74 by all particles which is representing 0.44% of the whole searching space.

7- In second scenario which was in middle of body of minaret with 90% damage percentage, the SHM technique detected the target (optimum) solution (damage) in iteration number 95 by all particles which is representing 0.57% of the whole searching space.

8- In third scenario which was in the balcony with 90% damage percentage, the SHM technique detected the target (optimum) solution (damage) in iteration number 84 by all particles which is representing 0.50% of the whole searching space.

9- In fourth scenario which was in the dome with 90% damage percentage, the SHM technique detected the target (optimum) solution (damage) in iteration number 83 by all particles which is representing 0.50% of the whole searching space.

10- In fifth scenario which was in the dome with 50% damage percentage, the SHM technique detected the target (optimum) solution (damage) in iteration number 80 by all particles which is representing 0.48% of the whole searching space.

11- In sixth scenario which was in the dome with 10% damage percentage, the SHM technique detected the target (optimum) solution (damage) in iteration number 67 by all particles which is representing 0.40% of the whole searching space.

12- From the results for the different damage scenarios of the adopted structural model, the proposed SHM technique using PSO method is very robustness and efficiency to detect the damage and its characteristics, location and percentage.

## **7.2. Recommendations**

- 1- Conducting studies with using different optimization methods in the structural health monitoring technique of the minaret.
- 2- Conducting the study by representing the damage in other ways, such as reducing the mass density or geometry of the element.
- 3- Modeling the structure with another element type or another element size and compare the results.
- 4- Implementing experimental modal analysis for such type of real structure using the Accelerometers and data acquisition devices.
- 5- Application of the proposed SHM technique for another important historical brick masonry structure.

# REFERENCE

## References

- [1] Qarib, Hossein, and Hojjat Adeli. "Recent advances in health monitoring of civil structures." *Scientia Iranica* 21.6 (2014): 1733-1742.
- [2] Farrar, Charles R., and Keith Worden. "An introduction to structural health monitoring." *Philosophical Transactions of the Royal Society A: Mathematical, Physical and Engineering Sciences* 365.1851 (2007): 303-315.
- [3] Merkle, Daniel, and Martin Middendorf. "Swarm intelligence." *Search methodologies*. Springer, Boston, MA, 2005. 401-435.
- [4] Khalifa, "Seismic Behavior of Imam Ali Holy Shrine Structure in Najaf Ashraf - Iraq ", *Master thesis of Science in Civil Engineering-Structural Engineering , Faculty of Engineering, University of Kufa, 2021.*
- [5] Chopra, Anil K. *Dynamics of structures*. Pearson Education India, 2007.
- [6] Inman, D. J. "Engineering Vibration, University of Michigan." *Ann Arbor, MI* (2014).
- [7] Doebling, Scott W., Charles R. Farrar, and Michael B. Prime. "A summary review of vibration-based damage identification methods." *Shock and vibration digest* 30.2 (1998): 91-105.
- [8] Al-Wazni, Saad JA. "Damage detection and localization for civil structural health monitoring." *Doctoral Thesis, University of Belgrade, Faculty of Civil Engineering, (2016).*
- [9] Garziera, R., M. Amabili, and L. Collini. "Structural health monitoring techniques for historical buildings." *Proceedings of the 4th Pan-American Conference for Non-Destructive Testing, Buenos Aires, Argentina. Vol. 2226. 2007.*

- [10] Abdalla, Musa O. "Particle swarm optimization (PSO) for structural damage detection." *ASMCSS'09 Proceedings of the 3rd International Conference on Applied Mathematics, Simulation, Modelling, Circuits, Systems and Signals*. 2009.
- [11] Bayraktar1a, Alemdar, Ahmet Can Altunişik, and Murat Muvafik2b. "Damages of minarets during Erciş and Edremit earthquakes, 2011 in Turkey." (2014).
- [12] Kang, Fei, Jun-jie Li, and Qing Xu. "Damage detection based on improved particle swarm optimization using vibration data." *Applied Soft Computing* 12.8 (2012): 2329-2335.
- [13] Cakti, E., et al. "A parametric study on earthquake behavior of masonry minarets." *Proceedings of the Tenth US National Conference on Earthquake Engineering Frontiers of Earthquake Engineering, 10NCEE, Anchorage, Alaska*. 2014.
- [14] Duvnjak, Ivan, Domagoj Damjanović, and Joško Krolo. "Structural health monitoring of cultural heritage structures: Applications on Peristyle of Diocletian's palace in Split." *8th European workshop on structural health monitoring, EWSHM*. Vol. 4. 2016.
- [15] Mehrian, Sh Zamani, et al. "Structural health monitoring using optimising algorithms based on flexibility matrix approach and combination of natural frequencies and mode shapes." *International Journal of Structural Engineering* 7.4 (2016): 398-411.
- [16] Livaoğlu, Ramazan, et al. "Effect of geometric properties on dynamic behavior of historic masonry minaret." *KSCE Journal of Civil Engineering* 20.6 (2016): 2392-2402.

- [17] Basaran, Hakan, et al. "Investigation of seismic safety of a masonry minaret using its dynamic characteristics." *Earthquakes and Structures* 10.3 (2016): 523-538.
- [18] Nohutcu, H., et al. "Collapse mechanism estimation of a historical slender minaret." *Structural Engineering and Mechanics* 64.5 (2017): 653-660.
- [19] Nohutcu, Halil, et al. "Evaluation of Dynamic Characteristics of Historical Masonry Structures by Operational Modal Analysis" *Proceedings of 3rd International Sustainable Buildings Symposium (ISBS 2017)*. 2019.
- [20] Ghannadi, Parsa, et al. "Efficiency of grey wolf optimization algorithm for damage detection of skeletal structures via expanded mode shapes." *Advances in Structural Engineering* 23.13 (2020): 2850-2865.
- [21] Nguyen, Quy Thue, and Ramazan Livaoğlu. "A health monitoring solution on damage detection of minarets." *Engineering Failure Analysis* 135 (2022): 106154.
- [22] Sun, Wenyu, and Ya-Xiang Yuan. *Optimization theory and methods: nonlinear programming*. Vol. 1. Springer Science & Business Media, 2006.
- [23] Arora, Rajesh Kumar. *Optimization: algorithms and applications*. CRC Press, 2015.
- [24] Yang, Shengxiang. "Evolutionary computation for dynamic optimization problems." *Proceedings of the 15th annual conference companion on Genetic and evolutionary computation*. 2013.
- [25] Lee, Kwang Y., and Mohamed A. El-Sharkawi, eds. *Modern heuristic optimization techniques: theory and applications to power systems*. Vol. 39. John Wiley & Sons, 2008.

- [26] Kitayama, Satoshi, Masao Arakawa, and Koetsu Yamazaki. "Differential evolution as the global optimization technique and its application to structural optimization." *Applied Soft Computing* 11.4 (2011): 3792-3803.
- [27] Merkle, Daniel, and Martin Middendorf. "Swarm intelligence." *Search methodologies*. Springer, Boston, MA, 2005. 401-435.
- [28] Al-Wazni, Saad, and Ahmed Y. Azainul-abideen. "Intelligent non-destructive technique for crack existence inspection in a structure using Particle Swarm Optimization (PSO)." *IOP Conference Series: Materials Science and Engineering*. Vol. 584. No. 1. IOP Publishing, 2019.
- [29] Wei, Zitian, Jike Liu, and Zhongrong Lu. "Structural damage detection using improved particle swarm optimization." *Inverse Problems in Science and Engineering* 26.6 (2018): 792-810.
- [30] Khalifa, Hayder, and Saad Al-Wazni. "Experimental testing and comparison between historical and traditional masonry brick." *Journal of Physics: Conference Series*. Vol. 1973. No. 1. IOP Publishing, 2021.
- [31] ANSYS Parametric Design Language Guide Release 14.0, ANSYS, Inc. certified to ISO 9001:2008. (2014).
- [32] ANSYS Modeling and Meshing Guide, ANSYS Release 9.0, ANSYS, Inc.
- [33] SOLID65 Element Description
- [34] Fu, Zhi-Fang, and Jimin He. *Modal analysis*. Elsevier, 2001.
- [35] ANSYS Mechanical APDL Structural Analysis Guide, ANSYS Release 13.0, ANSYS, Inc.
- [36] Al-Ghazali Karrar and Al-Wazni Saad "Investigation and Parametric Study of a Masonry Bricks Minaret Structure under Vibration", University of Kufa, Iraq, (2022).
- [37] MATLAB. (V0.9 Revision 104), {oUUID 1.858}. (2017).

[38] Bharadwaj Nanda, Damodar Maity and Dipak Kumar Maiti "Vibration Based Structural Damage Detection Technique using Particle Swarm Optimization with Incremental Swarm Size", Int'l J. of Aeronautical & Space Sci. 13(3), 323–331, (2012).

## الخلاصة

يعتبر هيكل ضريح الامام علي (ع) من الاماكن التاريخية والمهمة في العراق في النجف. في هذه الدراسة، تم تطبيق تقنية SHM مقترحة باستخدام طريقة تحسين سرب الجسيمات (PSO) لمنشأ منارة الإمام علي. تعتبر المئذنتان هما الجزء الأكثر أهمية من الهيكل الكلي بسبب حساسيتهما لأي تحميل غير متوقع بسبب الشكل ونسبة النحافة.

تم أخذ الأبعاد الحقيقية لهيكل المئذنة من الموقع وتم إنشاء نموذج العناصر المحددة (FEM) للمئذنة باستخدام برنامج ANSYS. تم إجراء دراسة بارامترية لتحديد حجم العناصر المناسب في نموذج المئذنة FE بناءً على التحليل المودولي. كان حجم العنصر ٥٠٠ مم مناسباً في استهلاك الوقت والدقة المناسبة للنتائج، حيث بلغ إجمالي عدد العقد والعناصر ٥٤٢٥ و ٢١٦٨٥ على التوالي. بالنسبة للتحليل الاستاتيكي غير الخطي للمئذنة، تم تبني موديل مادة ذات سلوك (multilinear isotropic hardening (MISO)) باستخدام نظرية فشل (von Mises). تم استخلاص الإجهاد والإزاحة والتشققات من التحليل غير الخطي لهيكل المئذنة. أقصى إجهاد فشل (von Mises) هو ٠,٣٣٦ ميغا باسكال في منتصف المئذنة بالقرب من الجزء الثابت من المئذنة. يبلغ الحد الأقصى للإزاحة ١,٣٠٦ ملم في أعلى قبة المئذنة، بينما ظهر الشق الأول في نفس موقع أقصى إجهادات للمئذنة.

تم إجراء التحليل الديناميكي الخطي (المودولي) باستخدام طريقة (block Lanczos) بواسطة برمجة لغة (APDL) برنامج ANSYS لاستخراج الخواص الديناميكية لنموذج المئذنة. تم اعتماد النماذج السبعة الأولى بنسبة مشاركة للكتلة الكلية ٩٩,٥٪ وقيم التردد الطبيعية تتراوح بين (٢٩,١٦٢-٣,٣٥٣) هرتز. شكل المودات السبعة الأولى هي كالاتي: وضع ذو انحناء واحد واثنين وثلاثة في المحور x و y للمئذنة بالإضافة إلى وضع الالتواء. تم إجراء دراسة بارامترية لنموذج مئذنة FE بناءً على التحليل المودولي باستخدام أربعة أنماط فقط من أجل التحقق من تأثير تغيير خصائص المواد (معامل المرونة وكثافة الكتلة) وابعاد المئذنة على الترددات الطبيعية و شكل المودات. لذلك أثبتت نتائج الدراسة البارامترية التأثير الفعال لمعامل المرونة وكثافة الكتلة والابعاد على الخصائص الديناميكية للمئذنة.

في هذه الدراسة، تم اقتراح إجراء تقنية SHM باستخدام طريقة PSO عن طريق كتابة برنامج في بيئة لغة MATLAB. نظرًا لأنه لم يكن بالأمكان وضع أجهزة استشعار وجمع البيانات على المئذنة بسبب الكلفة لغرض تنفيذ الأختبار المودولي الحقلي في الموقع ولأسباب أمنية أيضاً، فقد تمت محاكاة سيناريوهات الضرر باستخدام برنامج ANSYS. لذلك، تم تنفيذ إجراء SHM العددي باستخدام سيناريو الضرر المفترضة لتمثيل التحليل المودولي التجريبي للمنشأ المتضرر. لمحاكاة التشقق كضرر في نموذج المئذنة،

تم تقليل صلابة عنصر محدد في نموذج FE بتمثيله بالانخفاض في قيمة معامل المرونة. تم اختبار الإجراء المقترح لتقنية SHM على نوعين من الهياكل قبل نموذج المئذنة، عارضة فولاذية مثبتة من جهة واحدة وجدار مبني من الطابوق لمعرفة كفاءة تقنية SHM المقترحة المعتمدة. نتائج الاختبار أثبتت متانة وكفاءة تقنية SHM المقترحة.

في هذا البحث، تم أخذ ستة سيناريوهات مختلفة للضرر في النموذج الهيكلي للمئذنة بمواقع مختلفة ونسب ضرر مختلفة. تم اعتماد ثلاث نسب مختلفة للضرر تراوحت (١٠ و ٥٠ و ٩٠)٪ لموقع واحد في أعلى المنارة (في القبة) حيث حدوث أقصى إزاحة. كما تم اختيار ثلاثة مواقع للضرر وتوزيعها في مناطق الأجهادات الحرجة، بالقرب من القاعدة، وفي نهاية الجدار المثبت مع جدار الصحن وفي المئذنة بشدة ضرر ٩٠٪. تم تنفيذ تقنية SHM المقترحة لاكتشاف سيناريوهات الضرر ومواقعها وشدها. بالنسبة لسيناريو الضرر الموجود في الأعلى مع ضرر ١٠٪، تم الحصول على التقارب العالي لدالة الهدف للجسيمات و اكتشاف الضرر عند المحاولة رقم ٢٧، ولكن في منطقة ذات الاجهادات العالية في جسم المئذنة، تم الحصول على تقارب كبير لقيم دالة الهدف عند المحاولة رقم ٧٠.

تظهر نتائج تقنية SHM المقترحة كفاءة عالية ومتانة في اكتشاف الضرر لكل من الموقع والشدة ولجميع سيناريوهات الضرر.



جمهورية العراق

وزارة التعليم العالي والبحث العلمي

جامعة الكوفة - كلية الهندسة

قسم الهندسة المدنية

# مراقبة السلامة الانشائية لبناية مرقد الامام علي باستخدام طريقة تحسين سرب الجسيمات

رسالة

مقدمة لكلية الهندسة / جامعة الكوفة كجزء من متطلبات نيل شهادة الماجستير في علوم الهندسة المدنية

(هندسة إنشاءات)

من قبل

**كرار حسين دونه عبد الزهره**

(بكالوريوس في الهندسة المدنية ٢٠١٨)

بإشراف

**أ.م.د سعد جبار عباس الوزني**